

- I. QUASI-ELASTIC LIGHT SCATTERING FROM LIQUIDS AND LIQUID MIXTURES: A STUDY OF MASS AND THERMAL DIFFUSIVITIES
  
- II. OBSERVATION OF TRANSLATIONAL AND INTRAMOLECULAR DIFFUSION OF CIRCULAR DUPLEX DNA BY QUASI-ELASTIC LIGHT SCATTERING

Thesis by  
Ronald Jerome Brown

In Partial Fulfillment of the Requirements  
For the Degree of  
Doctor of Philosophy

California Institute of Technology  
Pasadena, California

1975

(Submitted July 31, 1974)

-ii-

*To my parents*

## ACKNOWLEDGMENTS

I am grateful to Professor C. J. Pings for his guidance and support during my studies at Caltech.

Without the advice and help of Hollis Reamer, the experimental work would not have been possible. George Griffith provided invaluable assistance in the design and construction of the apparatus.

J. Lee Compton and Robert Watson generously provided  $\phi\lambda$  and PM2 DNA samples and performed the necessary biophysical analyses.

During these studies I have received financial support from the National Science Foundation and the Donald E. Baxter Foundation. The research was supported by the Directorate of Chemical Sciences, AFOSR (SRC)-OAR, USAF Grant No. AFOSR-68-1382, by the Donald E. Baxter Foundation, and by National Science Foundation Grant GK-34045.

Finally, I am indebted to Patrice, who has been a source of encouragement and understanding during the conclusion of this work.

ABSTRACT

Part I

A quasi-elastic light scattering spectrometer has been constructed and used to measure the binary mutual diffusion coefficient  $D_{AB}$  as a function of concentration in eight binary mixtures and the thermal diffusivity  $\chi$  in nine pure liquids and two binary mixtures. The resulting values are in close agreement with the available bulk values and are accurate to within 3% for mass diffusivities and 5% for thermal diffusivities. Because neither type of measurement is dependent on the imposition of a macroscopic gradient, many of the problems associated with conventional bulk measurements are eliminated.

Determinations require less than 2 hours for thermal diffusivities and 30 minutes for mass diffusivities, in contrast to the more time consuming classical approaches.

On the basis of these experimental results, light scattering spectroscopy is established as an effective tool in the determination of liquid mass and thermal diffusivities. The technique should have wide industrial application.

Part II

Quasi-elastic light scattering experiments on solutions of  $\phi$ X174 RF DNA and PM2 I DNA reveal spectral contributions from translational and intramolecular motion. A tentative interpretation of the data in terms of Rouse-Zimm theory indicates lowest order relaxation

times qualitatively consistent with theoretical predictions. Further experiments on linear and form II DNA should provide information about the changes in molecular flexibility and translational diffusivity associated with an alteration in conformation.

TABLE OF CONTENTS

PART I: QUASI-ELASTIC LIGHT SCATTERING FROM LIQUIDS AND LIQUID MIXTURES: A STUDY OF MASS AND THERMAL DIFFUSIVITIES . . . . .	1
Chapter I Introduction . . . . .	2
II Theory . . . . .	6
III Apparatus and Experimental Methods . . . . .	22
IV Results and Discussion . . . . .	26
PART II: OBSERVATION OF TRANSLATIONAL AND INTRAMOLECULAR DIFFUSION OF CIRCULAR DUPLEX DNA BY QUASI-ELASTIC LIGHT SCATTERING . . . . .	33
Chapter V Introduction . . . . .	34
VI Theory . . . . .	38
VII Experimental . . . . .	43
VIII Results and Discussion . . . . .	45
Appendices . . . . .	58
Literature Cited . . . . .	79
Proposition . . . . .	140

LIST OF TABLES

1	$R_0$ Values for Pure Liquids, Liquid Mixtures, and Macromolecular Solutions . . . . .	86
2	Mass Diffusivity Measurements for Liquid Mixtures . . . . .	87
3	Previous Liquid Thermal Diffusivity Measurements by Quasi-Elastic Light Scattering . . . . .	89
4	Intensity of Scattering from Entropy Fluctuations . . . . .	90
5	$(\frac{\partial \epsilon}{\partial C})_{P,T}$ and Refractive Index Differences for Binary Mixtures . . . . .	91
6	Thermal Diffusivities of Pure Liquids and Binary Mixtures . . . . .	92
7	Values for the Scattering Parameter $\sqrt{x}$ for Circular $\phi$ X174 RF DNA . . . . .	93
8	Values for the Scattering Parameter $\sqrt{x}$ for Circular PM2 DNA . . . . .	93
9	Lower Bound Values on $\tau_1$ for $\phi$ X174 RF DNA . . . . .	94
10	Lower Bound Values on $\tau_1$ for PM2 I DNA . . . . .	94
III.1	Comparison of Light Sources and Photomultipliers Used In Light Scattering . . . . .	95

LIST OF FIGURES

1	A schematic drawing of the light scattering spectrometer used in this study . . . . .	97
2a	A typical correlogram for mass diffusion in a methanol-benzene mixture . . . . .	98
2b	A typical correlogram for thermal diffusion in a benzene-toluene mixture . . . . .	99
3	Mutual diffusion data for the nitromethane-benzene system . . . . .	100
4	Mutual diffusion data for the acetone-benzene system . . . . .	101
5	Mutual diffusion data for the n-hexane-benzene system . . . . .	102
6	Mutual diffusion data for the methanol-benzene system . . . . .	103
7	Mutual diffusion data for the ethanol-benzene system . . . . .	104
8	Mutual diffusion data for the systems toluene-bromobenzene and methanol-butanol . . . . .	105
9	The inverse decay time $(2\pi\tau)^{-1}$ vs. $K^2$ due to concentration fluctuations in a 10% (vol.) acetone-carbon disulfide mixture . . . . .	106
10	Inverse decay time vs. $K^2$ in the methanol-benzene system . . . . .	107
11	Inverse decay time vs. $K^2$ for pure carbon disulfide . . . . .	108
12	Inverse decay time vs. $K^2$ for pure carbon tetrachloride . . . . .	109
13	Inverse decay time vs. $K^2$ for pure toluene . . . . .	110
14	Inverse decay time vs. $K^2$ from entropy fluctuations in a toluene-benzene mixture . . . . .	111
15	Departure plot for thermal conductivity of liquid acetone . . . . .	112
16	Departure plot for thermal conductivity of liquid toluene . . . . .	113

17	Departure plot for thermal conductivity of liquid ethyl alcohol . . . . .	114
18	$P_{NM}(x)$ vs. $x^{1/2}$ at $\gamma_L \gg 1$ . . . . .	115
19	Inverse decay times versus scattering wave vector squared for a solution of polystyrene latex spheres. $\tau^{-1}$ is determined by an exponential fit with a variable baseline . . .	116
20	Inverse decay times versus scattering wave vector squared for the same data as in Figure 19. $\tau^{-1}$ is determined by an exponential fit with a zero baseline . . . . .	117
21	A typical correlation function collected for a solution of polystyrene latex spheres. Sample time increment is $5 \mu s$ .	118
22	A typical correlation function collected under conditions identical to those of Figure 21 except that $\Delta\tau = 10 \mu s$ . .	119
23	A typical correlation function collected under conditions identical to those of Figure 21 except that $\Delta\tau = 20 \mu s$ . .	120
24	Inverse decay times versus scattering wave vector squared for a solution of $\phi X174$ RF I and II DNA . . . . .	121
25	Inverse decay times versus scattering wave vector squared for a solution of PM2 I DNA . . . . .	122
26	A typical correlation function collected from a solution of PM2 I DNA. The sample time increment is $10 \mu s$ . . . . .	123
27	A typical correlation function for PM2 I DNA collected under conditions identical to those of Figure 26 except that $\Delta\tau = 20 \mu s$ . . . . .	124
28	A typical correlation function for PM2 I DNA collected under conditions identical to those of Figure 26 except that $\Delta\tau = 50 \mu s$ . . . . .	125
II.1	Details of the grounding scheme for the light scattering spectrometer . . . . .	126

III.1	Block diagram of the photon counting and data collection systems . . . . .	127
III.2	A pulse height distribution for the EMI 9789B photomultiplier tube in system 1, obtained using the E sweep with a window width of 0.04 volts and a power supply voltage of 1350 . . . . .	128
III.3	A pulse height distribution for the EMI 9789B photomultiplier tube in system 2, obtained using the E sweep with a window width of 0.04 volts and a power supply voltage of 1250 . . . . .	129
III.4	The photon count rate as a function of high voltage applied to the photomultiplier tubes. All other variables are fixed. . . . .	130
III.5	Counts per minute interval versus elapsed time. Upper curve corresponds to the reference channel and lower curve represents the analytical channel. The source is a sample of fluorescein irradiated by laser light and modulated with a variable attenuator . . . . .	131
III.6	Counts per minute interval versus elapsed time. The analytical count rate is normalized to the reference channel. Fluorescein source . . . . .	132
III.7	Percent departure of the analytical count rate from the reference count rate. Error bars represent one sigma due to counting statistics. Fluorescein source . . . . .	133
III.8	Counts per minute interval versus elapsed time. The upper curve corresponds to the reference channel and the lower curve represents the analytical channel. The source is a white light bulb powered by a battery and regulated with a variable resistor . . . . .	134
III.9	Counts per minute interval versus elapsed time. The analytical count rate is normalized to the reference channel. White light source . . . . .	135

III.10	Percent departure of the analytical count rate from the reference count rate. Error bars represent one sigma due to counting statistics. White light source . . . .	136
III.11	Counts per minute interval versus elapsed time. The upper curve corresponds to the reference channel and the lower curve represents the analytical channel. The source is an aqueous solution of polystyrene latex spheres . . . . .	137
III.12	Counts per minute interval versus elapsed time. The analytical count rate is normalized to the reference channel. Sphere solution source . . . . .	138
III.13	Percent departure of the analytical count rate from the reference count rate. Error bars represent one sigma due to counting statistics. Sphere solution source . . . . .	139

PART I

QUASI-ELASTIC LIGHT SCATTERING FROM LIQUIDS AND LIQUID MIXTURES:  
A STUDY OF MASS AND THERMAL DIFFUSIVITIES

## Chapter I

### INTRODUCTION

Because both the mutual diffusion coefficient  $D_{AB}$  and the thermal diffusivity  $\chi$  appear in transport equations, a knowledge of their values is of particular importance in many chemical engineering applications. However, reliable values of mass and thermal diffusivities are relatively scarce. The classical techniques for measuring these properties are both laborious and susceptible to large errors. In recent years an alternate approach has developed, optical-beating spectroscopy.

For almost half a century it has been known that the frequency spectra of light scattered from liquids by entropy and concentration fluctuations contain transport coefficient information (Landau and Placzek 1934). To resolve the extremely narrow lines predicted from the theory of the distributed spectra, the resolving power ( $\omega_0/\omega$ ) of the spectrometer must approach  $10^{14}$ . The best conventional spectroscopic method, the spherical Fabry-Perot interferometer, has a limiting resolution of  $1:10^8$ . Only with the advent of the laser as an intense, monochromatic light source and the development of optical homodyne and heterodyne spectroscopy has the study of the spectra from concentration and entropy fluctuations become possible. Benedek (1969), Cummins and Swinney (1970), and Chu (1970) have written extensive reviews of the optical-beating techniques.

The earliest quantitative spectral measurements were made on fluid systems near their critical point (Alpert 1965; Ford and Benedek 1965) and on macromolecular solutions (Dubin et al. 1967). In both cases light is scattered very strongly by the large temperature or concentration fluctuations. In contrast to the now extensive use of quasi-elastic light scattering techniques to study these phenomena, there have been only a few attempts to measure transport coefficients in systems removed from their critical point, largely because normal mixtures and pure liquids may scatter more than  $10^5$  times less than critical systems and macromolecular solutions. For example, if we compare the relative intensity of scattering from benzene, as expressed by the Rayleigh ratio  $R_0$ , to that from a 100  $\mu\text{g}/\text{cc}$  solution of  $\lambda\text{DNA}$ , we notice that benzene scatters approximately 10 times less than  $\lambda\text{DNA}$ , and only half of that intensity is located in the central peak. The situation is even more extreme, for the quantity of real experimental interest is the intensity of scattering per half-width of the resultant distributed spectra. In this case the DNA solution scatters approximately  $10^6$  times more per half-width than benzene. Table 1 contains further comparisons of scattering intensities. Critical systems are even more intense scatterers than macromolecular solutions.

The efforts to study liquids and liquid mixtures removed from their critical point by Lastovka and Benedek (1966), Aref'ev et al. (1967), Berge et al. (1969,1970), Dubois et al. (1970), Dubois and Berge (1971), and most recently Jamieson and Walton (1973) demonstrated the feasibility of using light scattering techniques to determine transport coefficients for certain systems. A compilation of all the

mass diffusivity data available prior to or concurrent with this work appears in Table 2. The first feature worth noting is the absence of conventionally determined data for comparison. Only in the case of diethyl diethylene glycol/carbon disulfide and ethyl ether/carbon disulfide do independent data exist, and these are by NMR, which is not a generally suitable technique for mass diffusivity measurements. It is further evident that the systems chosen for study were selected for their high degree of scattering, thus facilitating signal detection. Table 2 contains values for the magnitude of refractive index difference between solute and solvent  $|n_1 - n_2|$ . It will later be demonstrated that this quantity corresponds directly to the intensity of scattering; hence the predominance of carbon disulfide and nitrobenzene in the sample systems--both have unusually large refractive indices. Finally, at the time our studies began, there were no  $D_{AB}$  versus concentration data available, and only Dubois et al. (1970) had obtained angular scattering data for binary mixtures in order to confirm the expected wave vector dependence.

A similar situation existed in the measurement of thermal diffusivities. Table 3 contains all of the thermal diffusivity data prior to this work. Bulk data existed for comparison to the light scattering values, but a clear discrepancy existed between the two determinations which could not be definitively attributed to either type of measurement. The systems chosen for study were selected for their intensity of scattering, as Table 4 illustrates. The values which appear for the scattered intensity due to entropy fluctuations,  $I_E$ , are based on a theoretical expression derived from thermodynamic

fluctuation theory, which will be subsequently developed.

The objective of this study was to construct a spectrometer and obtain data which would firmly establish quasi-elastic light scattering as a reliable tool for the rapid and accurate determination of mass and thermal diffusivities. Mutual diffusion coefficients as a function of concentration are reported for eight systems. Extensive literature data exist for most of the mixtures studied. Thermal diffusivity measurements for nine pure liquids and two mixtures are also reported and compared to the values calculated from conventional measurements of density, heat capacity, and thermal conductivity. With both types of determinations angular studies were conducted in order to verify the anticipated scattering angle dependence. Sample systems for this study were chosen based on the availability of independent data and not their intensity of scattering.

## Chapter II

### THEORY

Light is scattered by optical inhomogeneities. The physical reason for optical inhomogeneities in pure fluids is density fluctuations, which concomitantly produce fluctuations in the dielectric constant. In solutions, concentration fluctuations are an additional cause of fluctuations in the dielectric constant. The modes of fluctuation dissipation are controlled by the transport properties of the medium and the scattered electric field mirrors the time dependence of these thermal fluctuations. The total scattered electric field consists of a superposition of phase changes which result from the dissipative motion of density and concentration fluctuations.

#### Continuum Theory

In developing the theory for light scattering from liquids and liquid mixtures we shall treat the medium as a continuum and concern ourselves only with Rayleigh scattering. As a light beam passes through a fluid its electric field induces an oscillating dipole moment in each differential scattering volume. Each of these oscillating dipoles then radiates an electric field which obeys the formula:

$$E_{scj}(\underline{R}, t) = \frac{\sin \phi}{c^2 |\underline{R} - \underline{r}|} \left[ \frac{\partial^2}{\partial t^2} P(\underline{r}, t') \right]_{t'} d^3 r \quad (1)$$

The total scattered field observed at a field point  $R$  is simply the sum (integral) of the individual  $E_{scj}$ 's.

$$E_{sc}(\underline{R}, t) = \int_V \frac{\sin \phi}{c^2 |\underline{R} - \underline{r}|} \left[ \frac{\partial^2}{\partial t^2} P(\underline{r}, t') \right]_t d^3r \quad (2)$$

where  $\phi$  is the angle between  $P(\underline{r}, t')$  and  $\underline{R}$

$c$  is the velocity of light in vacuum

$V$  is the illuminated volume

$t'$  is the retarded time,  $t' = t - \frac{|\underline{R} - \underline{r}|}{(c/n)}$

$n$  is the index of refraction.

If we assume the polarizability is a scalar (isotropic) then the dipole moment is expressed as

$$P(\underline{r}, t) = \alpha(\underline{r}, t) \underline{E}_0 e^{i(\underline{k}_0 \cdot \underline{r} - \omega_0 t)} \quad (3)$$

where  $\underline{k}_0$  is the wave vector of the incident light ( $k_0 = n\omega_0/c$ ). With the aid of the far field approximation ( $R \gg r$ ) and assuming the frequency of fluctuation of  $\alpha$  is small compared to that of the incident light, the scattered field is expressed as

$$E_{sc}(\underline{R}, t) = \left(\frac{\omega_0}{c}\right)^2 \sin \phi \frac{e^{i(\underline{k}_s \cdot \underline{R} - \omega_0 t)}}{R} \left[ \int_V \alpha(\underline{r}, t) e^{i(\underline{k}_0 - \underline{k}_s) \cdot \underline{r}} d^3r \right] \quad (4)$$

where the scattered light wave vector  $\underline{k}_s$  is colinear with  $\underline{R}$  and has a magnitude  $n\omega_0/c$ . The bracketed term is commonly referred to as the interference integral because it describes the superposition of the phases of the waves scattered from each point in the medium. The polarizability is reexpressed as

$$\alpha(\underline{r}, t) = \langle \alpha \rangle + \delta\alpha(\underline{r}, t)$$

where  $\langle \alpha \rangle$  is the average value of  $\alpha$  and  $\delta\alpha$  represents the fluctuations around the medium's average value.

The point of these manipulations is to show that of all of the fluctuations in the medium, only that of a particular wavelength and direction is responsible for scattering in the  $\underline{k}_s$  direction. Expressing the spatial Fourier components of the fluctuation in polarizability in terms of the fluctuation in dielectric constant,

$$\delta\alpha(\underline{r}, t) = \frac{\delta\epsilon(\underline{r}, t)}{4\pi} = \frac{(1/4\pi)}{(2\pi)^{3/2}} \int \delta\epsilon(\underline{q}, t) e^{i\underline{q}\cdot\underline{r}} d^3q \quad (5)$$

we now have for the total scattered field

$$\begin{aligned} E_{sc}(\underline{R}, t) &= \left(\frac{\omega_0}{c}\right)^2 \frac{\sin \phi}{4\pi R} e^{i(\underline{k}_s \cdot \underline{R} - \omega_0 t)} \frac{1}{(2\pi)^{3/2}} \\ &\times \int \delta\epsilon(\underline{q}, t) d^3q \int e^{i(\underline{k}_0 - \underline{k}_s + \underline{q}) \cdot \underline{r}} d^3r \end{aligned} \quad (6)$$

Clearly,

$$\int e^{i(\underline{k}_0 - \underline{k}_s + \underline{q}) \cdot \underline{r}} d^3r = (2\pi)^3 \delta^3(\underline{k}_0 - \underline{k}_s + \underline{q})$$

where  $\delta^3$  is the three-dimensional Dirac delta function. This equation indicates that a single wave vector component of the fluctuations is responsible for the scattering observed at the field point  $\underline{R}$ ; the interference integral is non-zero only when

$$\underline{k}_0 - \underline{k}_s = -\underline{q}$$

Defining  $\underline{K} = \underline{k}_s - \underline{k}_0$ , we can say that the scattering observed at  $\underline{R}$

is entirely due to the  $\underline{K}$  wave vector component of the fluctuation. The Bragg reflection condition also obtains, i.e.,

$$|\underline{K}| = 2\left(\frac{2\pi n}{\lambda_0}\right) \sin\left(\frac{\theta}{2}\right) \quad (7)$$

where  $\theta$  is the scattering angle between  $\underline{k}_0$  and  $\underline{k}_s$  and  $\lambda_0$  is the incident light wavelength.

Our final result for the scattered field is then (Dubin 1970)

$$E_{SC}(\underline{R}, t) = \left(\frac{\omega_0}{c}\right)^2 \frac{\sin \phi}{4\pi R} e^{i(\underline{k}_s \cdot \underline{R} - \omega_0 t)} (2\pi)^{3/2} \delta\epsilon(\underline{K}, t) \quad (8)$$

Thus description of the scattered field is reduced to the derivation of an expression for fluctuations in the dielectric constant  $\delta\epsilon(\underline{K}, t)$ . It is evident that the temporal changes of the optical inhomogeneities produce a modulation of the scattered light, while the nature of the modulation is closely connected with the physical process (i.e., mass and/or thermal diffusion) determining the particular form of the modulation function.

### Fluctuation Theory and Total Scattered Intensity

As a preliminary step to examining the temporal evolution of these fluctuations we shall employ elementary thermodynamic fluctuation theory to calculate the total intensity scattered by spatially independent fluctuations. The results will assist us in evaluating the coefficients of the distributed spectra. The total scattered intensity may be expressed as  $I \propto |E_{SC}|^2$ , hence

$$\langle I \rangle \propto \langle |\delta\epsilon(\underline{K}, t)|^2 \rangle \quad (9)$$

where  $\langle \rangle$  represents either a time or ensemble average. In order to evaluate  $\langle |\delta\varepsilon(\underline{k}, t)|^2 \rangle$  we write by definition

$$\langle |\delta\varepsilon(\underline{k}, t)|^2 \rangle = \frac{1}{(2\pi)^3} \int_V \int_V \langle \delta\varepsilon(\underline{r}, t) \delta\varepsilon^*(\underline{r}', t) e^{-i\underline{k} \cdot (\underline{r} - \underline{r}')} \rangle d^3r d^3r' \quad (10)$$

Assuming  $\delta\varepsilon(\underline{r}, t)$  is spatially invariant and a stationary random process, Equation (10) becomes

$$\langle |\delta\varepsilon(\underline{k}, t)|^2 \rangle = \frac{V}{(2\pi)^3} \int_V \langle \delta\varepsilon(\underline{r}, 0) \delta\varepsilon^*(0, 0) \rangle e^{i\underline{k} \cdot \underline{r}} d^3r \quad (11)$$

If we assume that (1) the fluctuations are correlated only over the dimensions of the fluctuation volume, (2) the fluctuations are constant within that volume, and (3) these dimensions are sufficiently small so that  $e^{i\underline{k} \cdot \underline{r}} \approx 1$  where the correlation is non-zero, we have

$$\langle |\delta\varepsilon(\underline{k}, t)|^2 \rangle = \frac{V}{(2\pi)^3} \langle |\delta\varepsilon(0, 0)|^2 \rangle V^* \quad (12)$$

These assumptions are completely valid for pure liquids and liquid mixtures, but for macromolecular solutions intramolecular interference effects appear which invalidate Equation (12) and lead to the molecular structure factor. For the cases of interest the Fourier transformed mean square fluctuation in  $\varepsilon$  reduces to the equilibrium value  $\langle |\delta\varepsilon|^2 \rangle$  and

$$\langle I \rangle = GV^* \langle |\delta\varepsilon|^2 \rangle \quad (13)$$

where  $G = \frac{I_0 \pi^2 V \sin^2 \phi}{2\lambda^4 R^2}$ ,  $V$  is the scattering volume, and  $V^*$  is the

volume of the fluctuation (Fabelinskii 1968).

Following the method of Leontovich (1944), variations in the dielectric constant  $\epsilon$  of a pure liquid can be expressed in terms of the experimentally measurable parameters, density  $\rho$  and temperature  $T$ , where  $\rho$  and  $T$  are statistically independent variables

$$\delta\epsilon = \left(\frac{\partial\epsilon}{\partial\rho}\right)_T \delta\rho + \left(\frac{\partial\epsilon}{\partial T}\right)_\rho \delta T \quad (14)$$

Einstein (1910) originally made the assumption that  $(\partial\epsilon/\partial T)_\rho$  is small, which allows  $\epsilon$  to be expressed solely in terms of density. The density can be written as a function of the two independent thermodynamic variables, pressure  $P$  and entropy  $S$ .

$$\delta\rho(P,S) = \left(\frac{\partial\rho}{\partial P}\right)_S \delta P + \left(\frac{\partial\rho}{\partial S}\right)_P \delta S \quad (15)$$

From Equations (13) and (14) we are able to write the intensity as

$$\langle I \rangle = GV^* \left(\frac{\partial\epsilon}{\partial\rho}\right)_T^2 \langle |\delta\rho|^2 \rangle \quad (16)$$

where

$$\langle |\delta\rho|^2 \rangle = \left(\frac{\partial\rho}{\partial P}\right)_S^2 \langle |\delta P|^2 \rangle + \left(\frac{\partial\rho}{\partial S}\right)_P^2 \langle |\delta S|^2 \rangle \quad (17)$$

The intensity is seen to be divided into two distinct components-- adiabatic pressure fluctuations

$$I_{ad} = V^* G(\rho) \left(\frac{\partial\epsilon}{\partial\rho}\right)_T^2 \left(\frac{1}{\rho} \frac{\partial\rho}{\partial P}\right)_S^2 \langle |\delta P|^2 \rangle \quad (18)$$

and isobaric entropy fluctuations

$$I_{is} = V^*G(\rho) \left(\frac{\partial \epsilon}{\partial \rho}\right)_T^2 \left(\frac{1}{\rho} \frac{\partial \rho}{\partial S}\right)_P^2 \langle |\delta S|^2 \rangle \quad (19)$$

Employing thermodynamic identities, Equations (18) and (19) simplify to

$$I_{ad} = G(\rho) \left(\frac{\partial \epsilon}{\partial \rho}\right)_T^2 \beta_S kT \quad (20)$$

where  $\beta_S$  is the adiabatic compressibility and

$$I_{is} = G(\rho) \left(\frac{\partial \epsilon}{\partial \rho}\right)_T^2 \frac{kT^2 \sigma^2}{c_p \rho} \quad (21)$$

where  $\sigma$  is the coefficient of volume expansion. All of these calculations are under the assumption that  $\left(\frac{\partial \epsilon}{\partial T}\right)_\rho^2 \langle (\delta T)^2 \rangle$  is close to zero. For most systems this requirement is fulfilled. Refer to Fabelinskii (1968) for a detailed discussion of this approximation.

A similar approach is used to calculate the intensity of scattering from solutions; density, temperature, and concentration are the statistically independent variables. If we assume that concentration fluctuations are the dominant source of scattering then

$$E_{sc}(\underline{R}, t) \propto \delta C(\underline{K}, t) \quad (22)$$

and

$$\langle I_{conc} \rangle = V^*G\left(\frac{\partial \epsilon}{\partial C}\right)_{\rho, T}^2 \langle |\delta C|^2 \rangle \quad (23)$$

### The Distributed Spectra from Macroscopic Equations

Landau and Placzek (1934) used thermodynamic fluctuation theory in conjunction with the macroscopic equations of heat conduction and

mass diffusion to describe the time decay of fluctuations in the dielectric constant and the shape of the resulting distributed spectra. They reasoned that fluctuations in density can be expressed in terms of the independent thermodynamic variables, pressure and entropy, that is, adiabatic and isobaric fluctuations. Modulation of light by adiabatic fluctuations of density physically represent local compressions and rarefactions of the fluid. Due to the elastic nature of the fluid, these fluctuations propagate throughout the sample and can be visualized as thermal elastic waves diffracted according to the Bragg condition. These waves result in the Brillouin peaks, which are displaced to either side of the Rayleigh peak. The width of the Brillouin peaks is a function of the sound absorption coefficient, which depends on heat capacity and shear and bulk viscosities. These peaks are sufficiently displaced that they do not interfere with observation of the Rayleigh peak, and hence are not of further concern in this work.

Scattering from isobaric fluctuations in density is associated with temperature or entropy fluctuations. The dissipation of these fluctuations obeys the Fourier heat equation

$$\frac{\partial \delta T(\underline{r}, t)}{\partial t} = \chi V^2 \delta T(\underline{r}, t) \quad (24)$$

and is controlled by the thermal diffusivity. The component responsible for scattering is then

$$\delta T(\underline{K}, t) = \delta T(\underline{K}, 0) \exp[-\chi K^2 t] \quad (25)$$

Thus, fluctuations in temperature or entropy are exponentially decaying functions localized in space. An analogous situation exists for the

dissipation of concentration fluctuations in binary mixtures. The diffusion equation

$$\frac{\partial \delta C(\underline{r}, t)}{\partial t} = D_{AB} \nabla^2 \delta C(\underline{r}, t) \quad (26)$$

is obeyed, and its solution yields

$$\delta C(\underline{K}, t) = \delta C(\underline{K}, 0) \exp[-D_{AB} K^2 t] \quad (27)$$

The expression for the scattered field now takes the form

$$E_{SC}(\underline{K}, t) \propto e^{-i\omega_0 t} e^{-\chi K^2 t} \delta T(\underline{K}, 0) \quad (28)$$

for pure liquids and an analogous form with  $D_{AB}$  replacing  $\chi$  and  $C$  replacing  $T$  for binary mixtures.

The quantities of direct interest in quasi-elastic light scattering are the dielectric constant (electric field) autocorrelation function  $C_E(\tau)$ , and its Fourier transform  $I(\underline{K}, \omega)$ , which is the spectrum of the electric field

$$C_E(\tau) = \langle E_{SC}^*(t) E_{SC}(t+\tau) \rangle \quad (29a)$$

$$\propto e^{-i\omega_0 \tau} \langle \delta \chi^*(\underline{K}, t) \delta \chi(\underline{K}, t+\tau) \rangle \quad (29b)$$

$$\propto \langle |\delta \chi(\underline{K}, 0)|^2 \rangle e^{-\chi K^2 |\tau|} e^{-i\omega_0 \tau} \quad (29c)$$

where  $\chi$  is either  $D_{AB}$  or  $\chi$ . It is apparent from the previous section that  $\langle |\delta \chi(\underline{K}, 0)|^2 \rangle \sim \langle |\delta \chi|^2 \rangle$ . Finally, with the aid of the Wiener-Khintchine theorem (see Appendix I) the spectrum is written as

$$I(\underline{K}, \omega) \propto \int_{-\infty}^{\infty} C_E(\tau) e^{i\omega\tau} d\tau \quad (30a)$$

$$= \langle I_x \rangle \frac{1}{\pi} \frac{\chi K^2}{\omega^2 + (\chi K^2)^2} \quad (30b)$$

$\langle I_x \rangle$  is  $\langle I_{is} \rangle$  for entropy (temperature) fluctuations and  $\langle I_{conc} \rangle$  for concentration fluctuations. As a check, the total intensity is

$$\int_{-\infty}^{\infty} I(\underline{K}, \omega) d\omega = \langle I_x \rangle \quad (31)$$

as previously derived.

Landau and Placzek's final results in expanded form (although never explicitly derived) are

$$C_E(\tau) = \langle I_{is} \rangle e^{-i\omega_0\tau} e^{-\chi K^2|\tau|} \quad (32a)$$

and

$$I(\underline{K}, \omega) = \langle I_{is} \rangle \frac{1}{\pi} \frac{\chi K^2}{\omega^2 + (\chi K^2)^2} \quad (32b)$$

for pure liquids and

$$C_E(\tau) = \langle I_{conc} \rangle e^{-i\omega_0\tau} e^{-D_{AB}K^2|\tau|} \quad (33a)$$

and

$$I(\underline{K}, \omega) = \langle I_{conc} \rangle \frac{1}{\pi} \frac{D_{AB}K^2}{\omega^2 + (D_{AB}K^2)^2} \quad (33b)$$

for binary mixtures, where as before

$$\langle I_{is} \rangle = G(\rho) \frac{\partial \epsilon}{\partial \rho} \frac{2}{T} \frac{kT^2 \sigma^2}{c_p \rho} \quad (21)$$

$$\langle I_{\text{conc}} \rangle = V^* G \left( \frac{\partial \epsilon}{\partial C} \right)_{\rho, T}^2 \langle |\delta C|^2 \rangle \quad (23)$$

The Distributed Spectra from Hydrodynamic Equations

Kadanoff and Martin (1963), Mountain (1966), and Mountain and Deutch (1969) have presented a more rigorous development in which the linearized hydrodynamic equations--the continuity equation, the Navier-Stokes equation, the diffusion equation, and the energy transport equation--were used to determine the modes by which the system relaxes back to equilibrium, and the amplitude of each mode. Thermodynamic fluctuation theory was employed to evaluate the coefficients of the spectral contributions, which are the mean square fluctuations of the statistically independent variables. The final results derived for a pure liquid are similar to those obtained from Landau and Placzek's treatment; for binary mixtures, Mountain and Deutch observed a term resulting from the dynamics, which does not appear in the thermodynamic theory (Miller 1967). This additional term is a result of the coupling of temperature and concentration dissipation, that is, the Dufour and Soret effects. Under the condition  $\chi \gg D_{AB}$ , which obtains for the systems studied here, the formulae are similar to those developed from the macroscopic transport equations and fluctuation theory, and the experimental separation of the contributions from entropy and concentration fluctuations is possible.

For a pure fluid (Mountain 1966)

$$\begin{aligned} C_E(\tau) &= \langle \delta\rho(\underline{K}, 0) \delta\rho(\underline{K}, \tau) \rangle \\ &\propto \langle |\delta\rho(\underline{K})|^2 \rangle \left\{ \frac{C_p - C_v}{C_p} \exp[-\chi k^2 |\tau|] \right\} e^{-i\omega_0 \tau} \end{aligned} \quad (34a)$$

and

$$I(\underline{K}, \omega) \propto \langle |\delta\rho(\underline{K})|^2 \rangle \left( \frac{c_p - c_v}{c_p} \right) \left( \frac{1}{\pi} \frac{\chi k^2}{\omega^2 + (\chi k^2)^2} \right) \quad (34b)$$

where  $\rho = \rho(P, S)$  and the pressure fluctuation terms (the Brillouin peaks) have been omitted.

For a binary mixture (Mountain and Deutch 1969)

$$C_E(\tau) \propto \left\{ \left( \frac{\partial \epsilon}{\partial C} \right)_{P, T}^2 \langle |\delta C(\underline{K})|^2 \rangle \exp[-D_{AB} k^2 |\tau|] + \left( \frac{\partial \epsilon}{\partial T} \right)_{P, C}^2 \langle |\delta T(\underline{K})|^2 \rangle \exp[-\chi k^2 |\tau|] \right\} e^{-i\omega_0 \tau} \quad (35a)$$

and

$$I(\underline{K}, \omega) \propto \left( \frac{\partial \epsilon}{\partial C} \right)_{P, T}^2 \langle |\delta C(\underline{K})|^2 \rangle \left\{ \frac{1}{\pi} \frac{D_{AB} k^2}{\omega^2 + (D_{AB} k^2)^2} + \left( \frac{\partial \epsilon}{\partial T} \right)_{P, C}^2 \langle |\delta T(\underline{K})|^2 \rangle \left\{ \frac{1}{\pi} \frac{\chi k^2}{\omega^2 + (\chi k^2)^2} \right\} \right\} \quad (35b)$$

subject to the condition  $\chi \gg D_{AB}$  (pressure fluctuations have again been suppressed). One can appreciate the approximations involved by observing that  $C$  and  $T$  (and implicitly  $P$ ) appear as statistically independent variables in Equations (35a) and (35b), while in actuality  $T$ ,  $\rho$ , and  $C$  are the independent thermodynamic variables.

Equation (34a) expresses the density correlation function in the real time domain as a decaying exponential with a decay time (the time required for the exponential to decay to  $e^{-1}$  of its initial value) of  $(\chi k^2)^{-1}$ . The corresponding spectrum in the frequency domain (Equation (34b)) represents a Lorentzian with a half-width at half-

height of  $\chi K^2/2\pi$  Hz. Hence the thermal diffusion process may be characterized by either an exponential decay time or its conjugate half-width. Similarly, for a binary mixture with concentration fluctuations as the dominant source of scattering, the concentration correlation function (Equation (35a)) is described by the decay time  $(D_{AB}K^2)^{-1}$  or the corresponding half-width of Equation (35b),  $D_{AB}K^2/2\pi$ . If temperature fluctuations should dominate, the characterization parameters are identical to those for a pure fluid.

### The Amplitude of Scattering

The amplitude of the mass diffusivity term in Equation (35b) is a function of the factors  $(\delta\varepsilon/\delta C)_{P,T}^2$  and  $\langle|\delta C|^2\rangle$ . The first term is dependent upon the difference between mass reduced polarizabilities of solute and solvent, as is evident from the Lorentz-Lorenz formula for a solution (Heller 1959):

$$\frac{\varepsilon - 1}{\varepsilon + 2} = \frac{4\pi\rho'}{3} \left[ C\left(\frac{\alpha_1}{m_1}\right) + (1-C)\left(\frac{\alpha_2}{m_2}\right) \right] \quad (36)$$

and its derivative

$$\left(\frac{\partial\varepsilon}{\partial C}\right)_{P,T} = \frac{4\pi}{3} \frac{(\varepsilon+2)^2}{3} \rho' \left[ \frac{\alpha_1}{m_1} - \frac{\alpha_2}{m_2} - \frac{3}{4\pi} \frac{\varepsilon-1}{\varepsilon+2} \left( \frac{1}{\rho_1} - \frac{1}{\rho_2} \right) \right] \quad (37)$$

where  $\rho' = [C/\rho_1 + (1-C)/\rho_2]^{-1}$  is the density of the mixture in grams of solution per  $\text{cm}^3$  of solution,  $C$  is solute concentration in grams of solute per gram of solution,  $\alpha_i$  is the molecular polarizability,  $m_i$  is the molecular mass, and subscript 1 refers to the solute and 2 to the solvent. As is evident from Table 5, the amplitude of the concentration term in Equation (35) for a fixed composition is proportional

to the difference between the refractive indices of the two components, which is what one would intuitively expect. Experimentally one should detect reduced scattered intensities for solutions with comparable solute-solvent refractive indices and a corresponding reduction in precision of the experimental results.

The mean square concentration fluctuation can be expressed by (Zimm 1945)

$$\langle |\delta g|^2 \rangle = \frac{kT}{\left(\frac{\partial^2 F}{\partial g^2}\right)_{P,T}} \quad (38)$$

where  $F$  is the Gibbs free energy of the fluid,  $g$  is the solute concentration in  $\text{g/cm}^3$  of solution, and  $k$  is Boltzmann's constant. With a change of variable, Equation (38) reduces to

$$\langle |\delta C|^2 \rangle = \frac{kT}{\left(\frac{\partial^2 F}{\partial C^2}\right)_{P,T}} \quad (39)$$

Expressing the differential of  $F$  as

$$dF = \mu_1 \frac{\rho}{M} dn_1^* + \mu_2 \frac{\rho}{M} dn_2^* \quad (40)$$

with  $n_i^*$  defined as the mole fraction of  $i$ , we are able to rewrite Equation (40) in the form

$$dF = \mu dC \quad (41)$$

where  $\mu = \rho(\mu_1 M_1^{-1} - \mu_2 M_2^{-1})$  is a chemical potential of solution.

Finally, the mean square fluctuation in concentration may be written as

$$\langle |\delta C|^2 \rangle = \frac{kT}{\left(\frac{\partial \mu}{\partial C}\right)_{T,P}} \quad (42)$$

$(\partial \mu / \partial C)_{P,T}$  is a complicated function of activities and molecular weights, but qualitatively, as solute and solvent approach equal concentrations, the term should increase in magnitude. Conversely, as the solution becomes more dilute in either component, the intensity of scattering should decrease and the precision of the associated data become poorer. Dubois and Berge (1971) have studied the functional dependence of the chemical potential derivative in detail.

#### Definitions of Mutual Diffusion Coefficients

Some confusion has arisen as to the exact nature of the binary diffusion coefficient  $D_{AB}$ . The diffusivity described in this work is derived directly from Fick's law

$$J_1 = \rho' D_{AB} \nabla C \quad (43)$$

$J_1$  represents the mass flux of solute. The theoretical foundation for this phenomenological equation is provided by irreversible thermodynamics; it can be shown that (De Groot 1959)

$$J_1 = -L_{11}(1-C)^{-1} (\partial \mu_1 / \partial C)_{T,P} \nabla C \quad (44)$$

where  $L_{11}$  is a phenomenological coefficient. It follows that  $D_{AB} = [L_{11} / \rho(1-C)] (\partial \mu_1 / \partial C)_{T,P}$ . Some authors use  $(\partial \mu_1 / \partial n_1)_{T,P} \nabla n_1$  instead of the mass concentration gradient and define the associated

coefficient  $D_{AB}^n$  by using  $\rho' D_{AB}^n$  for the coefficient of the molar gradient, i.e.,

$$-\rho' D_{AB} \nabla C = -\rho' D_{AB}^n \nabla n_1 \quad (45)$$

Consequently,

$$D_{AB}^n = D_{AB} (C/m_1 + (1-C)/m_2)^2 m_1 m_2 \quad (46)$$

and  $D_{AB}^n = D_{AB}$  only when  $m_1 = m_2$  .

Chapter III

APPARATUS AND EXPERIMENTAL METHODS

A schematic diagram of the light scattering spectrometer used in this study is given in Figure 1. Details of its construction and operation appear in Appendix II. The system was also designed to perform total intensity measurements using dual photon-counting (see Appendix III).

The laser, detection optics, and sample were mounted on a Newport Research Corp. vibration isolation table to prevent extraneous vibrations from contributing to the time dependence of the scattered light. Isolation was in both the horizontal and vertical directions. Using geophones, we determined the table's resonant frequency to be  $<3$  Hz. All optical devices were positioned rigidly on the stainless steel surface.

The incident light of approximately one watt was the  $4880\text{\AA}$  line of a Coherent Radiation 52A argon ion laser. Two pinholes with an angular acceptance of  $0.2^\circ$  defined the scattering volume, and the scattering angle was determined by triangulation to better than  $0.06^\circ$ . The sample volume was contained in a 10-cm path length cylindrical cell with optical quality flat windows. Stray light from imperfections and dust on the windows acted as a local oscillator source for the heterodyne spectroscopy. The detector, an EMI 9634QR phototube, carried the fluctuating photocurrent to a Saicor 43A correlator. The autocorrelation function was collected until the significant part of the function began to fill the memory--10 min to 2 hrs were required, depending upon the signal to noise ratio of the photocurrent. The 400-point autocorrelation

function (containing 13 bits plus sign) was then transferred in digital form from the correlator to paper tape for subsequent computer analysis. Typical correlograms appear in Figure 2.

Sample chemicals of reagent grade were used without further purification. The binary mixtures were prepared volumetrically with an estimated accuracy of 0.5%. All samples were multiply filtered through a fine fritted glass filter to remove dust. A Bausch and Lomb refractometer was used to measure refractive indices; values were corrected to  $\lambda = 4880\text{\AA}$ . The samples were maintained at room temperature, which did not drift more than  $1^{\circ}\text{C}$  during the course of an experiment. Because  $D_{AB}$  and  $\chi$  exhibit a weak temperature dependence (typically less than  $0.5\%/^{\circ}\text{C}$ ), we estimate the maximum error due to temperature control to be less than 1%.

Current correlation techniques were employed because of the speed and efficiency of data acquisition; the rate of data collection by correlating is faster than that of data collection with a spectrum analyzer by a factor which is of the order of the number of bandwidths swept. Spectrum analyzers scan in frequency (with the exception of real time analyzers), measuring only one bandwidth at a time, whereas a correlator (in principle) analyzes all of the signal all of the time. The correlator is also able to perform signal averaging on the correlation function, thus improving the statistical accuracy of the data.

In the case of heterodyne spectroscopy, the photocurrent autocorrelation function is an exact replica of the electric field autocorrelation function (see Appendix I), hence

$$C_i(\tau) = \langle i(t) i(t+\tau) \rangle \propto C_E(\tau) \quad (47)$$

and the decay time of the current exponential contains the coefficient of interest. The points of the correlation function were fit to a single exponential with a baseline using the Marquardt nonlinear least squares algorithm. The reciprocal decay time for a pure liquid

$$\tau^{-1} = \chi k^2 \quad (48)$$

and the value of  $k^2$  determine  $\chi$ . Values of  $\tau$  were collected over a range of scattering angles. For the binary mixtures two exponentials are observed. Because the magnitude of concentration fluctuations in binary mixtures is generally greater than the magnitude from temperature fluctuations, and because the decay time for thermal diffusivity is smaller than from mass diffusivity by approximately two orders of magnitude, the effect of thermal diffusion can be compressed into the initial part (approximately ten points) of the correlation function; these points are neglected in the fit to determine the mass diffusivity reciprocal decay time

$$\tau^{-1} = D_{AB} k^2 \quad (49)$$

$\tau$  values for  $D_{AB}$  were collected as a function of concentration for a single scattering angle, with the exception of one concentration of carbon disulfide/acetone and two of methanol/benzene, which were studied as a function of angle to verify the expected  $k^2$  dependence (Figures 9 and 10).

To measure thermal diffusivities for binary mixtures, one must in general perform a two exponential fit to the data. Under the special circumstances of similar refractive indices for solute and solvent, density fluctuations become the predominant source of scattering and the data may be analyzed solely in terms of thermal diffusion. One of the binary systems studied, toluene-benzene, satisfies the criterion of matched refractive indices and hence has been analyzed in terms of Equations (34a) and (48). The other binary system, toluene-bromobenzene, has been analyzed for both types of fluctuations by appropriately varying the sample time increment so as to emphasize either mass or thermal diffusion.

The components of the spectrometer primarily responsible for our ability to measure accurately mass and thermal diffusivities for weakly scattering systems are: (1) the argon-ion laser, which produces an extremely intense beam at a low wavelength (see Appendix III); (2) a photomultiplier with both high gain and quantum efficiency (the latter is possible due to the low wavelength); (3) a correlator, which enhances the S/N ratio and stores the data in digital form; (4) careful vibration isolation and elimination of low frequency noise (see Appendix II); and (5) careful alignment of the system (Appendix II).

Chapter IV

RESULTS AND DISCUSSION

The following data were taken in collaboration with Erdogan Gulari (Gulari et al. 1973, and thesis). In Figures 3 to 8, mutual diffusion coefficients from this study are plotted as a function of concentration with comparative literature data. Thermal diffusivity results are compared in Table 6 with the literature bulk values. Error bars in Figures 3 to 14 are based on two standard deviations of the single exponential fit plus an estimate of possible systematic errors. Errors appearing in Table 6 result from two standard deviations of the data to a best straight line plus possible systematic errors. Mass diffusivity values range in accuracy from 12% for dilute mixtures to better than 1% for more equal mass concentration solutions, thus confirming the theoretical prediction of Equation (42). Referring to Figures 3 to 8 and Table 5 (a tabulation of refractive index differences and  $(\partial\epsilon/\partial C)_{P,T}$  values for mixtures used in this study), we are able to observe the correlation between experimental uncertainty, refractive index differences, and the magnitude of  $(\partial\epsilon/\partial C)_{P,T}$ , which confirms the conclusion drawn from Equation (37). Comparing the entries of Tables 2 and 5 reveals that virtually all of the systems previously studied relied on a much greater level of scattering for their determinations.

The accuracy of  $\chi$  values in all cases is better than 10% and is typically 5%. Figures 9 to 14 exhibit values of the inverse decay time of the Rayleigh line as a function of the square of the scattering wave vector for light scattered from concentration fluctuations (Figures

9 and 10) and entropy fluctuations (Figures 11 to 14). Each datum represents a single correlation function. Half-widths are related to the exponential decay time  $\tau$  by

$$\Gamma = (2\pi\tau)^{-1} \quad (50)$$

where  $\Gamma$  represents the conjugate Lorentzian half-width of the spectrum [Equations (34b) and (35b)], thus the vertical axis represents both the inverse decay time of the exponential correlation function and the half-width of the corresponding Lorentzian.

As seen from these plots, the linear dependence predicted from theory by Equations (48) and (49) is accurately obeyed. Least squares fitting with statistical weighting has been used to determine the best straight lines.

Figures 3 through 8 show that our mutual diffusion coefficients are in excellent agreement with the bulk values reported in the literature. Three other light scattering measurements of mass diffusivities are available for comparison--all are from the system carbon disulfide-acetone. Berge et al. (1970) reported  $D_{AB} = 2.32 \times 10^{-5} \text{cm}^2/\text{s}$  at room temperature for a 10% by volume acetone mixture obtained at a single scattering angle of  $1.05^\circ$ . Aref'ev et al. (1967) reported  $D_{AB} = 0.30 \pm 0.04 \times 10^{-5} \text{cm}^2/\text{s}$  for a 10% by weight acetone mixture at room temperature. Their data were obtained at  $90^\circ$  using Fabry-Perot interferometry. Jamieson and Walton (1973) obtained a value of  $D_{AB} = 0.92 \times 10^{-5} \text{cm}^2/\text{s}$ , taken at  $10^\circ 34'$  for a 10% by volume mixture. In comparison, our values are  $2.42 \pm 0.04 \times 10^{-5}$  at  $20.0^\circ\text{C}$  for a 10% by volume mixture and  $2.23 \pm 0.06 \times 10^{-5}$  at  $18.5^\circ\text{C}$  for a 10% by weight

acetone in carbon disulfide solution.

Jamieson and Walton argued that Aref'ev did not employ signal averaging techniques, thereby introducing an inherent inaccuracy in his result. They attribute the disagreement between their value and Berge's to "the errors attendant in measuring spectra at scattering angles below  $5^{\circ}$ ". The theoretical basis for these errors has been discussed by Schaefer and Berne (1972), Edwards et al. (1971) and Yeh (1969). A finite scattering volume or, equivalently, an uncertainty in scattering vector caused by the focusing and collecting optics are responsible for the spectral distortion. Based on Yeh's work, Jamieson and Walton argued that at the scattering angle of  $1.05^{\circ}$  used by Berge the effect of a finite collection aperture would produce a significantly broadened spectrum, and consequently a large estimate for the diffusion coefficient. Czwozniak and Jones (1974) have recently demonstrated that finite-aperture broadening has an insignificant effect on the Rayleigh spectrum, which contradicts Jamieson and Walton's conclusions. While the finite collection aperture effects cannot explain the discrepancy between measurements, the effect of a focused beam in the sample could in principle be responsible for the differences.

Our data conclusively indicate that aperture or finite sample volume effects cannot explain the discrepancies between our values and Jamieson and Walton's. All of our measurements were performed with an unfocused beam, which eliminates the only other conjecture related to errors associated with small angle scattering. To further document the validity of our results, angular data have been taken for the carbon disulfide/acetone mixture. Figure 9 clearly indicates the anticipated

wave vector dependence; linearity would not have been observed had aperture effects been present. None of the other investigators conducted any angular studies to verify the predicted  $k^2$  dependence.

The agreement between our values of thermal diffusivity and the values calculated from bulk measurements of  $\lambda$ ,  $\rho$ , and  $C_p$  data is satisfactory as is evident from Table 6. Included in Table 6 are the only other light scattering determinations of thermal diffusivity. Our value of  $1.10 \pm 0.02 \times 10^{-3} \text{ cm}^2/\text{s}$  for pure carbon disulfide is the same as Berge's value of  $1.1 \times 10^{-3} \text{ cm}^2/\text{s}$  (Berge et al. 1970). Berge and Dubois (1969) in the first experimental work on benzene reported  $\chi = 0.655 \pm 0.070 \times 10^{-3} \text{ cm}^2/\text{s}$ . These authors subsequently improved their techniques and found  $\chi = 0.87 \pm 0.1 \times 10^{-3} \text{ cm}^2/\text{s}$  (unpublished work). Values obtained at higher angles by Fabry-Perot interferometry are  $\chi = 1.03 \pm 0.05 \times 10^{-3} \text{ cm}^2/\text{s}$  (Oliver and Pike 1970),  $0.90 \pm 0.02 \text{ cm}^2/\text{s}$  (Searby 1971), and  $0.94 \pm 0.05 \times 10^{-3} \text{ cm}^2/\text{s}$  (Beysens 1973). These are to be compared to our experimental value of  $\chi = 0.956 \pm 0.040 \text{ cm}^2/\text{s}$  and the bulk value of  $\chi = 0.963 \times 10^{-3} \text{ cm}^2/\text{s}$ . Other Fabry-Perot values available are  $0.84 \pm 0.05 \times 10^{-3} \text{ cm}^2/\text{s}$  for carbon tetrachloride and  $0.98 \pm 0.05 \times 10^{-3} \text{ cm}^2/\text{s}$  for toluene (Oliver and Pike 1970). Lastovka and Benedek (1966) reported  $\chi = 0.879 \pm 0.025 \times 10^{-3} \text{ cm}^2/\text{s}$  for toluene, which agrees with our value of  $0.849 \pm 0.038 \times 10^{-3} \text{ cm}^2/\text{s}$ .

#### Classical Thermal Conductivity Measurements

It should be noted that where possible the quoted literature values for thermal diffusivity are taken from Touloukian, Volumes 3 and 6. These volumes contain a comprehensive study of all the available data on liquid thermal conductivity and heat capacity for selected

substances; the recommended reference values cited for each liquid have been used in Table 1. The variation in experimentally determined thermal conductivities is of interest.

Figures 15, 16, and 17 are thermal conductivity departure plots taken from Touloukian (1970). All points are plotted relative to the author's recommended values based on an evaluation of the data. Each point corresponds to a different experimental work. Notice that results for the same system commonly vary by over 25%, thus reflecting the difficulties associated with the conventional thermal conductivity measurements. The most significant problems are conduction corrections, convection currents, and radiation between the surfaces enclosing the liquid. In contrast, quasi-elastic light scattering does not require the imposition of macroscopic temperature gradients; thus convection is not a serious source of error. Spectrometers can easily be constructed which do not suffer from the problems of radiation and conduction associated with classical methods.

#### Classical Mass Diffusivity Measurements

The limitations inherent to classical diffusion measurements are not so serious, although large discrepancies exist between values obtained by different investigators on the same system. Johnson and Babb (1956) discuss the different conventional techniques for determining mass diffusivities as well as their limitations and the consistency of data taken by several investigators. The most important limitation of these techniques is the requirement of a macroscopic concentration gradient. As a result, one generally obtains an integral diffusion coefficient rather than the more meaningful differential coefficient. One

of the more popular methods, the diaphragm cell technique, requires calibration and is subject to bulk flows (Board and Spalding 1966); both can contribute to errors in the measurements of  $D_{AB}$ . Quasi-elastic light scattering needs no macroscopic concentration gradients and is not subject to calibration errors or bulk flow. Scattering arises from microscopic fluctuations in concentration, hence the measured diffusion coefficient is of a differential form. Some techniques, such as the diaphragm cell, may require days of operation for a single point, while light scattering determinations take less than an hour. The most precise conventional techniques employ interferometric methods (Dunlop et al. 1972) for continuously analyzing the changes of concentration with distance and time in a cell. Analysis of the data requires involved mathematical analysis. These measurements are limited in the same way as light scattering--they require a difference in refractive index between sample and solvent. This is the most serious limitation of the light scattering technique. Determinations of  $D_{AB}$  improve in accuracy and precision with (1) increasing refractive index differences between the binary components as is evident from the  $(\partial\epsilon/\partial C)_{P,T}$  factor of Equation (37) and Table 5; and (2) the approach to equal concentrations, which is expressed in the  $\langle |\delta C|^2 \rangle$  factor of the same equation.

#### Conclusions and Recommendations

A sensitive quasi-elastic light scattering spectrometer has been constructed and used to collect diffusivity data for a wide class of pure liquids and binary mixtures. Independent bulk data confirm

the accuracy of the technique. The light scattering approach has several advantages over conventional techniques for determining mass and thermal diffusivities. It is not dependent on the imposition of a macroscopic gradient, a problem which seriously complicates bulk measurements. Using light scattering, diffusivity determinations take from 15 minutes to 2 hours; this is in contrast to conventional methods which may take weeks.

The approach we have developed should have important industrial applications. Transport properties have always been of importance in the design of chemical processing facilities. Now that pilot plant operations are being bypassed in favor of the computer design of full scale plants, precise and accurate values of mass and thermal diffusivities are at even more of a premium. Another possible industrial application is the continuous monitoring and control of processes in chemical plants.

Now that it has been demonstrated that diffusivities can be measured under standard conditions, the work could be extended to cover elevated temperatures and pressures. Neither condition would present serious design problems. Light scattering studies in our laboratory have already been conducted at several hundred pounds pressure and temperatures approaching 80°C.

PART II

OBSERVATION OF TRANSLATIONAL AND INTRAMOLECULAR DIFFUSION OF  
CIRCULAR DUPLEX DNA BY QUASI-ELASTIC LIGHT SCATTERING

Chapter V

INTRODUCTION

As demonstrated in Part I of this thesis, light scattering spectroscopy is a valuable tool for the study of liquid mass and thermal diffusivities. However, the domain of the technique is not confined to just liquids and liquid mixtures, but is becoming increasingly useful in the study of macromolecular Brownian motion. Under appropriate conditions the light scattered from long-chain molecules will be modulated by the dynamics of the molecule. Since the pioneering theoretical paper by Pecora (1964), numerous studies have been conducted using light scattering to study macromolecular translational Brownian motion (Cummins et al. 1964; Dubin et al. 1967; Foord et al. 1970).

The rotational motion of macromolecules has also been studied using quasi-elastic scattering, beginning with the theoretical work of Pecora (1964, 1968a, 1968b) and followed by the experimental determination of the rotational diffusion constant  $\Theta$  for TMV by Cummins et al. (1969), Wada et al. (1969), and Fujime (1970a). The expressions developed are valid only for rigid, rod-like molecules.

Most molecules of biological interest have some degree of flexibility in solution and are not rod-like. The dynamics of large, flexible molecules in solution is a classical problem in polymer physics. Since the initial efforts of Rouse (1953) and Zimm (1956), theoreticians have been attempting to quantitatively describe the motion of large, flexible chains. Expressions for the distributed spectra of flexible-coil macromolecules have been derived using the Rouse-Zimm bead and spring model (Pecora 1965; 1968). Harris and Hearst (1966),

Saito et al. (1967), Saito and Ito (1968), Fujime (1970b), and Fujime and Maruyama (1973) have written expressions for the spectra based on the Kratky-Porod worm-like coil theory for semi-flexible molecules. Recently the worm-like coil model has received serious criticism (Soda 1973). The experimental implications of the models' inconsistencies and ambiguities are at present uncertain.

The experimental work in the area of flexible macromolecules is limited. Fujime (1970b) has reported measurement of the lowest order internal mode of bending motion of a semi-flexible polymer F-actin. Fujime and Ishiwata (1971) have studied the dynamic interaction of F-actin with other muscle proteins, heavy meromyosin, and tropomyosin. Further work by Ishiwata and Fujime (1972) has indicated the effect of calcium ions on the flexibility of thin filaments of muscle. Fujime et al. (1972) have also studied the flexural rigidity of bacterial flagella. These studies rely on an interpretation of the data which does not appear to be totally consistent with the theoretical formulation by Fujime (1970b). The authors mention other ambiguities related to concentration effects and polydispersity.

Schmidt (1973) has reported observation of the internal motion of NI-DNA in solution; again the same ambiguities are unresolved. Furthermore, the data analysis is based on a misinterpretation of other investigators' remarks (Dubin et al. 1967). Schmidt's four data points are fitted to a model with five independent parameters, a model which lacks any foundation in the formalism for the spectral distribution of light scattered from flexible chains.

Reed and Frederick (1971) have studied the spectral distribution of light scattered from solutions of polystyrenes in cyclohexane. For high molecular weight samples (4,500,000) they reported a departure from a single Lorentzian fit, which they attributed to intramolecular Brownian motion. In more recent work, Huang and Frederick (1974) have determined the translational diffusion coefficient  $D$  and the longest internal relaxation time  $\tau_1$  for a polystyrene of molecular weight  $27.3 \times 10^6$  in cyclohexane and 2-butanone. The values of  $\tau_1$  obtained are consistent with values calculated from Rouse-Zimm theory.

The purpose of this study was to conduct preliminary investigations on the flexibility and conformational states of two samples of circular duplex DNA, PM2 I and a mixture of  $\phi$ X174 RF I and II. Form I of these DNA's appears in nature as a covalently closed superhelical structure. It is possible to unwind the supercoil using a variety of techniques (Bauer and Vinograd 1971) to produce a relaxed circular molecule (form II). It is proposed that by comparing the spectra of light scattered from relaxed and supercoiled molecules we may infer conformational changes through changes in the diffusion coefficient, and on a more careful examination of the spectra extract information on the changes in flexibility between forms I and II. Studies on linear forms of  $\phi$ X174 RF and PM2 should reveal even more dramatic changes in flexibility.

These systems were selected for study because  $\phi$ X174 RF and PM2 DNA exist in a variety of conformations, are well characterized and monodisperse, have a size suitable for flexibility studies using light scattering, and are molecules of biological importance. With regard to

the last point, relatively little is understood of how DNA may coil in more highly organized structures, such as a phage head. Gray and Hearst (1968) have attempted a study of the bending energetics using sedimentation data. It is hoped that information on the flexibility of  $\phi X$  and PM2 molecules from light scattering may eventually elucidate some of the energetics involved in the packaging process.

Chapter VI

THEORY

Scattering Theory

Pecora (1964) has shown that the field autocorrelation function for isotropic systems may be written

$$C_E(\tau) \propto \langle \alpha^*(\underline{K}, 0) \alpha(\underline{K}, \tau) \rangle \quad (51)$$

where  $\alpha(\underline{K}, \tau)$  is the spatial Fourier component of the local fluid polarizability  $\alpha(r, t)$ . In the first part of this thesis we chose to expand  $\alpha$  for liquids in terms of hydrodynamic parameters. Here we shall treat dilute macromolecular solutions and assume that the solvent scattering is negligible. By dividing the molecule into  $n$  segments, each with polarizability  $\alpha_i$ , Equation (51) becomes

$$C_E(\tau) \propto \frac{\alpha^2}{n^2} \sum_{i,j} \langle \exp\{i\underline{K} \cdot [\underline{r}_i(t) - \underline{r}_j(0)]\} \rangle \quad (52)$$

The location of segment  $i$  on the molecule may be written

$$\underline{r}_i = \underline{R} + \underline{b}_i$$

where  $\underline{R}$  is a vector to the molecular center of mass and  $\underline{b}_i$  is a vector describing the segmental position relative to the center of mass. Then,

$$\begin{aligned} C_E(\tau) &\propto \langle \exp\{i\underline{K} \cdot [\underline{R}(t) - \underline{R}(0)]\} \rangle \\ &\times \langle \frac{1}{n^2} \sum_{i,j} \exp\{i\underline{K} \cdot [\underline{b}_i(t) - \underline{b}_j(0)]\} \rangle \end{aligned} \quad (53)$$

It has been assumed that center of mass motion is independent of internal motion. Internal motion will not affect the spectrum if the molecules are small, i.e.,

$$\underline{k} \cdot (\underline{b}_i(t) - \underline{b}_i(0)) \ll 1 \quad (54)$$

in which case

$$C_E(\tau) \propto \langle \exp\{i\underline{k} \cdot [\underline{R}(t) - \underline{R}(0)]\} \rangle \quad (55)$$

and the spectrum is determined solely by translational motion of the center of mass. In effect, the light wave sees the time dependence of polarizability changes; for translational diffusion the polarizability moves with the molecule. If the polymer is a rigid, uniform sphere, the light is unable to observe any internal motion (in this case rotational diffusion) because there is no change in the molecular polarizability distribution of the segments on rotation.

The center of mass motion for polymers can be described by the diffusion equation

$$\frac{\partial P(\underline{r}, t)}{\partial t} = D \nabla^2 P(\underline{r}, t) \quad (56)$$

where  $P(\underline{r}, t)$  is the conditional probability of finding a molecule at position  $\underline{r}$  at time  $t$  if it is at the origin at time zero, and  $D$  is the translational diffusion coefficient. The conditional probability can be used to evaluate the ensemble average of Equation (55) with the result (Cummins et al. 1969)

$$C_E(\tau) \propto \exp[-DK^2\tau] \quad (57)$$

The decay time is

$$\tau^{-1} = DK^2 \quad (58)$$

a result which we previously found for binary mixtures by using the fluctuation approach.

When the molecules are large (or  $K$  is large), condition (54) does not hold and we should expect to see intramolecular motion. The solution to this problem requires a detailed knowledge of polymer chain hydrodynamics.

### Flexible Polymer Theory Applied to Light Scattering

The basic problem confronting us in finding an expression for the spectral distribution of light scattered from flexible macromolecules is the evaluation of the expression

$$\sum_{i,j}^n \langle \exp\{i\mathbf{K} \cdot [\mathbf{r}_i(t) - \mathbf{r}_j(0)]\} \rangle \quad (59)$$

To evaluate this term we need the probability  $\psi(\mathbf{r}_0, \mathbf{r}_1, \dots, \mathbf{r}_n)$  of finding each segment  $i$  with coordinates between  $\mathbf{r}_i$  and  $\mathbf{r}_i + d\mathbf{r}_i$  at time  $t$ , as well as a description of  $\mathbf{r}_i(t)$ . Either Rouse-Zimm theory or the worm-like coil formalism provide the needed information. The two treatments reduce to the same expressions (Fujime 1973) when  $\gamma L \gg 1$ , where  $\gamma^{-1}$  is the statistical segment length and  $L$  is the contour length of the molecule. This condition applies for the DNA of this study, hence, we shall confine our discussion to Rouse-Zimm theory because of its conceptual simplicity.

The basic model consists of a series of beads interconnected by ideal springs. Each segment of the molecule is represented by a Gaussian random coil, and the beads are located at the junctions of these segments. The beads act as centers of hydrodynamic resistance, each with frictional constant  $\rho$ . For such a model Zimm (1956) has derived an equation of motion using normal-mode coordinates. The equation expresses the influence of the Hookean restoring forces, hydrodynamic forces, and the forces of Brownian motion. Zimm (1956) has solved for the eigenvalues of the problem with the result

$$\lambda_k = \pi^2 k^2 / n^2 \quad (60)$$

and normal-mode relaxation times of

$$\tau_k = \frac{\rho}{6\lambda_k kT \gamma^2} \quad (61)$$

Substituting the infinite dilution value of the diffusion coefficient  $D_0$  for  $kT/\rho n$  gives

$$\tau_k = \frac{n(\frac{1}{\gamma})^2}{6\pi^2 k^2 D_0} \quad (62)$$

For a linear Gaussian coil the mean square radius of gyration is

$$\langle R_G^2 \rangle = \frac{n(\frac{1}{\gamma})^2}{6} \quad (63)$$

hence

$$\tau_k = \frac{\langle R_G^2 \rangle}{\pi^2 k^2 D_0} \quad (64)$$

We should also note that

$$n\left(\frac{1}{\gamma}\right)^2 = \langle \ell^2 \rangle_e \quad (65)$$

where  $\langle \ell^2 \rangle_e$  is the mean square end-to-end distance.

Under the absence of any externally applied forces the equation of motion is formally equivalent to a system of coupled harmonic oscillators. The solution in terms of  $\psi(\underline{r}_0, \underline{r}_1, \dots, \underline{r}_n)$  was first derived by Wang and Uhlenbeck (1945).

Pecora has used  $\psi$  and the normal coordinate expressions for  $\underline{r}_i$  to evaluate the expression

$$\left\langle \sum_{i,j}^n \exp\{i\underline{K} \cdot [\underline{r}_i(t) - \underline{r}_j(0)]\} \right\rangle$$

The final expression for  $C_E(\tau)$  is of the form (Fujime 1973)

$$C_E(\tau) \propto \sum_{N,M:\text{even}} P_{NM}(x) \exp[-(DK^2 + N/\tau_1 + M/\tau_2)\tau] \quad (66)$$

for  $\gamma L \gg 1$ , where higher order relaxation times have been neglected. The scattering form factors have been numerically evaluated and are plotted versus the scattering parameter  $x (= K^2 n (\frac{1}{\gamma})^2 / 6)$  in Figure 18 (Fujime 1973). It is evident that as we move to higher angles, higher order intramolecular terms begin to contribute significantly to the spectral distribution. For molecules that have a large  $\langle \ell^2 \rangle_e$ , higher order terms will contribute even at low scattering angles.

## Chapter VII

### EXPERIMENTAL

#### Materials

##### Polystyrene latex spheres

Dow polystyrene latex spheres (run number LS-1044-E) were diluted to 0.01 mg/cc in a 0.01% SDS aqueous solution. Before use, the sphere solution was subjected to sonication to remove aggregates.

##### $\phi$ X174 RF DNA

The  $\phi$ X174 RF DNA was the gift of J. Lee Compton; it was isolated and purified according to the procedure of Johnson and Sinsheimer (1974). Characterization by banding in an EB CsCl gradient indicated that over 93% of the original preparation consisted of RFI. We are unable to make any definitive statements about the exact composition of our sample because no analyses were performed. It is probably safe to assume that all of the DNA was circular; EB CsCl bandings on irradiated aliquots of the original preparation (diluted to 10  $\mu$ g/cc) indicated no visible nicking.

The light scattering experiments were performed using 120  $\mu$ g/cc of  $\phi$ X174 RF in 0.05 M tris, 0.02 M EDTA at a pH of 7.5.

##### PM2 I DNA

The PM2 I DNA was the gift of Robert Watson. The PM2 bacteriophage was grown, harvested, and isolated by the method of Espejo and Canelo (1968). Final purification was according to the procedure of Revet et al. (1971) using CsCl-PI buoyant banding as described by Hudson

et al. (1969). A concentration of 75  $\mu\text{g}/\text{cc}$  in 0.01M tris, 0.002 M EDTA, 0.5M NaCl, pH 7.4, was used for this study. The initial preparation and the irradiated sample (after completion of the experiment) were simultaneously examined by band sedimentation velocity to determine the extent of nicking. The velocity patterns appeared virtually identical, indicating  $\approx 3\%$  nicked rings both before and after irradiation.

#### Apparatus and Procedure

The spectrometer was as described in Part I of this thesis. A C105 Brice Phoenix cell with flat entrance and exit windows contained the sample. A teflon plug placed in the bottom of the cell reduced the required sample volume to 7 ml. The incident laser beam was focused in the center of the cell using a 10 cm focal length lens.

Data acquisition for both experiments was identical to that of Part I and required less than 3 hours for completion. All correlation functions were of the homodyne type.

Chapter VIII  
RESULTS AND DISCUSSION

Polystyrene Latex Spheres Experiment

As a control experiment data were taken on the Dow polystyrene latex spheres. These spheres were chosen for study because the sample time increments used completely encompassed the  $\Delta\tau$  needed to examine the DNA spectra. In Figure 19 each datum represents a single autocorrelation function collected using the sample time increment represented by the corresponding symbol. The correlation functions of Figure 19 were fitted to the form

$$C_1(\tau) = A(1) + A(2) \exp[-A(3)\tau] \quad (67)$$

where  $A(3)$  is defined as  $\tau^{-1}$ , the inverse exponential decay time. (We have used  $\tau$  to denote both elapsed time  $\tau$  and the exponential decay constant  $\tau$ . The desired usage should be obvious.) The narrow spread in decay times when  $\Delta\tau$  varied by a factor of 10 indicates that the parent function is close to a true exponential. Typical fits are shown in Figures 21-23; the quality of the fits is in all cases precise (1 standard deviation) to better than 1%. The source of the small systematic differences in  $(2\pi\tau)^{-1}$  observed as a function of  $\Delta\tau$  in Figure 19 is not known at present. Because the spheres are intense scatterers, the S/N ratio is good and all of the correlation functions collected had baselines close to 0. Figure 20 consists of the same data fitted to a single exponential with a zero baseline. The systematic deviations of Figure 19 disappear when this is done. For low level signals the data must be fitted with a baseline because the S/N

ratio is not sufficient to mask low frequency noise which is correlated and appears as a baseline offset.

From theory we expect the sphere data to exhibit an inverse decay time for the correlation function of  $2DK^2$ . A plot of  $\tau^{-1}$  versus  $K^2$  should produce a straight line with a slope proportional to the diffusion coefficient  $D$ . A fit to the data of Figure 19 yields a value for  $D$  of  $0.359 \times 10^{-7} \text{cm}^2/\text{sec}$ . Assuming the diffusion coefficient for the spheres can be represented by the Stokes-Einstein relation

$$D = kT/\zeta \quad (68)$$

where  $\zeta = 6\pi\eta r$ , the average radius of the spheres can be calculated. The value determined in this manner is

$$r = 595\text{\AA}$$

An accuracy of 5% is estimated based on the value of the slope of a line drawn through the  $(2\pi\tau)^{-1}$  values which best represent the entire correlation functions. Our value is to be compared to Dow's quoted value of  $545 \pm 14\text{\AA}$ , measured by electron microscopy. Considerable evidence has accumulated which indicates that values obtained from electron microscopy are consistently low (Kratohvil and Smart 1965; Phillips et al. 1970). In a thorough particle size determination using total intensity light scattering from single latex particles, Phillips et al. (1970) measured the sphere size as  $600 \pm 50\text{\AA}$ , which is in agreement with our experimental results.

φX174 RF and PM2 I Experiments

The experimental results for the solutions of φX174 RF and PM2 I DNA appear in Figures 24 and 25, respectively. Again each datum represents the decay time determined from a fit to a single correlation function. The correlation functions are fitted to a single exponential with a variable baseline. The reproducibility of the data is better than that shown in the figures. Figures 26-28 display typical autocorrelation functions collected for PM2 I DNA. The reproducibility of the correlation functions is thought to be ≈1%; the variation of results in Figures 24 and 25 is a reflection of the uncertainty in the fit (a standard error of ≈2%)--the parent function is presumably a sum of exponentials while the fitting function is a single exponential.

The data for both DNA solutions have been analyzed in terms of the prior theoretical discussion. The initial assumption, to be revised later, is that only the translational component and the lowest order intramolecular term contribute significantly to the scattering. Then the field correlation function is expressed as

$$\begin{aligned}
 C_E(\tau) \propto & P_{00}(x) \exp \{-(DK^2)\tau\} \\
 & + P_{20}(x) \exp \{-[DK^2 + \frac{2}{\tau_1}]\tau\}
 \end{aligned} \tag{69}$$

and the current autocorrelation function becomes

$$\begin{aligned}
 C_i(\tau) \propto & P_{00}^2(x) \exp \{-(2DK^2)\tau\} \\
 & + 2P_{00}(x) P_{20}(x) \exp \{ -[2DK^2 + \frac{2}{\tau_1}]\tau\} \\
 & + P_{20}^2(x) \exp \{-[2DK^2 + \frac{4}{\tau_1}]\tau\}
 \end{aligned} \tag{70}$$

We further assume that  $2P_{00}P_{20} \gg P_{20}^2$  so that the last term of Equation (70) may be ignored. The effect of such an assumption will be discussed later. The current correlation function finally simplifies to

$$C_i(\tau) \propto P_{00}^2(x) \exp\{-(2DK^2)\tau\} + 2P_{00}(x) P_{20}(x) \exp\{-[2DK^2 + \frac{2}{\tau_1}]\tau\} \quad (71)$$

Translational diffusion

The value for the diffusion coefficient  $D$  is estimated from the analysis of low angle data using the following reasoning. In the low angular region the dominant contribution to the scattering is from center of mass translation. Figure 18 illustrates the prediction for the translational scattering amplitude from Rouse-Zimm theory.

With Equation (71) in mind, it will be useful to adopt the notation

$$\Gamma_{\tau} \equiv 2/\tau_1$$

and

$$\Gamma_D \equiv 2DK^2$$

where the  $\Gamma$ 's are components of the relaxation times. The ratio

$$\frac{\Gamma_{\tau}}{\Gamma_D} = \frac{6\pi^2}{\langle \rho^2 \rangle_e K^2} \quad (72)$$

can be evaluated for the two solutions with the result (for  $30^\circ$ )

$$\Gamma_{\tau}/\Gamma_D = 5.5 \quad (\phi X \text{ RF})$$

$$\Gamma_{\tau}/\Gamma_D = 3.2 \quad (\text{PM2})$$

$\langle \ell^2 \rangle_e$ , the mean square end-to-end distance, is estimated using a statistical segment length of  $1200\text{\AA}$  (Schmid et al. 1971) and contour lengths of  $1.78 \times 10^{-4}\text{cm}$  for  $\phi X$  and  $3.06 \times 10^{-4}\text{cm}$  for PM 2 (Espejo and Sinsheimer 1969).

Considerable ambiguity exists in the estimation of  $\Gamma_{\tau}/\Gamma_D$  because the expression for  $\tau_1$  [Equation (62)] is derived for infinite dilution. It is unknown whether Rouse-Zimm theory holds for finite concentration and  $\tau_1$  has the same concentration dependence as  $D$ . For the moment it is sufficient to say that

$$\Gamma_{\tau} > \Gamma_D$$

for low angles.  $C_i(\tau)$  may now be expressed as

$$C_i(\tau) \propto P_{00}^2(x) \exp\{-\tau/\tau_{cm}\} + 2P_{00}(x) P_{20}(x) \exp\{-\tau/\tau_{int}\} \quad (73)$$

where  $\tau_{cm}^{-1} \equiv \Gamma_D$  and  $\tau_{int}^{-1} \equiv \Gamma_{\tau} + \Gamma_D \approx 5\Gamma_D$ . For the case of low scattering angles the prediction is then a rapidly decaying exponential (the intramolecular component) of low amplitude with a characteristic time of

$$\tau_{int} = (2DK^2 + 2/\tau_1)^{-1} \quad (74)$$

superimposed on an exponential (the pure translational component) with a much longer relaxation time of

$$\tau_{cm} = (2DK^2)^{-1} \quad (75)$$

The fractional intensity of the latter term is large compared to the internal term. It follows that for long sample time increments the intramolecular contribution is compressed into the initial part of the curve and the contribution to the correlation function is primarily from the pure translational term.

The inverse decay time  $(2\pi\tau)^{-1}$  of the correlation function provides an estimate of  $D$ . The slope of a line drawn through the  $(2\pi\tau)^{-1}$ 's for low angle correlation functions should be equal to  $D/\pi$ . This procedure has been followed with the results

$$D = 0.7 \times 10^{-8} \text{ cm}^2/\text{sec} \quad (\phi X \text{ RF})$$

$$D = 0.7 \times 10^{-8} \text{ cm}^2/\text{sec} \quad (\text{PM2 I})$$

These compare to infinite dilution values based on sedimentation data (Espejo et al. 1969) of

	I	$D_0 = 2.32 \times 10^{-8}$
PM2	II	$D_0 = 1.87 \times 10^{-8}$
	I	$D_0 = 3.29 \times 10^{-8}$
$\phi X \text{ RF}$	II	$D_0 = 2.54 \times 10^{-8}$

Considerable uncertainty exists in our experimental values because even at low angles ( $30-40^\circ$ ) and long  $\Delta\tau$  the values of  $x$  (Figure 18) for these DNA molecules are sufficiently large and  $\tau_{int}$  is sufficiently short that intramolecular contributions cannot be totally neglected;

Tables 7 and 8 contain scattering parameter values for the range of  $k^2$ . Such an effect would falsely increase the measured value of  $D$ . A second possibility exists--partial heterodyning due to stray or reflected light would reduce  $(2\pi\tau)^{-1}$  and therefore decrease the observed  $D$ . Either of these possibilities could seriously affect the result because of the sensitivity of  $D$  to small variations in  $(2\pi\tau)^{-1}$  at low angles. The possibility of scattering at even lower angles using heterodyning would eliminate these problems. The difficulty is that at  $(2\pi\tau)^{-1}$  values of several Hz, low frequency noise may seriously distort the data.

#### Intramolecular diffusion

Having established the form of the correlation function as

$$C_i(\tau) \propto P_{00}^2 \exp\{-\tau/\tau_{cm}\} \\ + 2P_{00}P_{20}\{\exp -\tau/\tau_{int}\}$$

it is worthwhile to examine its behavior at higher angles. Reevaluating  $\Gamma_\tau/\Gamma_D$  for  $120^\circ$ ,

$$\Gamma_\tau/\Gamma_D = 0.6 \quad (\phi X \text{ RF})$$

$$\Gamma_\tau/\Gamma_D = 0.4 \quad (\text{PM2})$$

The values of  $\Gamma_\tau/\Gamma_D$  are probably too small because  $\langle \ell^2 \rangle_e$  for form I is reduced by approximately 15-20% from form II (Jolly and Campbell 1972a; 1972b). These molecules should also be treated as non-free-draining, which further reduces  $\tau_1$  and increases  $\Gamma_\tau/\Gamma_D$ .

At these concentration levels the occupation density for PM2 is 0.17 and for  $\phi X$  it is 0.22. For comparable levels of high molecular weight polystyrenes in solution, Huang and Frederick (1974) observed no systematic variation in  $\tau_1$  with concentration. If  $\tau_1$  does not change, then

$$\Gamma_\tau/\Gamma_D = \frac{6\pi^2 D_0}{\langle \ell^2 \rangle_e DK^2} \quad (76)$$

If we tentatively assume that  $\tau_1$  is less sensitive to concentration than  $D$ , then in view of Equation (76) and the preceding arguments it is reasonable to say that

$$\Gamma_\tau/\Gamma_D \gtrsim 1$$

As we move to lower angles this will most certainly be true. As for the low angle case, the decay of the intramolecular term is faster than the translational motion term, but in this instance we wish to study the  $\tau_{int}$  component in order to determine  $\tau_1$ . Fortunately, at high scattering angles the intramolecular amplitude  $P_{20}(x)$  contributes significantly to the total intensity (see Figure 18). We can envision the intramolecular term of reasonable amplitude decaying on top of a more slowly dying exponential resulting solely from mass diffusion.  $\tau_1$  may be estimated for such a case by using the short sample time increments, which have the effect of emphasizing the  $\tau_{int}$  term.

Two complementary methods have been employed to analyze the data. Both are based on the notion that at high angles and short  $\Delta\tau$ ,  $C_i(\tau)$  can be approximated with a single exponential

$$C_i(\tau) \propto 2P_{00}P_{20} \exp[-\tau/\tau_{int}] \quad (77)$$

where  $\tau_{int}^{-1} = 2DK^2 + 2/\tau_1$ . Using the experimentally determined values for  $D$  in the expression for  $\tau_{int}$ , a fit to the data yields values for  $\tau_1$ . The  $\tau_1$  values obtained at different scattering angles are not expected to remain constant because the slope of the baseline from translational diffusion will become flatter as  $K \rightarrow 0$ . The sloping baseline has the effect of reducing  $\tau_{int}$  and consequently

$$\tau_1(\text{measured}) < \tau_1(\text{actual})$$

at a given value of  $K$ . As  $K = 0$  is approached  $\tau_1(\text{measured})$  approaches  $\tau_1(\text{actual})$ ; thus, we are able to place a lower limit on  $\tau_1$  by calculating  $\tau_1$  as a function of decreasing  $K^2$ . The limitation of this approach for determining  $\tau_1$  is the reduction in amplitude of the internal term at low angles, which has the effect of producing falsely high values for  $\tau_1$ . Tables 9 and 10 contain determined  $\tau_1$ 's as a function of  $\theta$ . As the theory predicts,  $\tau_1(\text{measured})$  increases monotonically with decreasing scattering angle. The lower values of  $\theta$  chosen to estimate  $\tau_1$  have been somewhat arbitrarily chosen based on the predicted contribution to the correlation function from Figure 18.

An upper limit may be placed on  $\tau_1$  by extrapolating the high angle, short  $\Delta\tau$  data through the axis. Because  $\tau_1^{-1}(\text{measured}) > \tau_1^{-1}(\text{actual})$  and  $\tau_1^{-1}(\text{measured}) \rightarrow \tau_1^{-1}(\text{actual})$  as  $K \rightarrow 0$ , the line of  $(2\pi\tau)^{-1}$  versus  $K^2$  should yield a  $K = 0$  intercept with  $\tau_1(\text{intercept}) >$

$\tau_1(\text{actual})$ . With this procedure the following values were obtained:

$$\tau_1(K=0) \approx 4 \text{ msec} \quad (\phi X \text{ RF using } \Delta\tau \text{ of } 5 \mu\text{s})$$

$$\tau_1(K=0) \approx 6 \text{ msec} \quad (\text{PM2 I using } \Delta\tau \text{ of } 5 \text{ and } 10 \mu\text{s})$$

These are to be compared to the Rouse-Zimm theoretical values [Equation (64)] of

$$\tau_1 \approx 2.6 \text{ msec} \quad (\phi X \text{ RF})$$

$$\tau_1 \approx 4.4 \text{ msec} \quad (\text{PM2})$$

based on the experimentally determined values of  $D$ . If infinite dilution values are used the  $\tau_1$ 's are reduced by the ratio  $D_0/D$ . The supercoiling and non-free-draining contributions further reduce  $\tau_1$ .

We have proceeded under the assumption that  $C_i(\tau)$  contains only two terms. But at high angles  $C_i(\tau)$  has higher order intramolecular contributions containing decay times of  $(2DK^2 + 4/\tau_1)^{-1}$ ,  $(2DK^2 + 6/\tau_1)^{-1}$ , etc. These terms all have the effect of increasing the observed inverse exponential decay time, or analogously decreasing the measured intramolecular relaxation time. The enhanced  $\tau^{-1}$  values further contribute to the departure of the  $K = 0$  extrapolation from the correct values. The sloping baseline effect and the higher or intramolecular terms thus combine to produce an intercept value for  $\tau_1$  which is greater than the actual value (assuming the model to be correct). We see that the real  $\tau_1$  should be in between the high

angle fitted value and the intercept value.

Considering the large uncertainty in the  $\tau_1$ 's determined by these upper and lower bound procedures, the most we can conclude is that the experimental values appear to be qualitatively correct. A more thorough analysis must be performed in order to reach a firm conclusion.

#### Suggestions for Further Analysis

An alternate and more rigorous data analysis method exists which relies on graphical inspection of the data. We have seen that the correlation function has a quasi-exponential form. Plots on a semi-logarithmic scale of  $C_i(\tau)$  versus elapsed time  $\tau$  give straight lines at low scattering angles provided the  $\Delta\tau$  are sufficiently long. The single time constant estimated from the slope gives directly a value for  $D$ . For large angles, however, one should expect several decay times, of which two may be readily studied. If long  $\Delta\tau$  are used the asymptotic slope of the semilogarithmic data yields the translational constant; the amplitude of this longer time constant term is given by the intercept of the asymptote extrapolated back to  $\tau = 0$ . A second time constant is found by determining the initial slope of the data for short  $\Delta\tau$ . If the data are of a quasi-exponential form then

$$C_i(\tau) = \exp \{-\langle I \rangle \tau\} \quad (78)$$

where  $-\langle I \rangle$  is the initial slope. The theory predicts

$$C_i(\tau) \propto P_{00}^2 \exp\{-\Gamma_D \tau\} + 2P_{00}P_{20} \exp\{-(\Gamma_D + \Gamma_\tau)\tau\} \\ + P_{20}^2 \exp\{-(\Gamma_D + 2\Gamma_\tau)\tau\} \quad (79)$$

then

$$\left(\frac{d \ln C_i(\tau)}{d\tau}\right)_{\tau=0} = - \{P_{00}^2 \Gamma_D + 2P_{00}P_{20}(\Gamma_D + \Gamma_\tau) \\ + P_{20}^2(\Gamma_D + 2\Gamma_\tau)\} \quad (80)$$

Thus, the initial slope is

$$-\langle\Gamma\rangle = -\{P_{00}^2 \Gamma_D + 2P_{00}P_{20}(\Gamma_D + \Gamma_\tau) + P_{20}^2(\Gamma_D + 2\Gamma_\tau)\} \quad (81)$$

and the semi-logarithmic plot yields a value for  $\langle\Gamma\rangle$ . The two time constants thus separated can be plotted against  $k^2$ . The value of such a plot is that (1) the anticipated linear behavior for  $(2\pi\tau)^{-1}$  versus  $k^2$  for the low angle and high angle long  $\Delta\tau$  data can be checked, and (2) theoretical values for  $\langle\Gamma\rangle$  can be generated and compared to the experimental  $\langle\Gamma\rangle$ . The extension to higher order internal terms is straightforward. A complimentary check is available by plotting the theoretical fractional amplitudes versus the experimental values determined by extrapolation.

This approach should allow a more precise analysis of the data and could prove to be a convenient means for checking new molecular theories for the dynamics of polymer chains.

### Conclusions and Recommendations

Translational and internal diffusion have been observed for  $\phi$ X174 RF and PM2 I DNA using light scattering spectroscopy. A tentative interpretation of the data in terms of Rouse-Zimm theory yields internal relaxation times in qualitative agreement with theoretical predictions. Statements of quantitative agreement are probably unjustified until a more detailed analysis of the data has been performed and further information on concentration effects is obtained.

Experiments on systems related to those of this study should provide interesting information on changes in flexibility and tertiary structure of DNA. For example, PM2 II should exhibit internal relaxation times different from those of PM2 I, and linear PM2 should have a lowest order mode of relaxation four times that of circular PM2 (Bloomfield and Zimm 1966).  $\tau_1$  happens to be the hydrodynamic quantity most sensitive to a loss of circularity. Comparative studies are valuable because they do not rely heavily on the quantitative validity of Rouse-Zimm theory for the extraction of useful information. A similar study could be performed on a family of  $\phi$ X174 DNA:  $\phi$ X single-stranded linear, double-stranded linear, RF I, and RF II.

Using relaxed circular forms of  $\phi$ X and PM2 and the single-stranded linear form of  $\phi$ X DNA, it should be possible to compare experimental results to data generated from polymer dynamics theory using an approach similar to that previously discussed. This could prove to be a useful method for examining the validity of theories of macromolecular motion.

APPENDICES

Appendix I

Signal Processing

Coherence Theory

Now that the theory for the spectral distribution has been developed we need a method for information collection and translation. Random signal theory provides the theoretical framework for signal processing techniques. Cummins and Swinney (1970) discuss the application of these techniques to light-scattering in detail.

According to the Wiener-Khintchine theorem, the power spectrum  $P_i(\omega)$  of the photocurrent (from a photomultiplier) and the current correlation function  $C_i(\tau)$  are Fourier transform pairs

$$P_i(\omega) = \frac{1}{2\pi} \int_{-\infty}^{\infty} e^{i\omega\tau} C_i(\tau) d\tau \quad (I.1)$$

where

$$C_i(\tau) = \langle i(t) i(t+\tau) \rangle = \lim_{T \rightarrow \infty} \frac{1}{2T} \int_{-T}^T i(t+\tau) i(t) dt \quad (I.2)$$

and  $i(t)$  is the photoelectric current. In addition, Mandel (1963) has shown that

$$i(t) = eW^{(1)}(t) = e\sigma E^*(t) E(t) = e\sigma I(t) \quad (I.3)$$

where  $\sigma$  is the quantum efficiency and  $W^{(1)}(t)$  is the probability per unit time of photoelectron emission from a photocathode illuminated by the scattered field. The joint probability that one photoelectron will be emitted at time  $t$  (per unit time) and another at

time  $t+\tau$  (per unit time) is

$$W^{(2)}(t, t+\tau) = \sigma^2 E^*(t) E(t) E^*(t+\tau) E(t+\tau) \quad (I.4)$$

Also, for stationary fields,

$$\langle i(t) \rangle = e \langle W^{(1)}(t) \rangle = e \sigma \langle I \rangle \quad (I.5)$$

$$\begin{aligned} \langle W^{(2)}(t, t+\tau) \rangle &= \sigma^2 \langle E^*(t) E(t) E^*(t+\tau) E(t+\tau) \rangle \\ &= \sigma^2 \langle I \rangle^2 g^{(2)}(\tau) \end{aligned} \quad (I.6)$$

where

$$g^{(2)}(\tau) = \frac{E^*(t) E(t) E^*(t+\tau) E(t+\tau)}{\langle E^*(t) E(t) \rangle^2}$$

On substitution of (I.3) into (I.2)

$$C_i(\tau) = \langle i(t) i(t+\tau) \rangle = e^2 \langle W^{(1)}(t) W^{(1)}(t+\tau) \rangle \quad (I.7)$$

and  $C_i(\tau) = C_i^*(-\tau)$ .

The photocurrent  $i(t)$  actually consists of a series of infinitely narrow discrete pulses. Therefore  $C_i(t)$  has contributions from pulses caused by distinct electrons and those caused by the same electron, i.e., if the electrons at  $t$  and  $t+\tau$  are distinct,

$$\langle W^{(1)}(t) W^{(1)}(t+\tau) \rangle_{\text{distinct}} = \langle W^{(2)}(t, t+\tau) \rangle = \sigma^2 \langle I \rangle^2 g^{(2)}(\tau)$$

while if we observe the same electron at  $t$  and  $t+\tau$ ,

$$\langle W^{(1)}(t) W^{(1)}(t+\tau) \rangle_{\text{same}} = \langle W^{(1)}(t) \rangle \delta(\tau) = \sigma \langle I \rangle \delta(\tau)$$

This term gives rise to the shot noise in the photocurrent. As a result

$$\begin{aligned} C_i(\tau) &= e^2 \sigma \langle I \rangle \delta(\tau) + e^2 \sigma^2 \langle I \rangle^2 g^{(2)}(\tau) \\ &= e \langle i \rangle \delta(\tau) + \langle i \rangle^2 g^{(2)}(\tau) \end{aligned} \quad (I.8)$$

This expression relates the photocurrent correlation function to the second-order field correlation function. We consider below three different detection schemes which utilize this result.

### Optical Beating

Homodyne (self-beating) spectroscopy operates on the principle that as the intensity of the optical field at the detector fluctuates in time, so will the photocurrent since the photoelectric emission rate is proportional to the optical intensity. Thus by measuring the spectrum of the fluctuations we can determine the spectrum of the scattered field.

Homodyning transfers the spectral information to much lower frequencies where conventional electrical filters can handle the spectrum. Since the output current of the phototube is proportional to the square of the incident electric field, the photocurrent contains beat notes between each of the spectral components of scattered light.

For laser scattering by a dilute solution of scatterers, the optical field is a narrow band Gaussian random field with the autocorrelation function

$$C_E(\tau) = \langle E^*(t) E(t+\tau) \rangle = \langle I \rangle g^{(1)}(\tau) \quad (I.9)$$

For such a field Mandel (1965) has shown that

$$g^{(2)}(\tau) = 1 + |g^{(1)}(\tau)|^2 \quad (I.10)$$

Using this relation simplifies  $C_i(\tau)$  :

$$C_i(\tau) = e \langle i \rangle \delta(\tau) + \langle i \rangle^2 (1 + |g^{(1)}(\tau)|^2) \quad (I.11)$$

From Equation (I.1) it follows that

$$P_i(\omega) \propto \langle i \rangle^2 \int_{-\infty}^{\infty} e^{i\omega\tau} |g^{(1)}(\tau)|^2 d\tau \quad (I.12)$$

Using the convolution theorem

$$FT[f_1(t)f_2(t)] = F_1(\beta) * F_2(\omega-\beta) d\beta \quad (I.13)$$

where  $FT[f(t)] = F(\omega)$ , we arrive at the expression

$$P_i(\omega) = \frac{\langle i \rangle^2}{2\pi} \int_{-\infty}^{\infty} I(\beta) I(\omega-\beta) d\beta \quad (I.14)$$

Equation (I.14) relates the power spectrum of the photomultiplier tube current to the convolution of the power spectrum of the electric field with itself, from which the notion of self-beating naturally arises.

For diffusion the correlation function  $g^{(1)}(\tau)$  has the form

$$g^{(1)}(\tau) = e^{-i\omega_0\tau} e^{-X|\tau|} \quad (I.15)$$

hence

$$I(\omega) = \frac{\langle I \rangle}{2\pi} \int_{-\infty}^{\infty} e^{i(\omega - \omega_0)\tau} e^{-X|\tau|} d\tau = \langle I \rangle \frac{X/\pi}{X^2 + (\omega - \omega_0)^2} \quad (I.16)$$

and

$$\begin{aligned} P_i(\omega) &= \frac{1}{2\pi} \int_{-\infty}^{\infty} e^{i\omega\tau} \{e^{\langle i \rangle} \delta(\tau) + \langle i \rangle^2 + \langle i \rangle^2 e^{-2X|\tau|}\} d\tau \\ &= \frac{1}{2\pi} e^{\langle i \rangle} + \langle i \rangle^2 \delta(\omega) + \langle i \rangle^2 \frac{(2X/\pi)}{\omega^2 + (2X)^2} \end{aligned} \quad (I.17)$$

The photocurrent spectrum contains three terms; the shot noise, the d.c. component, and a Lorentzian, in that order. The third term is the actual light-beating spectrum with a half-width twice the optical width, and centered at  $\omega = 0$ . Thus an optical signal originally in the  $10^{15}$  Hz range is now in the low-frequency range due to self-beating.

The limitation of this technique is that the field be Gaussian. If not, there is no simple relationship between  $I(\omega)$  and  $P_i(\omega)$ .

An alternate detection method is heterodyne spectroscopy. The detector is illuminated simultaneously by the scattered field and a coherent local oscillator signal (usually the incident laser beam). In analyzing heterodyning we find that the light beating spectrum depends on  $g^{(1)}$  rather than  $g^{(2)}$ , and is therefore independent of the field statistics. In this case the power spectrum is an exact replica of the optical spectrum centered at  $|\omega_0 - \omega_{LO}|$ . If the local oscillator is the laser, the spectrum is centered around  $\omega = 0$ .

### Correlating

Signal correlation determines the photocurrent autocorrelation function directly. The quantities of interest are then extracted from  $C_i(\tau)$ , e.g., for a Gaussian field

$$C_i(t) = e \langle i \rangle \delta(\tau) + \langle i \rangle^2 + \langle i \rangle^2 |g^1(\tau)|^2$$

Assuming we are detecting a mass diffusion process

$$g^{(1)}(\tau) = e^{-i\omega_0\tau} e^{-D_{AB}K^2|\tau|}$$

and

$$C_i(\tau) = e \langle i \rangle \delta(\tau) + \langle i \rangle^2 + \langle i \rangle^2 e^{-2D_{AB}K^2|\tau|}$$

The shot noise and d.c. components are easily subtracted off, leaving

$$C_i(\tau) \propto e^{-2D_{AB}K^2|\tau|} \tag{I.18}$$

from which  $D_{AB}$  is readily obtained. For heterodyning, the current autocorrelation function is

$$C_i(\tau) \propto e^{-D_{AB}K^2|\tau|} \tag{I.19}$$

## Appendix II

### Details of the Spectrometer

Numerous precautions were taken to ensure proper performance of the spectrometer. The most important were optical alignment and the elimination of low frequency noise.

#### Axis of Rotation and Optical Alignment

The optical rail is attached to the turntable of a granite microscope base. Because the floor and table are neither flat nor level, the rail when rotated from  $0^{\circ}$  to  $130^{\circ}$  did not move in a horizontal plane perpendicular to the direction of polarization of the incident beam. In order to achieve the desired rotation plane the stops on the three air-pistons supporting the table were adjusted so that when the table was lowered onto its supports the rotating base projected a vertical axis of rotation. The direction of the axis was ascertained by inspecting the bubble level mounted on the rail as it was rotated over its full angular range. The stops were repeatedly adjusted until the rail could be rotated without moving the bubble by more than one division, which corresponds to motion out of the horizontal plane of less than  $0.01^{\circ}$ .

A dial gauge was next mounted to the foot of the rail. With the table lowered, the elevation of the rail was calibrated by recording the dial gauge reading as a function of angle. This procedure allowed the rail to be rotated in the desired plane when the table was under air-suspension.

To be sure that the optical system viewed the correct illuminated volume, a careful alignment scheme was devised. The procedure follows:

1. The table is lowered onto its mounts.
2. The rail is rotated to approximately  $90^{\circ}$  and the cathetometer is positioned so that it is roughly in line with the rail.
3. The cathetometer is leveled.
4. The rail is leveled using the adjustable rail support to properly position the bubble.
5. A pinhole assembly is placed in the approximate center of rotation and the cathetometer viewer is used to sight the pinhole.
6. The pinhole is moved to the near end of the rail and the rail is rotated until the pinhole is centered on the cross-hairs of the cathetometer telescope.
7. Steps 5 and 6 are repeated until the rail is aligned parallel to the viewer.
8. A plumb line is positioned at the center of the pinhole and the telescope is lowered to the rail. If the plumb line is not centered on the rail the pinhole is moved and the step repeated. The rail should now be in a line extending parallel to the telescope, the center of the rail, and the center of rotation.
9. The two separate pinhole assemblies are placed at designated positions on the rail, one close to the center of rotation and the other at the end of the rail. The plumb line is centered on the pinhole at the end of the rail; this pinhole is then removed and the position of the other pinhole is centered.

10. Both pinholes are sighted through by adjusting the focus of the telescope. A white illuminated card is held behind the pinholes.
11. Both pinhole assemblies are removed. A taut, vertical wire, positioned at the center of the sample platform, is sighted. If the wire is not centered the base must be translated. If the wire is to the left of the cross-hairs as viewed through the telescope, the wheel located at the front of the optical rotary base is moved to a lower setting.
12. If the wire is not centered, a pinhole is positioned near the center of rotation and the telescope is used to focus on its center. The second pinhole is added at the end of the rail and the rail is rotated until the pinhole is centered. The procedure is repeated until the telescope and pinholes are aligned.
13. The wire is again sighted. Its position is adjusted if necessary and 12 is repeated.
14. The rail is rotated to approximately  $0^{\circ}$  actual (in line with the laser beam) and the cathetometer is moved so as to be approximately aligned with the rail.
15. The pinholes are again aligned to the telescope, the pinhole assemblies are removed and the wire is sighted. If it is not on the cross-hairs, the other translational adjustment is turned until the wire is centered.
16. The rail is returned to its original position and 5-7 are repeated keeping the pinholes in the same position. Steps 11-15 are then executed.
17. Without moving the pinholes, the position of the laser beam is

adjusted so as to pass through both pinholes. Possible adjustments include the beam director horizontal, vertical, and angular (side to side) adjustments, and the angle of the rail. Once completed, the turntable dial reading becomes  $0^0$ . This procedure guarantees a scattering volume located at the center of the cell and the center of rotation, and an optical alignment completely independent of the rail. We have discovered that optical rails are not sufficiently straight in either direction; our alignment scheme eliminates this problem.

### Low Frequency Noise

#### Vibration isolation

As mentioned previously, the optical system is mounted on a Newport Research Corp. vibration-isolated optical table. The isolation is achieved through air-pistons and damping chambers operating in both the horizontal and vertical directions. Low frequency seismometers placed on the table and floor were used to check the degree of isolation. In the horizontal direction frequencies above 5 Hz were not transmitted. In the vertical direction only frequencies below 3 Hz could be detected.

#### Elimination of ground loops

Ground loops can pose a serious problem in the detection of the scattered spectrum unless elaborate precautions are taken. Figure II-1 details the grounding scheme we implemented.

#### System performance

With the entire spectrometer operating under typical experimental conditions (Fluke 415B high voltage power supply, Hewlett-Packard 3590A wave analyzer, 3594A sweeping local oscillator, EMI 9634QR

photomultiplier, and the Ar laser) the noise level as measured on the wave analyzer rms meter on its most sensitive scale was less than  $0.5 \mu\text{V}$ . When the correlator replaced the wave analyzer, the developing correlation function contained a small 120 Hz sine wave due to the laser. The correlation function did not exhibit any periodic components when an He-Ne laser was substituted for the Ar laser.

### Appendix III

#### The Measurement of Total Intensity

The light scattering spectrometer was constructed so that it was suitable for total intensity measurements. The two features which make this apparatus far more sensitive than conventional photometers are the use of a laser light source and dual photon counting.

#### Advantages of a Laser Light Source

Table III.1 describes the advantages of an argon-ion laser over conventional light sources and the He-Ne laser. The collimation of the laser light permits a directional intensity far greater than from a mercury lamp. For a photomultiplier to detect sufficient light intensity from a mercury lamp, the optical system must contain wide slits or apertures with a large angular acceptance. The degree of angular acceptance determines the lower scattering angle limit. But to perform angular studies on macromolecules, low angle studies are necessary, thus mercury light sources place severe limitations on the size of the molecule that can be studied.

Comparing the He-Ne and argon-ion lasers, we notice that the Ar laser has far greater power, and the intensity of scattering for a given incident intensity is almost three times that of the He-Ne laser because of the  $\lambda^{-4}$  wavelength dependence. In addition, photomultipliers have greater quantum efficiency in the blue region and a slightly higher gain. These factors make the Ar laser the overwhelming choice for total intensity measurements.

## Signal Detection Techniques

The basic problem in the detection of the total intensity of scattered light is the measurement of the signal in the presence of noise. Before describing photon counting, a brief explanation of alternate approaches is given.

### DC detection and lock-in amplification

In a dc system the signal-to-noise (S/N) improvement of experimental signals is limited by low frequency noise. Simple low-pass filtering is not effective on drift or  $1/f$  noise. Improvement can be achieved by modulating that portion of the total experimental signal which contains the desired information. Thus any dc signals, offsets, or drifts introduced following the modulation stage are not passed by the ac amplifier. If one now uses asynchronous demodulation (wide-band ac amplification followed by full-wave rectification and low-pass filtering) an offset and variations in the offset are introduced in the signal.

In contrast, lock-in amplification takes the same ac signal after amplification (the modulation frequency is selected for a minimum of  $1/f$  noise) and synchronously demodulates the signal by cross-correlating the amplifier output signal with a reference waveform of the same frequency. The result is that only the desired signal is full-wave rectified. Random noise and extraneous signals which are not phase-synchronized with the reference waveform will not produce any dc offset, but only ac noise which can be eliminated with low-pass filtering. The effective ac bandwidth is equal to the bandwidth of the low-pass filter.

The lock-in approach, while superior to dc detection, has some fundamental limitations. In a signal-limited experiment where counting statistics are important, synchronous detection eliminates half of the signal through modulation. In the case of light scattering the chopping of the incident beam reduces the intensity by two.

The other limitations are related to the spectral distribution of the noise and its origin. The lock-in system is no better than dc measurements for the elimination of wide-band noise. In both cases the low-pass filter bandwidth determines the level of noise reduction. If  $1/f$  noise is important, the effectiveness of the system depends on whether the noise is additive or multiplicative. Additive noise adds to the dc level but does not change the ac signal amplitude. These types of noise are not a problem with lock-in systems. Multiplicative noise multiplies the modulated signal, producing a variation in signal amplitude. Typical examples of multiplicative noise are gain-variation noise in the lock-in system and changes in the high voltage power supply of a photomultiplier. Lock-in amplifiers, like dc systems, cannot deal with noises of this type.

Young (1969) and Robben (1971) have demonstrated that photomultipliers show no increase in the noise power spectrum at low frequencies, thus phase-sensitive detection in the case of light scattering is useful only for eliminating dc offset resulting from additive noise.

#### Photon counting

Photon counting has advantages over both dc detection and phase-sensitive amplification. Gain drift, which has an important

effect on the accuracy of the previous techniques, is eliminated with photon counting conducted under proper conditions. Foord et al. (1969) and Jones et al. (1971) specify the requisites of proper counting operation. Specifically, the gain of the photomultiplier must be high enough to allow virtually every photoelectron pulse to be counted; that is, the pulse height distribution must be sufficiently narrow that a minor variation in gain does not alter the count rate. A closely related advantage accrues from the decrease of dark current and leakage current through pulse height discrimination. Provided the signal pulse height distribution amplitude is greater than that of the dark current, discrimination with a baseline threshold setting will effectively reduce the dark count contribution.

Other advantages include the detection of low light levels with good S/N ratios, the direct processing of inherently digital data, the elimination of statistical variations resulting from reading error and not from the noise in the signal, and improved precision.

### Instrumentation

#### Mechanical and optical systems

The photometer construction is basically the same as that previously described. An additional dove-tail rail, aperture system, and photomultiplier are positioned at  $\approx 100^\circ$  and held stationary by two large magnets mounted over the rail base and attached to the magnetic table surface. The aperture systems consist of two sets of modified milling attachments which can be translated in three mutually orthogonal directions. These two aperture systems define the solid angles and the irradiated volumes seen by the detectors. The angular divergence for

both systems is chosen to be identical while the illuminated volumes are in general different because system 1 is on a rotating rail while system 2 is fixed in position as a reference unit. Aperture system 1 is aligned with the cathetometer as outlined in Appendix II. Aperture system 2 is aligned by sighting the center of the focused light beam in the sample volume and positioning the rail and apertures such that one can also sight through the center of the pinholes. The cathetometer is then left in position as a reference check.

#### Photon counting system

The advantages of single photon detection over dc and synchronous detection were discussed in a previous section. Here we discuss the advantage of this particular photon counting system over others previously constructed. The dual system as designed by Wims and Myers (1972) contains a reference channel for normalizing the data to the incident intensity, which may vary as a function of time. Part of the incident beam is split off and directed to the reference photomultiplier. This arrangement eliminates incident intensity variation as a source of error, thus giving it an advantage over a single detection system, but it does not correct for changes in the position of the scattering volume.

Our system was designed with the reference detector viewing the sample volume. Variations in the height of the sample volume as viewed through the aperture systems are then compensated for by normalizing the data to the reference level. This approach proved to be essential for accurate total intensity measurements because the position of the laser beam drifted with time.

Our Coherent Radiation 52A argon-ion laser contains a feedback light-stabilization unit which varies the current on the plasma tube in order to compensate for drifts in intensity. We began to question its effectiveness of operation when the intensity as monitored directly with the photomultiplier and/or a Schottky barrier photodiode recorded drifts of several percent on a strip chart recorder sensitive to 0.1%. The manufacturer's specifications were noise  $< 0.2\%$ , and long term amplitude stability, better than 0.1% rms. A microammeter was installed directly behind the light control diode detector mounted on the head of the laser. We then proceeded to vary the plasma current by detuning the laser. Monitoring the head detector while simultaneously recording the light level from the photomultiplier or other diode (both positioned  $\approx 6$  feet from the first diode) indicated that the intensity as seen by the light stabilization detector was constant while the intensity drifted considerably for the other two detectors. As further evidence for the motion of the beam, a double concave lens was inserted in the beam and the position of the beam was visually observed as the current was slowly varied by detuning. As expected, the beam moved up with detuning in one direction and down with detuning in the other direction. To compensate for these variations in beam position we had to resort to the dual counting system with both detectors viewing the sample volume. On general principles this approach is preferred; the more advanced the stage in an experiment at which one can monitor a reference signal, the greater the likelihood of accurate measurements. The laboratory temperature is now controlled to  $0.2^{\circ}\text{C}$ , so that current variations resulting from temperature drift are

not as serious a problem.

A block diagram of our system is shown in Figure III.1. The photomultiplier and counting equipment meet the requirements that have been outlined by Foord et al. (1969). The EMI9789B photomultiplier has a fast rise time and generates a narrow pulse output. The output pulse height distribution is Poisson with a definite peak corresponding to single photoelectron emission from the cathode surface (see Figures III.2 and III.3). The quantum efficiency (C.B. index of  $\approx 9.0$ ) and gain ( $\approx 3.7 \times 10^7$ ) are high and the dark count is low ( $< 0.1$  nA).

The sockets and housings used were produced by Products for Research and specifically designed for photon counting applications. Both housings (PR2200-RF) contained interchangeable potted dynode assemblies, mu metal shielding, and RF shielding. The output pulses were fed into the charge sensitive Canberra 805 preamplifier. The model 805 contains a white emitter follower which enables it to drive long lengths of RG 62/U cable which are terminated into 93 ohms. The output tail pulse (rise time  $< 50$  nanoseconds) was fed into a Canberra 6018 amplifier which forms near-Gaussian pulse shapes. The 6018 is capable of handling over 50 KHz without appreciable gain change. The pulses from the amplifier were then fed to the Canberra model 6031 analyzer which generates logic pulse outputs of 0.4 microseconds wide and rise and fall times less than 25 nanoseconds. The analyzer has both lower and upper level discrimination with a minimum baseline threshold of 25 mv. The logic pulses then entered the Canberra 6324 dual counter/timer which has a 20 MHz counting rate and a range of  $1 \times 10^6$ . Output of the analyzer can also be fed to the Canberra 6080

analog ratemeter and the 6033 E sweep, which is able to perform automatic pulse height scans (for a single channel) with a preselected window width. The number of counts in both channels next entered the data control and output system which consists of the Canberra 6712 multi-axis programmer, 6832 teletype transmitter, 6834 teletype receiver, and the teletype. As an option, the data may be recorded on magnetic tape.

#### Photon counting system performance

With the system intact but the high voltage off on both tubes, neither channel recorded any counts, which indicated a noise free system. The tubes were operated in a voltage range such that pulse height distributions similar to Figures III.2 and III.3 were obtained. Dark current levels were negligible compared to the light count rates measured. A plot of the count rate as a function of tube voltage with fixed input light levels, amplifier gains, and baseline thresholds is shown in Figure III.4. In the plateau region almost every photoelectron pulse is being counted. In this region the count rate for a fixed light flux tends to become insensitive to tube gain and high voltage levels.

Figures III.5-13 attest to the success of the dual counting system. Figures III.5,8, and 11 show raw count rates for three different samples. In the case of the white light source and fluorecein the count rate was intentionally modulated. Figures III.6,9, and 12 exhibit the normalized count rates arrived at by calculating a mean ratio based on the ratio for each pair of points. Figures III.7, 10 and 13 display the percent departure of the analytical channel count

rate from the reference channel count rate. Error bars are based on one sigma assuming random counting statistics. In all three cases the deviations can be attributed solely to statistics.

LITERATURE CITED

LITERATURE CITED

- Alpert, S. S., Proc. Conf. on Phenomena in the Neighborhood of Critical Points, N.B.S. Misc. Publ. 273 National Bureau of Standards, Washington, D. C. (1965).
- Anderson, D. K., J. R. Hall, and A. L. Babb, J. Phys. Chem. 62, 404 (1958).
- Aref'ev, I. M., B. D. Kopylovskii, D. Sh. Mash, and I. L. Fabelinski, J.E.T.P. Letters 5, 355 (1967).
- Bauer, W., and J. Vinograd, in Progress in Molecular and Subcellular Biology 2 (Springer-Verlag, 1971), pp. 181-215.
- Benedek, G. B., in Polarization, Matiere and Rayonnement (Presses Universitaire de France, Paris, 1969).
- Berge, P., unpublished work (1969).
- Berge, P., P. Calmettes, M. Dubois, and C. Laj, Phys. Rev. Letters 24, 89 (1970).
- Berge, P., and M. Dubois, C. R. Acad. Sc. Paris 269B, 842 (1969).
- Beysens, D., Rev. Phys. Appl. 8, 175 (1973).
- Bloomfield, V., and B. H. Zimm, J. Chem. Phys. 44, 315 (1966).
- Board, W. J., and S. C. Spalding, AIChE J. 12, 349 (1966).
- Bridgman, P. W., Proc. Am. Acad. Arts Sci. 59, 141 (1923).
- Burchard, J. K., and H. L. Toor, J. Phys. Chem. 66, 2015 (1962).
- Caldwell, C. S., and A. L. Babb, J. Phys. Chem. 59, 1113 (1955).
- Chu, B., Ann. Rev. Phys. Chem. 21, 145 (1970).
- Cummins, H. Z., F. D. Carlson, T. J. Herbert, and G. Woods, Biophys. J. 9, 518 (1969).
- Cummins, H. Z., N. Knable, and Y. Yeh, Phys. Rev. Lett. 12, 150 (1964).
- Cummins, H. Z., and H. L. Swinney, Progr. Opt. 8, 135 (1970).
- Czworniak, K. J., and D. R. Jones, J. Opt. Soc. Amer. 64, 86 (1974).

- Dawson, J. R., and J. A. Harpst, *Biopolymers*, 10, 2499 (1971).
- DeGroot, S. R., *Thermodynamics of Irreversible Processes* (North Holland, Amsterdam, 1959).
- Deville and Landesman, personal communication to Berge.
- Dubin, S. B., Ph.D. thesis, M.I.T. (1970).
- Dubin, S. B., J. H. Lunacek, and G. B. Benedek, *Proc. Nat. Acad. Sci. U.S.* 57, 1164 (1967).
- Dubois, M., and P. Berge, *Phys. Rev. Letters* 26, 121 (1971).
- Dubois, M., P. Berge, and C. Laj, *Chem. Phys. Letters* 6, 227 (1970).
- Dunlop, Peter J., B. J. Steel, and J. E. Lane in *Physical Methods of Chemistry Part IV: Determination of Mass, Transport, and Electrical Magnetic Properties*, Arnold Weissberger and Bryant W. Rossiter (eds), *Techniques of Chemistry, Vol. I* (Interscience, New York, 1972) , pp. 205-349.
- Edwards, R. V., J. C. Angus, M. J. French, and J. W. Dunning, Jr., *J. Appl. Phys.* 42, 837 (1971).
- Einstein, A., *Ann. Physik* 33, 1275 (1910).
- Espejo, R., and E. S. Canelo, *Virology* 34, 738 (1968).
- Espejo, R., E. Canelo, and R. L. Sinsheimer, *Proc. Nat. Acad. Sci. U.S.* 63, 1164 (1969).
- Fabelinskii, I. L., *Molecular Scattering of Light* (Plenum Press, New York, 1968).
- Foord, R., E. Jakeman, C. J. Oliver, E. R. Pike, R. J. Blagrove, E. Wood, and A. R. Peacocke, *Nature* 227, 242 (1970).
- Foord, R., R. Jones, C. J. Oliver, and E. R. Pike, *Appl. Opt.* 8, 1975 (1969).
- Ford, N. C., and G. B. Benedek, *Phys. Rev. Letters* 15, 649 (1965).
- Fujime, S., *J. Phys. Soc. Jap.* 29, 416 (1970a).
- Ibid.*, 29, 751 (1970b).

- Fujime, S., and S. Ishiwata, J. Mol. Biol. 62, 251 (1971).
- Fujime, S., and M. Maruyama, Macromolecules 6, 237 (1973).
- Fujime, S., M. Maruyama, and S. Asakura, J. Mol. Biol. 68, 347 (1972).
- Gray, H. B., Jr., and J. E. Hearst, J. Mol. Biol. 35, 111 (1968).
- Gulari, E., Ph.D. thesis, C.I.T. (1973).
- Gulari, E., R. J. Brown, and C. J. Pings, AIChE J. 19, 1196 (1973).
- Harris, R. A., and J. E. Hearst, J. Chem. Phys. 44, 2595 (1966).
- Heller, W., Rec. Chem. Prog. 20, 209 (1959).
- Huang, W.-N., and J. E. Frederick, Macromolecules 7, 34 (1974).
- Hudson, B., W. B. Upholt, J. Deviny, and J. Vinograd, Proc. Nat. Acad. Sci. U.S. 62, 813 (1969).
- Huglin, M. B., Light Scattering from Polymer Solutions (Academic Press, 1972), p. 27.
- Ishiwata, S., and S. Fujime, J. Mol. Biol. 68, 511 (1972).
- Jamieson, A. M., and A. G. Walton, J. Chem. Phys. 58, 1054 (1973).
- Johnson, P., and R. S. Sinsheimer, J. Mol. Biol.    , (1974).
- Johnson, P. A., and A. L. Babb, Chem. Revs. 56, 387 (1956).
- Jolly, D. J., and A. M. Campbell, Biochem. J. 128, 569 (1972a).
- Ibid., 130, 1019 (1972b).
- Jones, R., C. J. Oliver, and E. R. Pike, Appl. Opt. 10, 1673 (1971).
- Kadanoff, L. P., and P. C. Martin, Ann. Phys. N.Y. 24, 419 (1963).
- Krasna, A. I., J. R. Dawson, and J. A. Harpst, Biopolymers 9, 1017 (1970).
- Kratochvil, J. P., and C. Smart, J. Colloid Interface Sci. 20, 875 (1965).
- Landau, L. D., and G. Placzek, Physik Z. Sovjetunion 5, 1972 (1934).
- Lastovka, J. B., and G. B. Benedek, Phys. Rev. Letters 17, 1039 (1966).
- Lemondé, H., Ann. Phys. (Paris) 9, 399 (1938).

- Leontovich, M. A., Statistical Physics, Gostekhizdat (1944).
- Mandel, L., Progr. Opt. 2, 181 (1963).
- Mandel, L., and E. Wolf, Rev. Mod. Phys. 37, 231 (1965).
- Miller, G. A., J. Phys. Chem. 71, 2305 (1967).
- Miller, L., and P. C. Carman, Trans. Farad. Soc. 55, 1831 (1959).
- Mountain, R. D., Revs. Mod. Phys. 38, 205 (1966).
- Mountain, R. D., and J. M. Deutch, J. Chem. Phys. 50, 1103 (1969).
- Oliver, C. J., and E. R. Pike, Phys. Letters 31a, 90 (1970).
- Pecora, R., J. Chem. Phys. 40, 1604 (1964).
- Ibid., 43, 1562 (1965).
- Ibid., 49, 1032 (1968).
- Ibid., 48, 4126 (1968a).
- Ibid., 49, 1036 (1968b).
- Phillips, D. T., P. J. Wyatt, and R. M. Berkman, J. Colloid Interface Sci. 34, 159 (1970).
- Reed, T. F., and J. E. Frederick, Macromolecules 4, 72 (1971).
- Revet, B.M.J., M. Schmir, and J. Vinograd, Nature New Biol. 229, 10 (1971).
- Riedel, L., Chem. Ing.—Techn. 13, 321 (1951).
- Robben, F., Appl. Opt. 10, 776 (1971).
- Rouse, P. E., Jr., J. Chem. Phys. 21, 1272 (1953).
- Saito, N., and S. Ito, J. Phys. Soc. Jap. 25, 1446 (1968).
- Saito, N., K. Takahashi, and Y. Yunoki, J. Phys. Soc. Jap. 22, 219 (1967).
- Schaefer, D. W., and B. J. Berne, Phys. Rev. Lett. 28, 475 (1972).
- Schmid, C. W., F. P. Rinehart, J. E. Hearst, Biopolymers 10, 883 (1971).
- Schmidt, R. L., Biopolymers 12, 1427 (1973).

- Searby, G. M., Ph.D. thesis, Oxford (1971).
- Shaw, R., J. Chem. Eng. Data 14, 461 (1969).
- Soda, K., J. Phys. Soc. Jap. 35, 866 (1973).
- Touloukian, Y. S., P. E. Liley, and S. C. Saxena, Thermophysical Properties of Matter 3, Y. S. Touloukian and C. Y. Ho (eds), The TPRC Data Series (IFI/Plenum, New York, 1970).
- Touloukian, Y. S., and T. Makita, Thermophysical Properties of Matter 6, Y. S. Touloukian and C. Y. Ho (eds), The TPRC Data Series (IFI/Plenum, New York, 1970).
- Wada, A., N. Suda, T. Tsuda, and K. Soda, J. Chem. Phys. 51, 31 (1969).
- Wang, M. C., and G. E. Uhlenbeck, Rev. Mod. Phys. 17, 323 (1945).
- Wims, A. M., and M. E. Myers, Jr., J. Colloid Interface Sci. 39, 447 (1972).
- Yeh, Y., Appl. Opt. 8, 1254 (1969).
- Young, A. T., Appl. Opt. 8, 2431 (1969).
- Zimm, B. H., J. Chem. Phys. 24, 269 (1956).
- Zimm, B. H., R. S. Stein, and P. Doty, Polymer Bull. 1, 90 (1945).

TABLES

Table 1

$R_0$  Values for Pure Liquids, Liquid Mixtures, and  
Macromolecular Solutions

<u>System</u>	<u><math>R_0 \times 10^6 \text{ cm}^{-1} (\lambda=4358\text{\AA})</math></u>	<u><math>R_0/X^*</math> <math>\text{sec-cm}^{-3}</math></u>
Carbon disulfide	151-240 (Fabelinskii 1968)	0.180
Toluene	32.2-60 (ibid)	0.053
Benzene	28-55.1 (ibid)	0.042
Carbon tetrachloride	12.5-15.40 (ibid)	0.019
Acetone	14.80 (ibid)	0.017
Methanol	11.4 (ibid)	0.010
Acetone (10% mole)/ Carbon Disulfide	400 (Berge et al. 1970)	0.360
$\lambda$ DNA @ $18.1\mu\text{g}/\text{cm}^3$	220 (Dawson and Harpst 1971)	$3.6 \times 10^4$
Calf Thymus DNA @ $63\mu\text{g}/\text{cm}^3$	788 (Krasna et al. 1970)	$9.4 \times 10^4$
T7 DNA @ $19.5\mu\text{g}/\text{cm}^3$	320 (ibid)	$5.5 \times 10^4$

---

\* X denotes either  $\chi$  or  $D_{AB}$ ; values of  $R_0/X$  are approximate.

Table 2

Mass Diffusivity Measurements for Liquid Mixtures

System	$\frac{ n_1 - n_2 }{\lambda_0 = 5461 \text{ \AA}}, 25^\circ\text{C}$	$D_{AB} \times 10^5, \text{ cm}^2/\text{s}$
carbon disulfide/acetone (10% vol)	0.2727	0.30 (Are'fev et al. 1967)
n-propanol/bromoform 1M	0.2141	0.70 $\pm$ 0.09 (ibid)
2M		0.94 $\pm$ 0.08
3M		1.098 $\pm$ 0.120
4M		1.10 $\pm$ 0.125
benzene/acetone (10% wt)	0.1439	Values not available (Dubois and Berge 1971)
benzene/chloroform (10% wt)	0.0574	Values not available (ibid)
carbon disulfide/acetone (8% wt)	0.2727	Values not available (ibid)
diethyl diethylene glycol/ carbon disulfide (single concentration study)		1.85 $\pm$ 0.15 (Dubois et al. 1970) 1.55 $\pm$ 0.4 (by NMR) (Deville & Landesman in private communication to Dubois)
acetone (10% vol)/carbon disulfide (single concentration; single angle)	0.2727	2.32 (Berge et al. 1970)

Table 2 (continued)

n-propanol/carbon disulfide (seven concentrations at single angle)	0.2461		(Jamieson & Walton 1973)
n-propanol/nitrobenzene (six concentrations at single angle)	0.1719		(ibid)
acetone (10% vol)/carbon disulfide (single angle)	0.2727	0.92	(ibid)
n-hexane/carbon disulfide (dilute solution; single concentration)	0.2571		(ibid)
n-hexane/nitrobenzene (dilute solution; single concentration)	0.1829		(ibid)

	carbon disulfide	nitrobenzene	
MeOH	0.304	0.2282	
EtOH	0.2686	0.1954	
n-PrOH	0.2461	0.1719	(ibid)
n-BuOH	0.2320	0.1578	
t-BuOH	0.2441	0.1699	
1-Pentanol	-	-	
1-Octanol	0.2008	0.2266	

(all single concentration measurements)

Table 3

Previous Liquid Thermal Diffusivity Measurements by Quasi-Elastic Light Scattering

System	$I_E/I_E(\text{benzene})$	$\chi \times 10^3 \text{ cm}^2/\text{s}$	$T^\circ\text{C}$	Bulk value $\times 10^3 \text{ cm}^2/\text{s}$ 20°C
toluene	0.923	$0.879 \pm 0.025$ (Lastovka and Benedek 1966)	20°C	0.922 (Touloukian, vols. 3&6, 1970)
benzene	1.00	$0.655 \pm 0.070$ (Berge and Dubois 1969)	room temperature	0.963 (ibid)
carbon disulfide	1.32	1.1 (Berge et al 1970)	room temperature	1.29 (Bridgman 1923; Shaw 1969)
acetone (10% vol)/ carbon disulfide	$\approx 1.32$	1.2 (ibid)		—

Table 4  
Intensity of Scattering from Entropy Fluctuations<sup>†</sup>

	$\rho$	$n$	$c_p \times 10^{-7}$ erg/deg	$dn/dT \times 10^5$ deg <sup>-1</sup>	$I_E$	$I_E/I_E(\text{Benz})$
Water	0.997	1.3397	4.18	-11	$2.47 \times 10^{-12}$	.00082
MeOH	0.791	1.338	2.56	-40.5	$6.87 \times 10^{-11}$	.228
EtOH	0.789	1.369	2.39	-41	$7.92 \times 10^{-11}$	.263
Benzene	0.879	1.5220	1.70	-64	$3.01 \times 10^{-10}$	1.00
CS <sub>2</sub>	1.262	1.67377	1.0	-81.5	$3.97 \times 10^{-10}$	1.32
Toluene	0.865	1.5130	1.68	-61	$2.78 \times 10^{-10}$	.923
Acetone	0.791	1.3677	2.21	-50	$1.27 \times 10^{-10}$	.422
Chloroform	1.489	1.4582	0.966	-61	$2.61 \times 10^{-10}$	.867
CCl <sub>4</sub>	1.595	1.4720	0.841	-56	$2.40 \times 10^{-10}$	.797

<sup>†</sup>Values taken from Fabelinskii, 1968

20°C;  $\lambda = 4358\text{\AA}$  ;

$$I_E = \left(\frac{\partial \epsilon}{\partial T}\right)^2 kT^2 / \rho c_p$$

$$= 4n^2 \left(\frac{\partial n}{\partial T}\right)^2 kT^2 / \rho c_p$$

Table 5

$(\frac{\partial \epsilon}{\partial C})_{P,T}$  and Refractive Index Differences for Binary Mixtures

System	$ n_1 - n_2 $ 25°C, $\lambda_0 = 5461\text{Å}$	$ A(\partial \epsilon / \partial C)_{P,T} ^*$
carbon disulfide/ acetone	0.2727	0.571
methanol/benzene	0.1736	0.364
acetone/benzene	0.1439	0.294
ethanol/benzene	0.1408	0.292
n-hexane/benzene	0.1283	0.271
nitromethane/benzene	0.1202	0.243
methanol/butanol	0.0704	0.154
toluene/bromobenzene	0.0636	0.143
toluene/benzene	0.0040	0.026

Source for n and  $\rho$  : Huglin 1972.

---

\* A is defined as  $\frac{3}{4\pi} \frac{3}{(\epsilon+2)^2}$ , which is nearly constant.

Table 6

Thermal Diffusivities of Pure Liquids and Binary Mixtures

$$\chi \times 10^3 (\text{cm}^2/\text{s})$$

System (pure liquids)	This study	T, °C	Bulk value, 20°C	Other light scattering determinations, 20°C unless otherwise specified
Acetone	0.881 ± 0.033	(18.2)	0.934 (Touloukian, vols. 3 & 6)	
Benzene	0.956 ± 0.040	(19.5)	0.963 ( <i>ibid.</i> )	0.655 ± 0.070* (Berge and Dubois, 1969) 0.87 ± 0.1 (Berge, unpublished) 1.03 ± 0.05 (Oliver and Pike, 1970) 0.90 ± 0.02 (Searby, 1971) 0.94 ± 0.05 (Beysens, 1973)
Bromobenzene	0.518 ± 0.025	(20.0)	0.749 (Riedel, 1951; Shaw, 1969)	
Carbon disulfide	1.10 ± 0.04	(19.3)	1.29 (Bridgman, 1923; Shaw, 1969)	1.1* (Berge et al., 1970)
Carbon tetrachloride	0.719 ± 0.016	(20.0)	0.771 (Touloukian, vols. 3 & 6)	0.84 ± 0.05 (Oliver and Pike, 1970)
Ethanol†	0.839 ± 0.046	(19.8)	0.889 ( <i>ibid.</i> )	
N-hexane	0.740 ± 0.033	(20.0)	0.837 ( <i>ibid.</i> )	
Methanol†	1.16 ± 0.10	(18.2)	1.035 ( <i>ibid.</i> )	
Toluene	0.849 ± 0.039	(19.0)	0.922 ( <i>ibid.</i> )	0.879 ± 0.025 (Lastovka and Benedek, 1966) 0.98 ± 0.05 (Oliver and Pike, 1970)
(binary mixtures)				
Toluene-bromobenzene				
12.5% toluene	0.649 ± 0.025	(19.9)		
62.5%	0.688 ± 0.039	(19.9)		
Toluene-benzene				
30.0% toluene	0.869 ± 0.040	(20.0)		
50.0%	0.815 ± 0.035	(20.0)		
70.0%	0.772 ± 0.030	(20.0)		
90.0%	0.847 ± 0.035	(20.0)		

† Single data were collected for methanol and ethanol.

\* Room temperature.

Table 7

Values for the Scattering Parameter  $\sqrt{x}$  for Circular  $\phi$ X174 RF DNA

$K^2 \times 10^{10} (\text{cm}^{-2})$	x	$\sqrt{x}$
2	3.57	1.89
4	7.14	2.67
6	10.71	3.27
8	14.28	3.78
9	16.10	4.01

Table 8

Values for the Scattering Parameter  $\sqrt{x}$  for Circular PM2 DNA

$K^2 \times 10^{10} (\text{cm}^{-2})$	x	$\sqrt{x}$
2	6.10	2.47
4	12.20	3.49
6	18.30	4.28
8	24.40	4.94
9	27.45	5.24

Table 9

Lower Bound Values on  $\tau_1$  for  $\phi$ X174 RF DNA

$\theta$	$\Delta\tau(\mu\text{s})$	$\tau_{\text{eff}}(\text{msec})$	$\tau_1(\text{msec})$
120	5	0.308	0.76
110	5	0.344	0.85
100	5	0.385	0.95
90	5	0.454	1.12
80	5	0.508	1.23
70	5	0.605	1.45

Table 10

Lower Bound Values on  $\tau_1$  for PM2 I DNA

$\theta$	$\Delta\tau(\mu\text{s})$	$\tau_{\text{eff}}(\text{msec})$	$\tau_1(\text{msec})$
120	2	0.189	0.43
110	2	0.214	0.49
100	2	0.243	0.55
90	2	0.290	0.66
80	2	0.354	0.81
70	5	0.661	1.62
60	10	0.940	2.34

Table III.1  
Comparison of Light Sources and Photomultipliers  
Used in Light Scattering

	Mercury Lamp		He-Ne Laser	Argon-Ion Laser
$\lambda$ (Å)	4358	5461	6328	4880
Power output (w)	500		0.005	1.0
Directional intensity (w-sr <sup>-1</sup> )	1	1	$2 \times 10^4$	$4 \times 10^6$
Wavelength dependence of scatter $\left  \frac{4880}{\lambda} \right ^4$	1.571	0.639	0.353	1.000
Quantum efficiency of optimum photocathode (%)	23 EMI9635B (K-C <sub>s</sub> )	14 EMI9558B S-20	8 EMI9658R extended S-20	17 EMI9634QR "super"S-11
Typical gain of PMT	$6.7 \times 10^6$	$1.3 \times 10^7$	$6.7 \times 10^6$	$5.5 \times 10^7$
Typical dark current (nA)	7.5	20	20	75
Available power in commercial products	800 w		50 mw	5 w

FIGURES

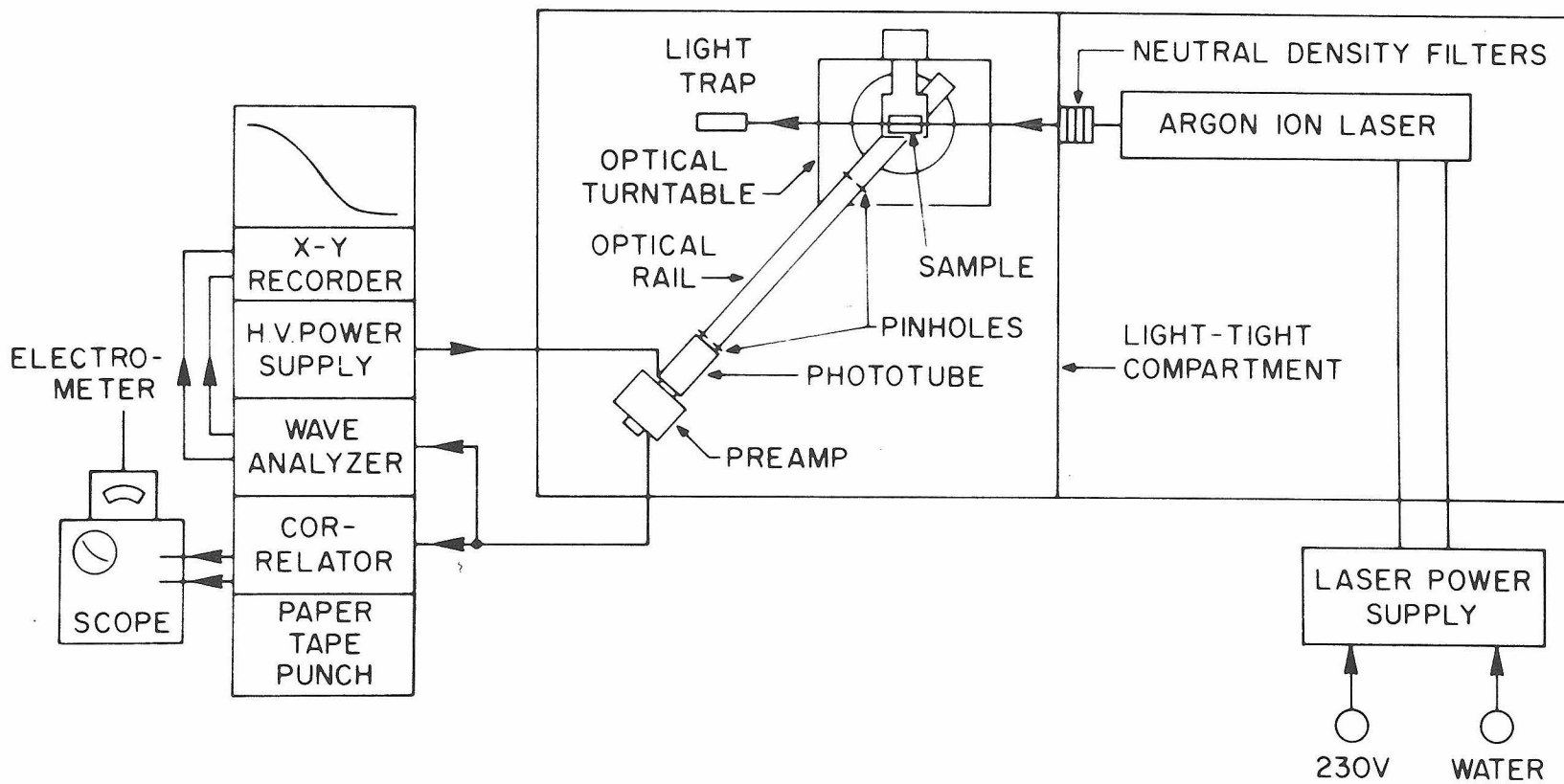


Fig. 1. A schematic drawing of the light scattering spectrometer used in this study.

METHANOL-BENZENE MASS DIFFUSIVITY

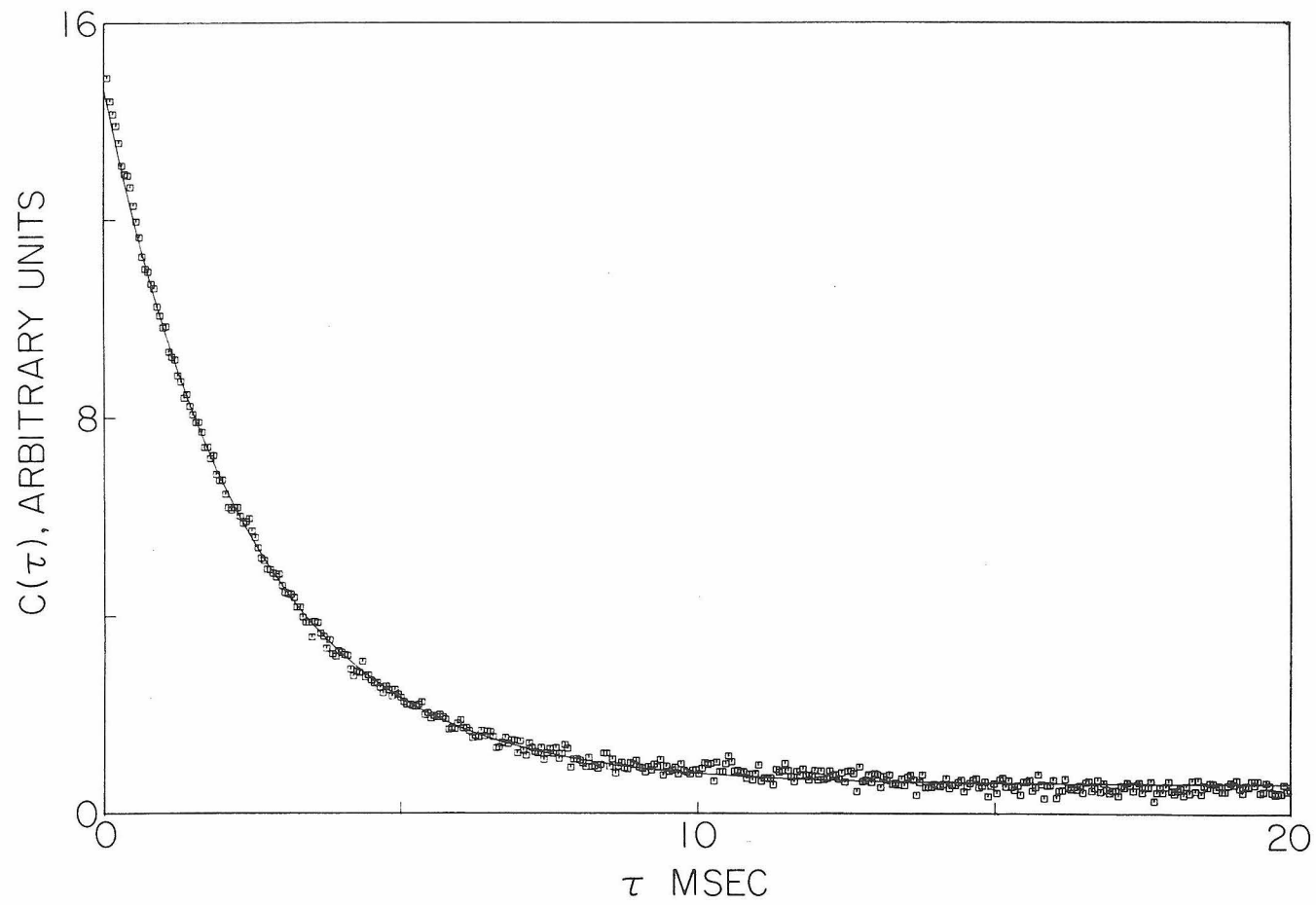


Fig. 2a. A typical correlogram for mass diffusion in a methanol-benzene mixture

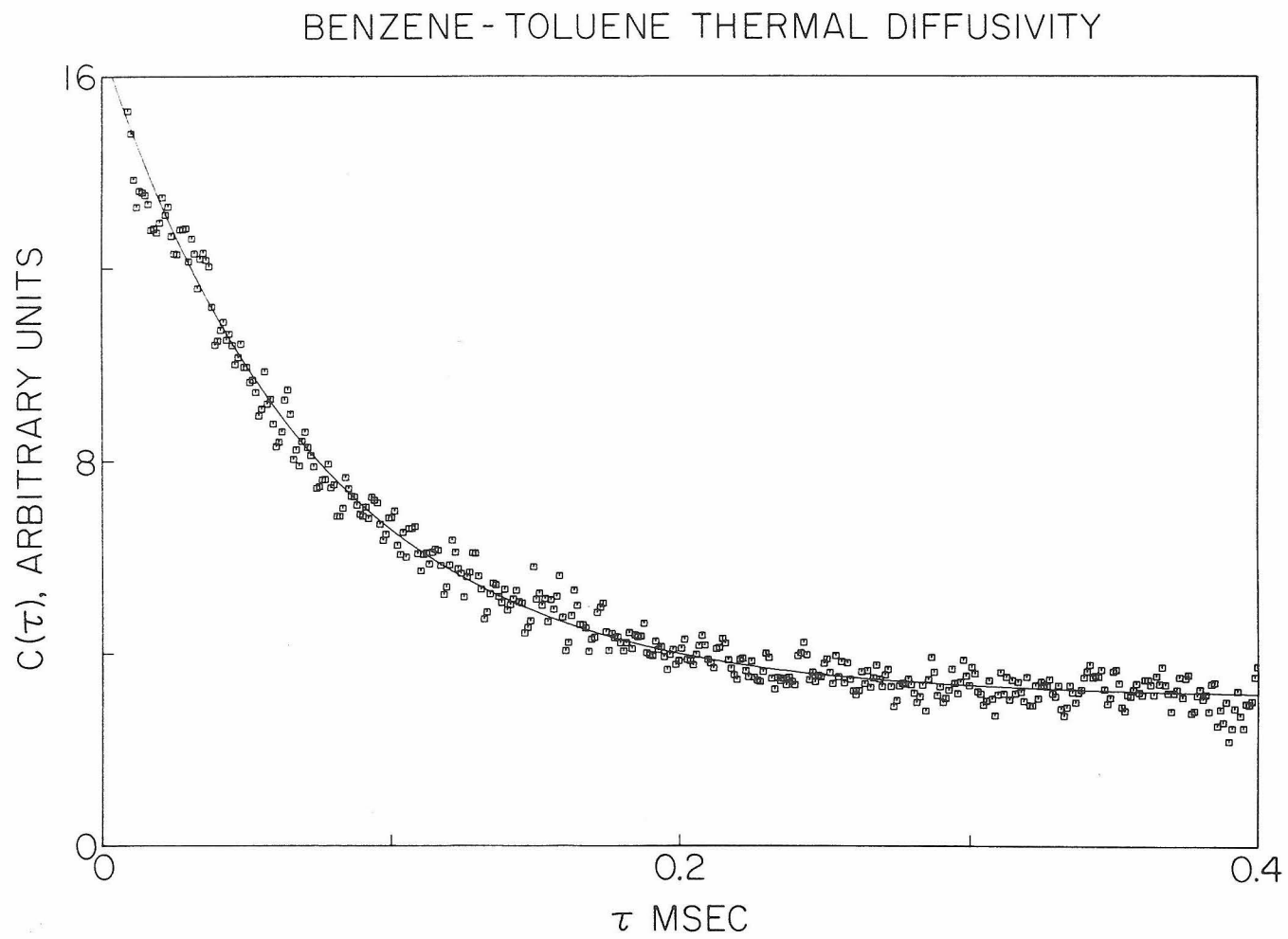


Fig. 2b. A typical correlogram for thermal diffusion in a benzene-toluene mixture

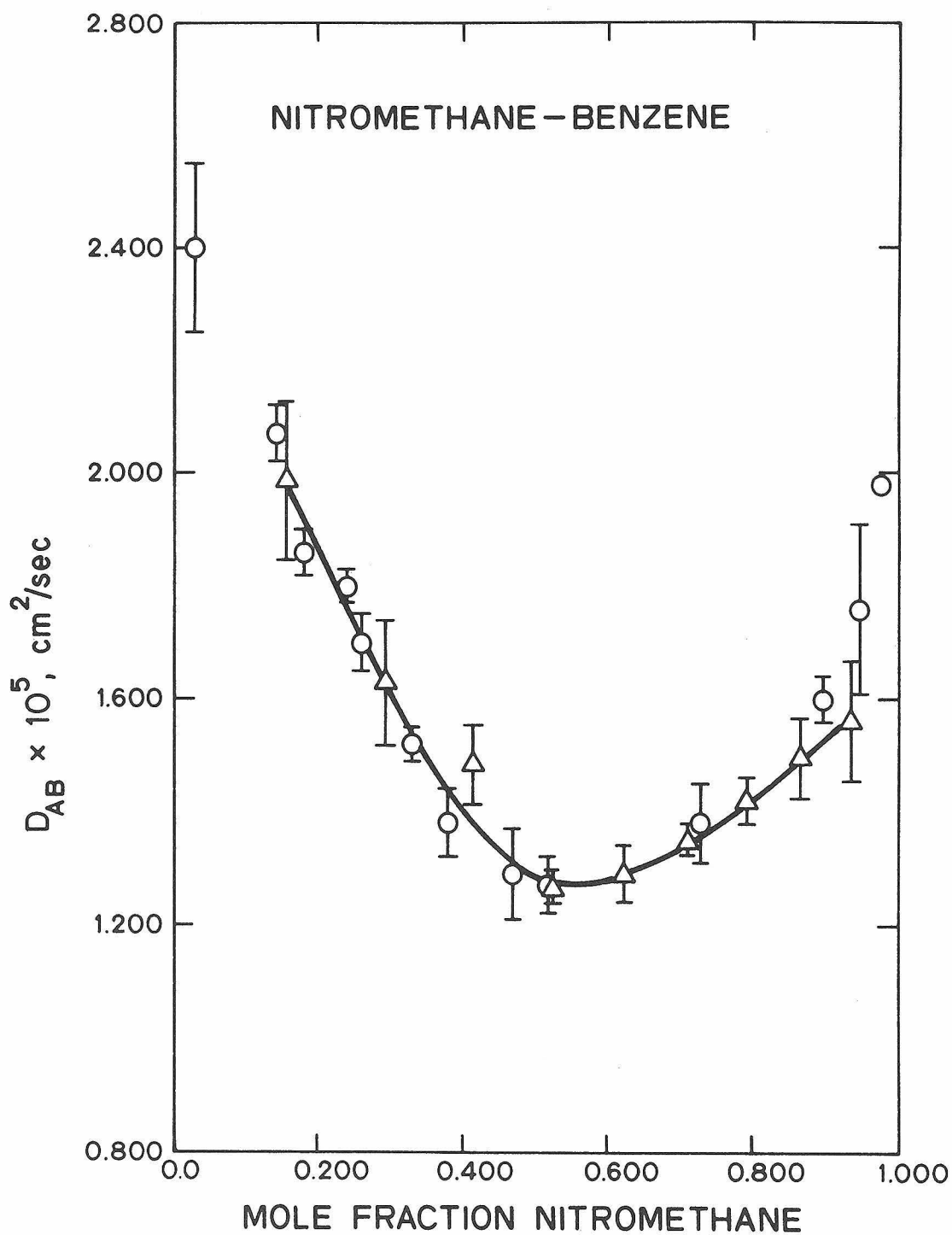


Fig. 3. Mutual diffusion data for the nitromethane-benzene system;  $\Delta$  this work,  $T = 20.0 \pm .2^\circ\text{C}$ ;  $\circ$  Miller and Carman (1959),  $T = 20.0^\circ\text{C}$ .

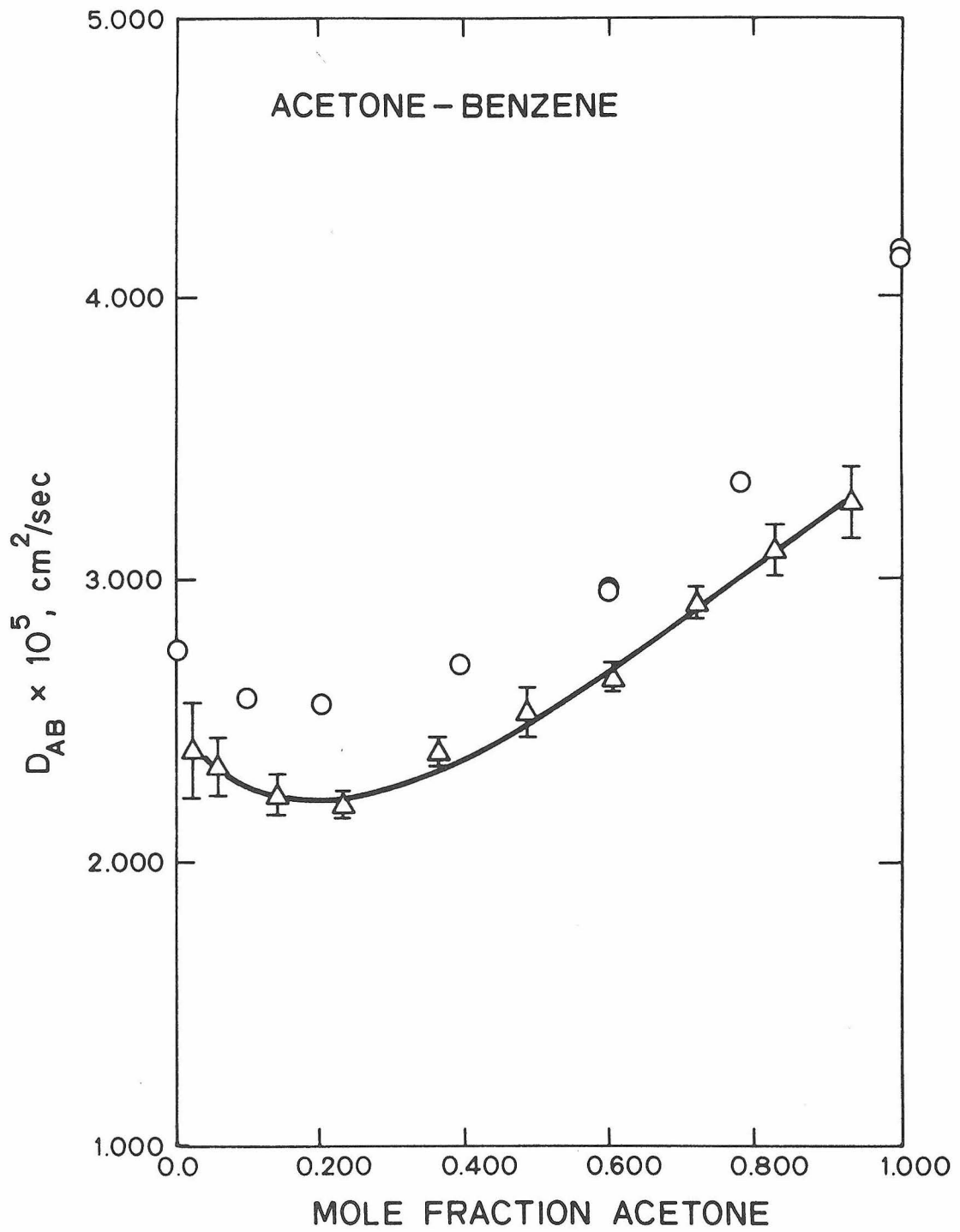


Fig. 4. Mutual diffusion data for the acetone-benzene system;  $\Delta$  this work,  $T = 1.99 \pm 0.2^\circ\text{C}$ ;  $\circ$  Anderson et al (1958),  $T = 25.15^\circ\text{C}$ .

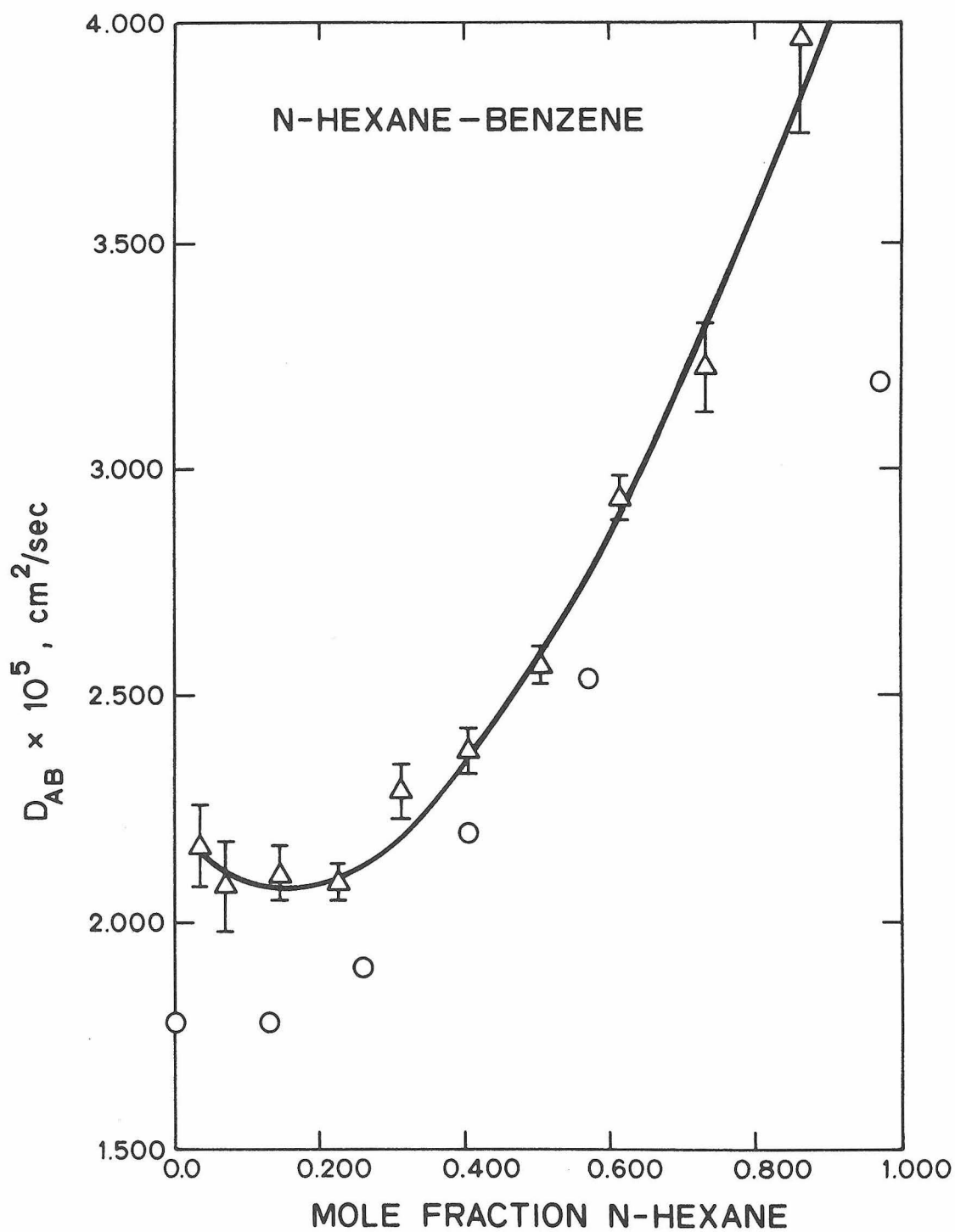


Fig. 5. Mutual diffusion data for the n-hexane-benzene system;  $\Delta$  this work,  $T = 19.9 \pm .2^\circ\text{C}$ ;  $\circ$  Lemonde (1938),  $T = 5^\circ\text{C}$ .

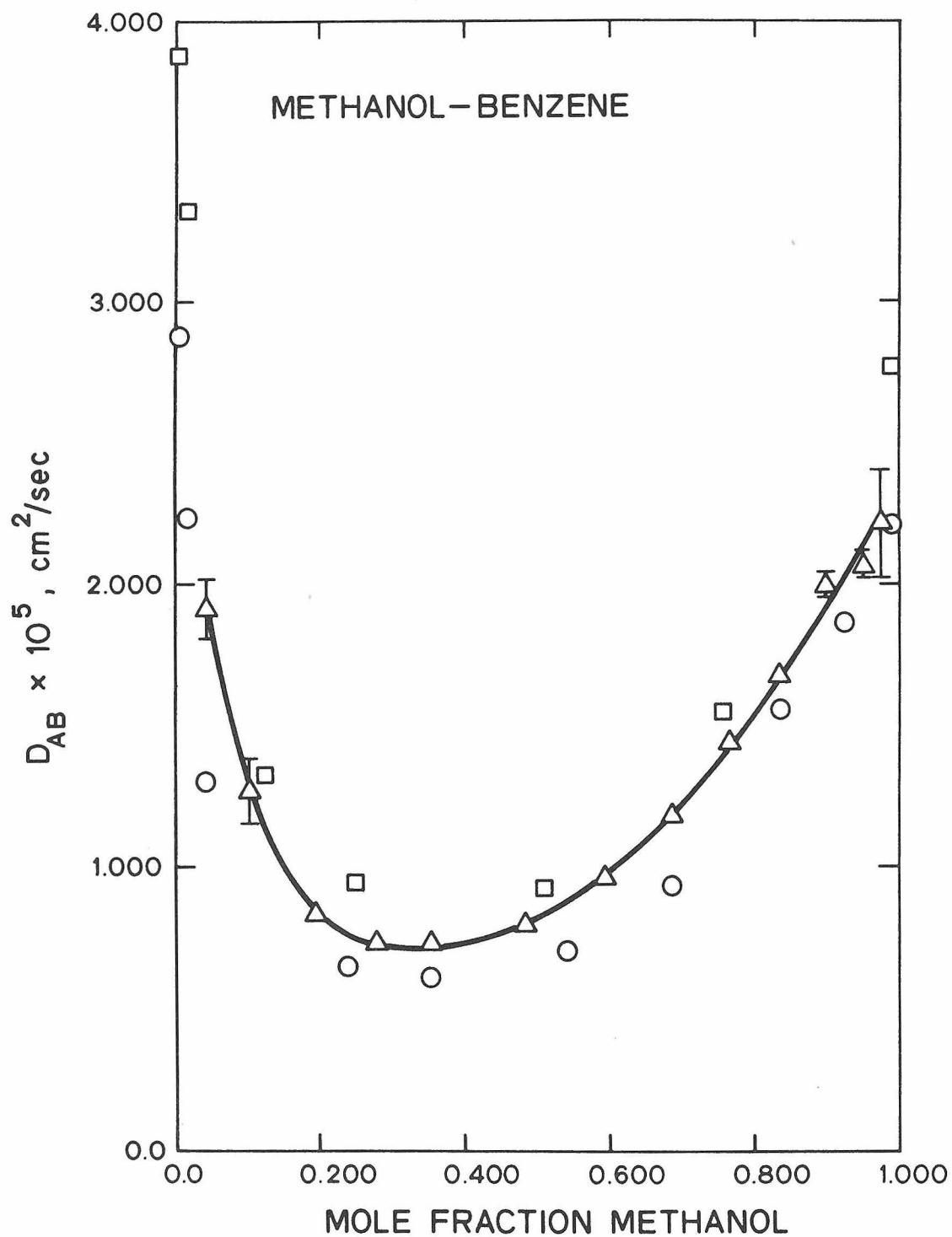


Fig. 6. Mutual diffusion data for the methanol-benzene system;  $\Delta$  this work,  $T = 20.0 \pm 0.2^\circ\text{C}$ ; Caldwell and Babb (1955),  $T = 27.06^\circ\text{C}$ ;  $\circ$  Lemondé (1938),  $T = 11^\circ\text{C}$ .

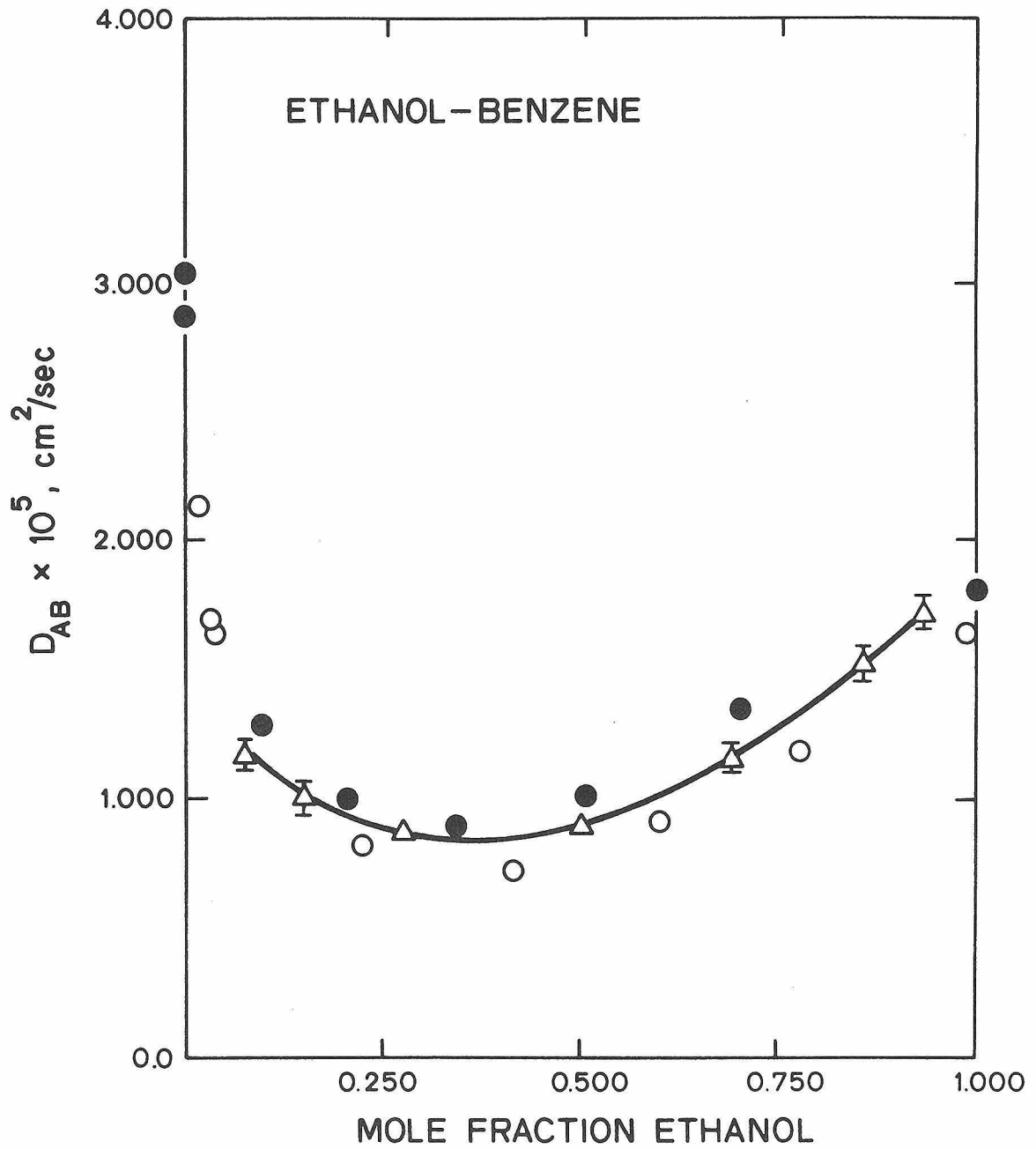


Fig. 7. Mutual diffusion data for the ethanol-benzene system;  $\Delta$  this work,  $T = 18.6 \pm 0.2^\circ\text{C}$ ;  $\circ$  Anderson et al. (1958),  $T = 25.15^\circ\text{C}$ ;  $\circ$  Lemondé (1938),  $T = 15^\circ\text{C}$ .

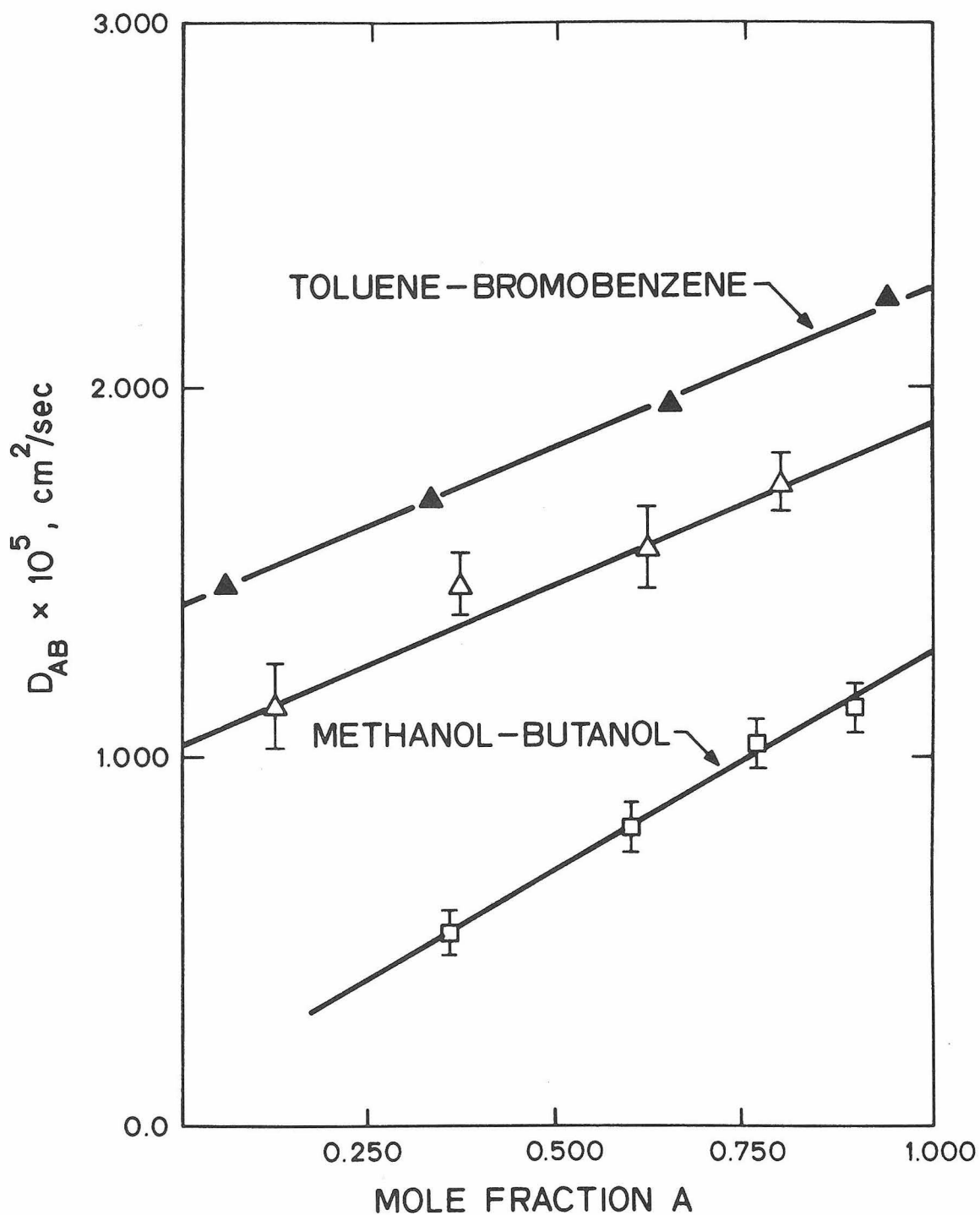


Fig. 8. Mutual diffusion data for the systems toluene-bromobenzene and methanol-butanol. Toluene-bromobenzene:  $\Delta$  this work,  $T = 19.9 \pm .2^\circ\text{C}$ ;  $\blacktriangle$  Burchard and Toor (1962),  $T = 29.6 \pm .03^\circ\text{C}$ . Methanol-butanol:  $\square$  this work,  $T = 19.5 \pm .2^\circ\text{C}$ .

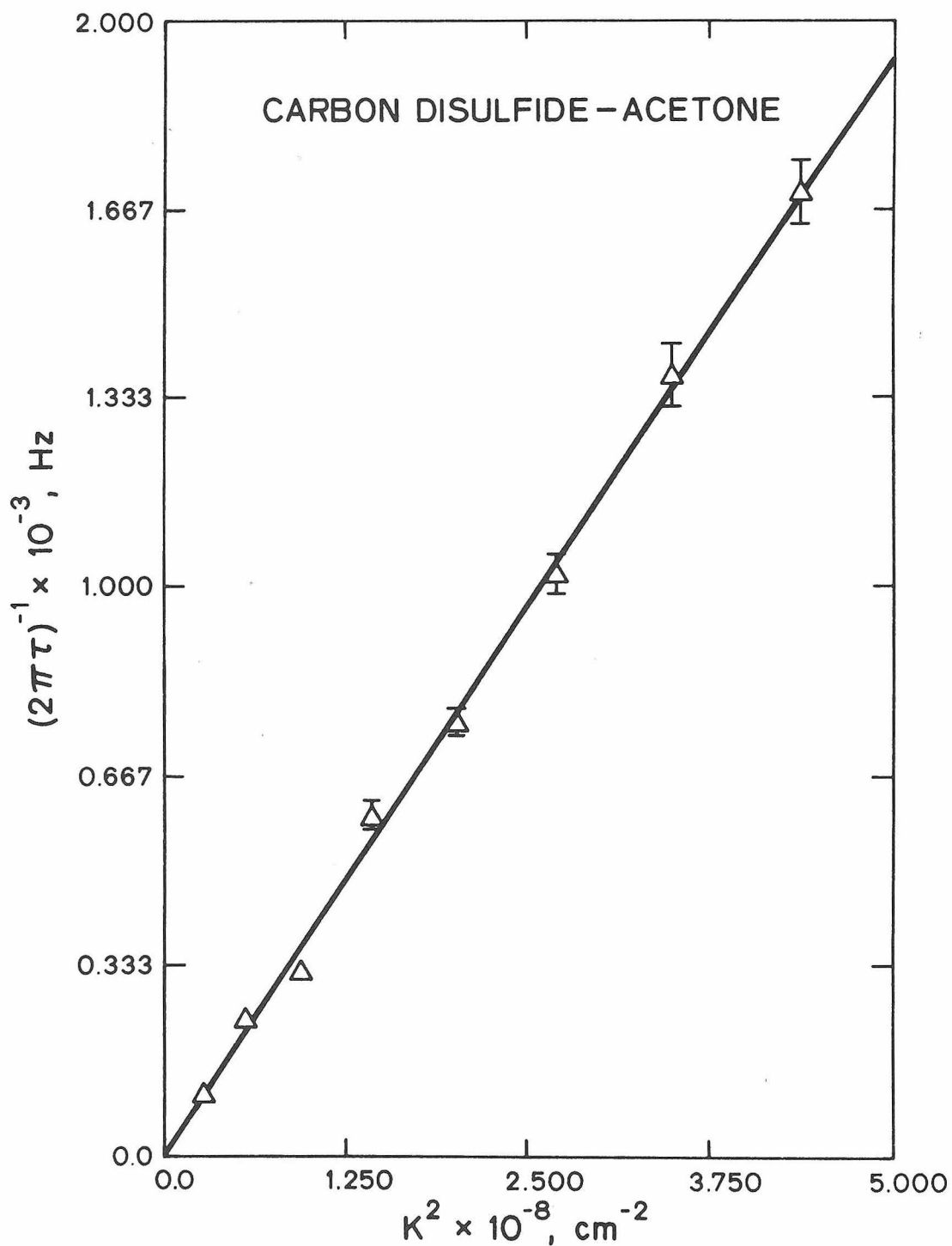


Fig. 9. The inverse decay time  $(2\pi\tau)^{-1}$  vs.  $K^2$  due to concentration fluctuations in a 10% (vol.) acetone-carbon disulfide mixture.  $(2\pi\tau)^{-1}$  for the exponential correlation function corresponds to the Lorentzian halfwidth  $\Gamma$  (in Hz) of the spectrum.

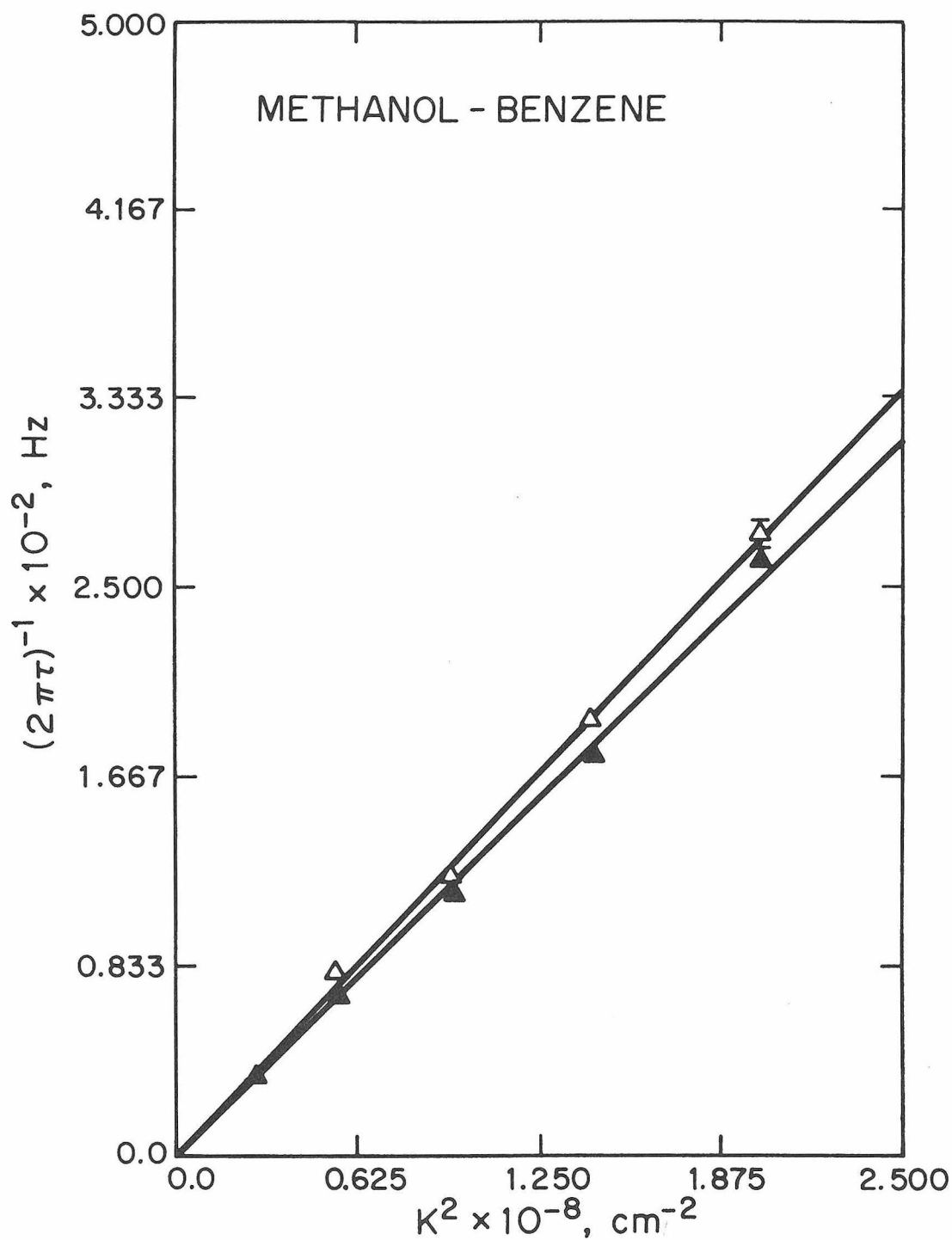


Fig. 10. Inverse decay time vs.  $K^2$  in the methanol-benzene system:  
 $\Delta$  10% (vol.) methanol;  $\blacktriangle$  30% (vol.) methanol.

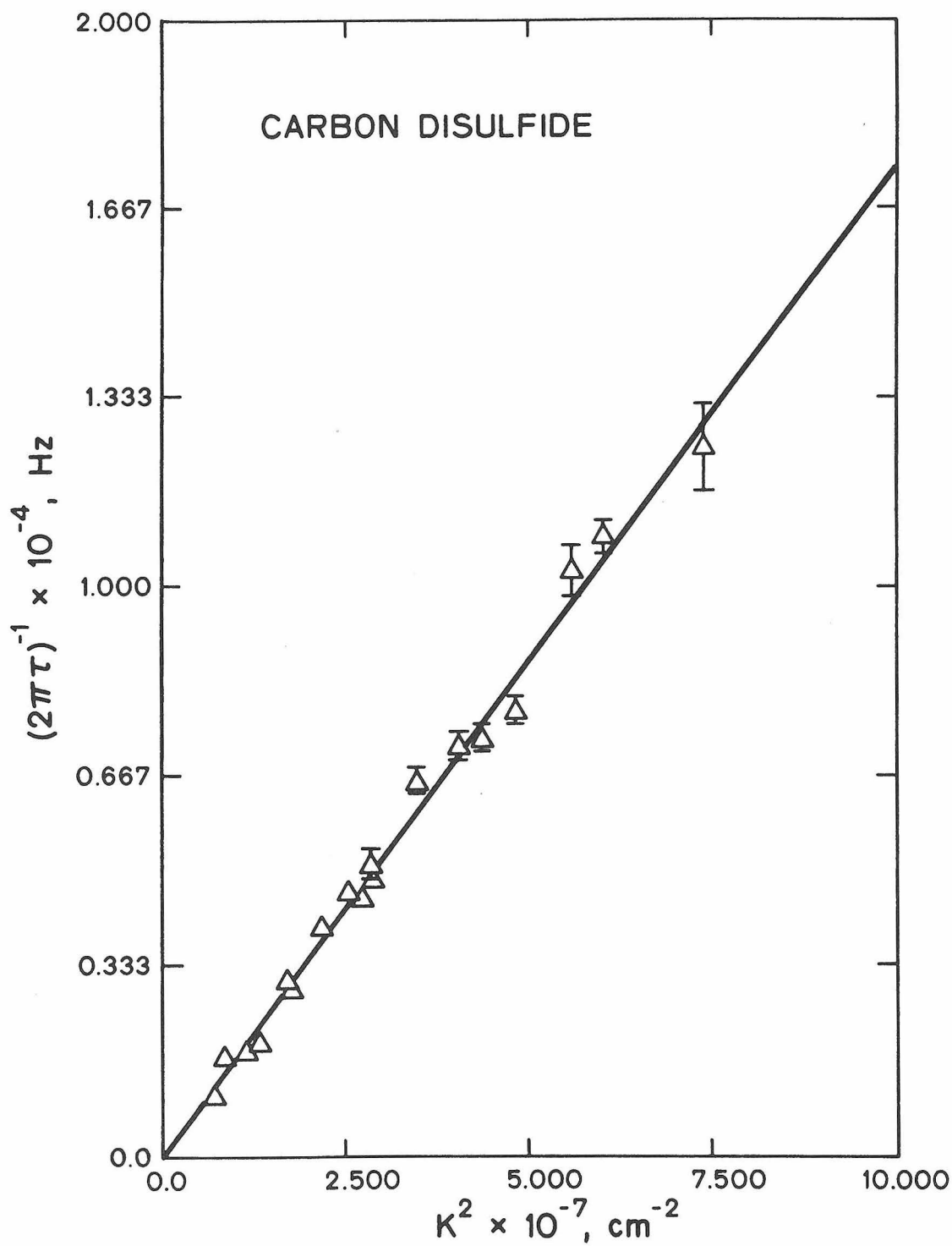


Fig. 11. Inverse decay time vs.  $K^2$  for pure carbon disulfide.

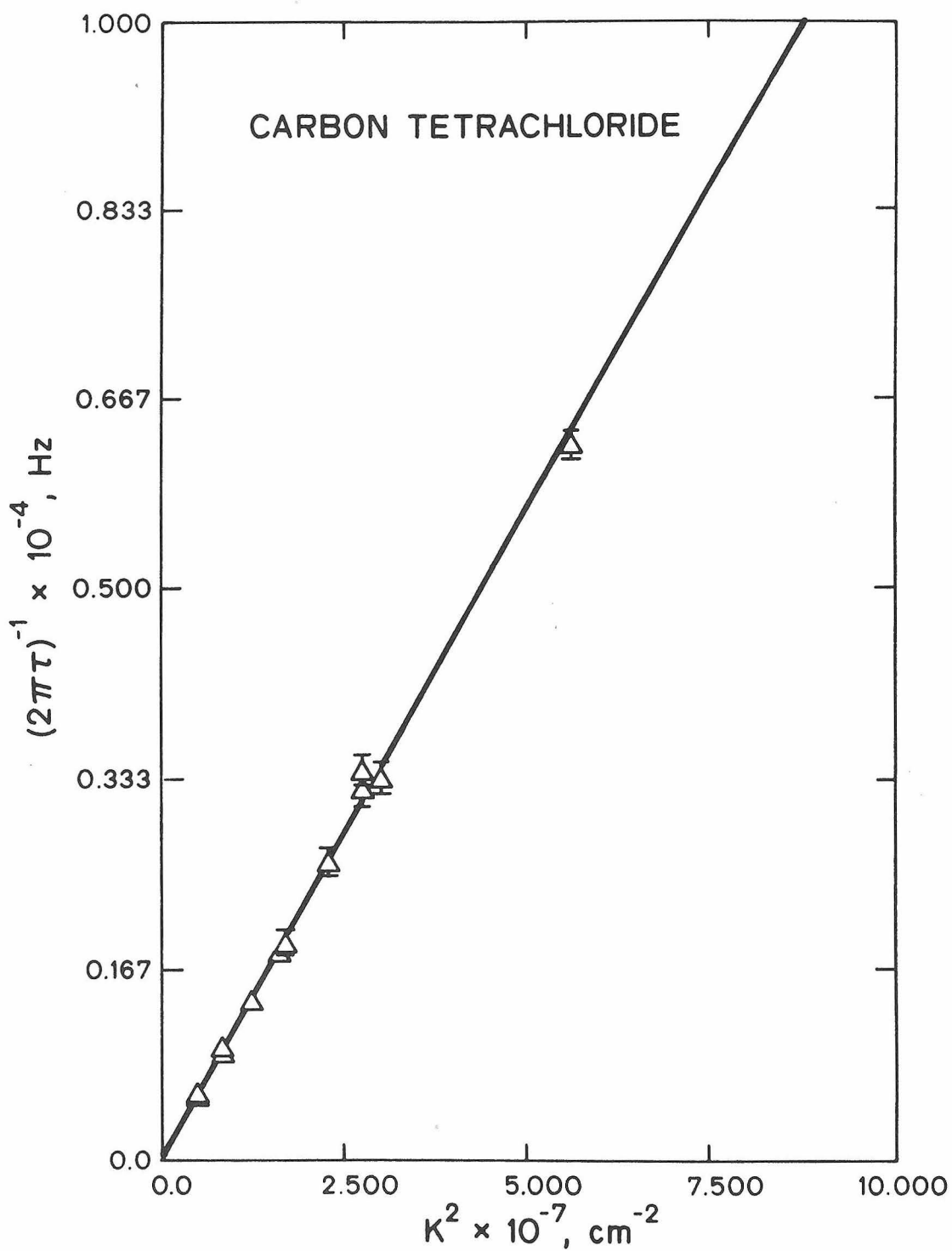


Fig. 12. Inverse decay time vs.  $K^2$  for pure carbon tetrachloride.

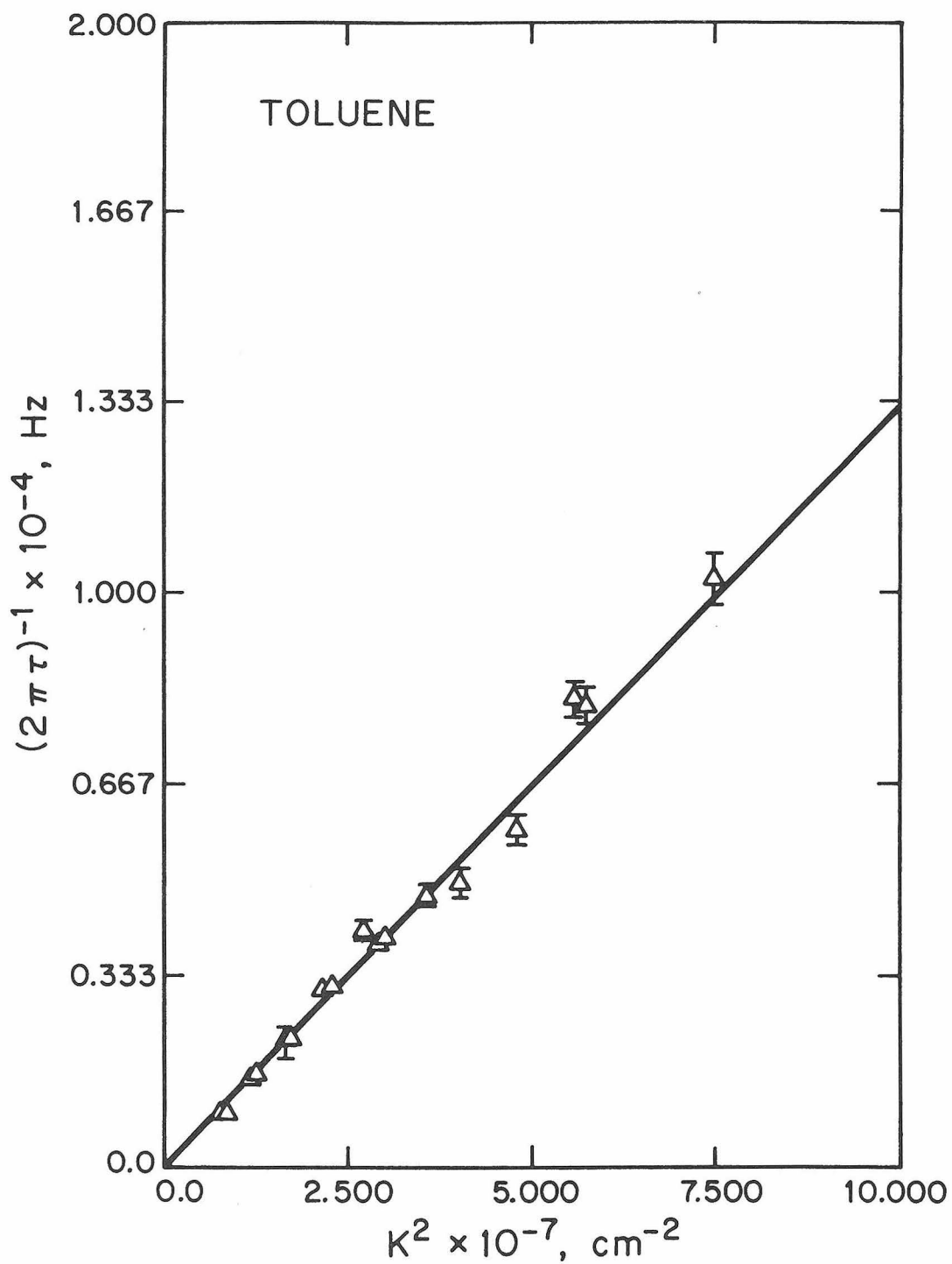


Fig. 13. Inverse decay time vs.  $K^2$  for pure toluene.

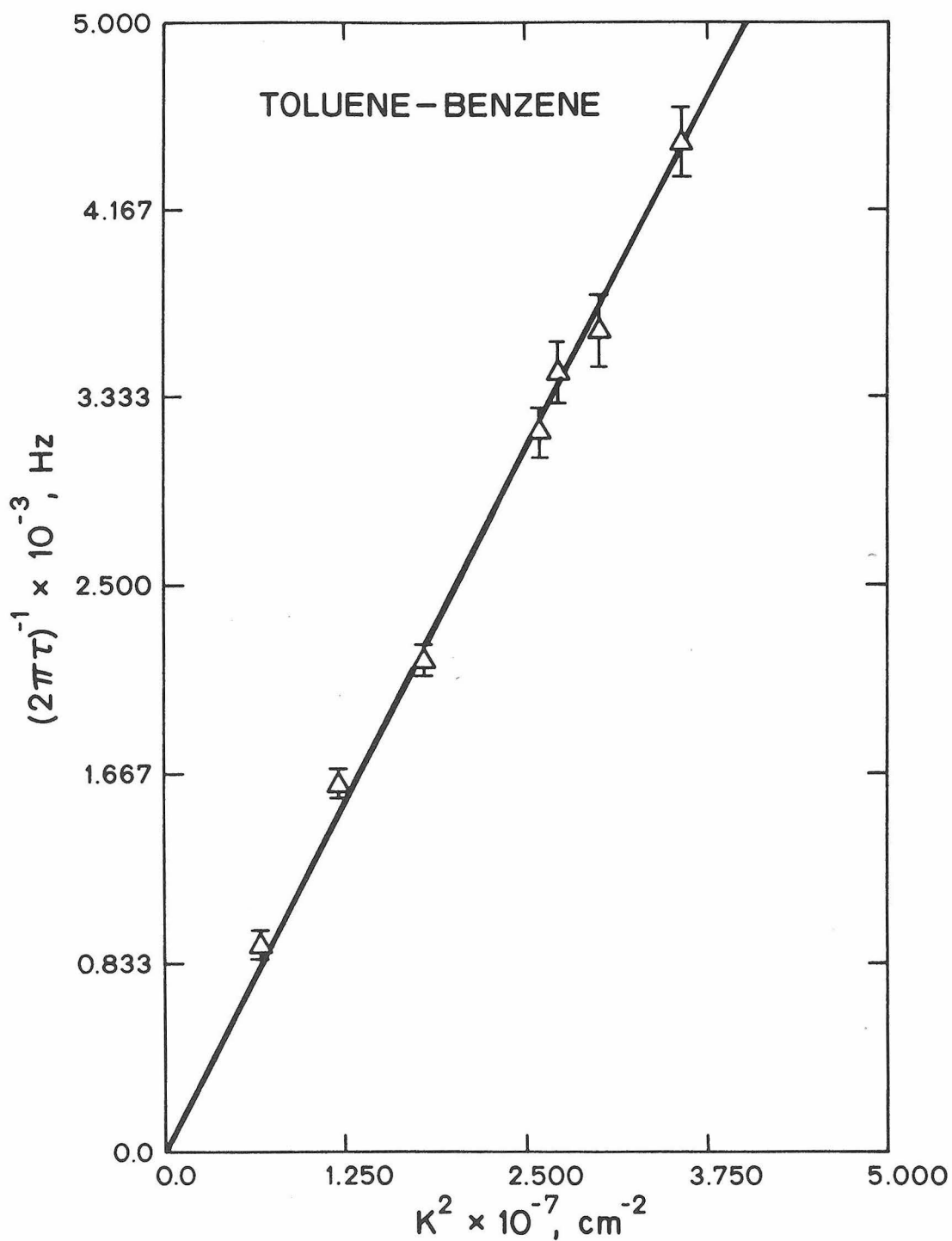


Fig. 14. Inverse decay time vs.  $K^2$  from entropy fluctuations in a toluene-benzene mixture.

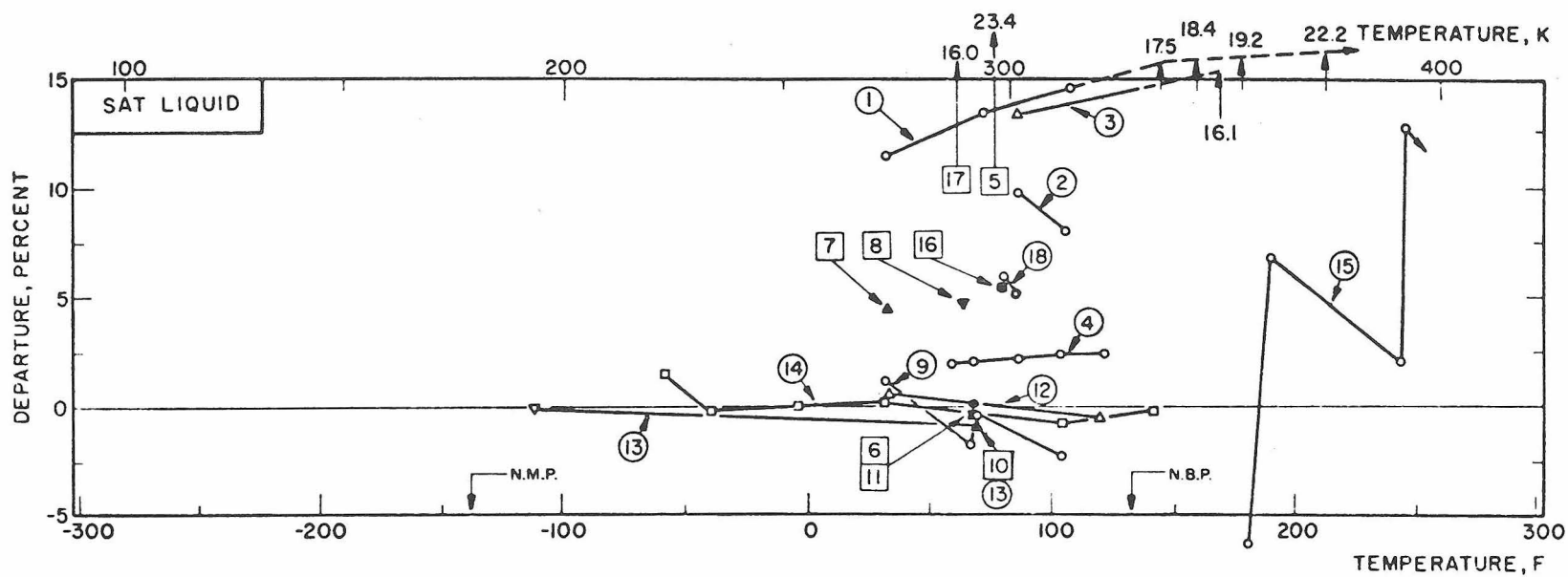


Fig. 15. Departure plot for thermal conductivity of liquid acetone. (From Touloukian, vol. 3, 1970).

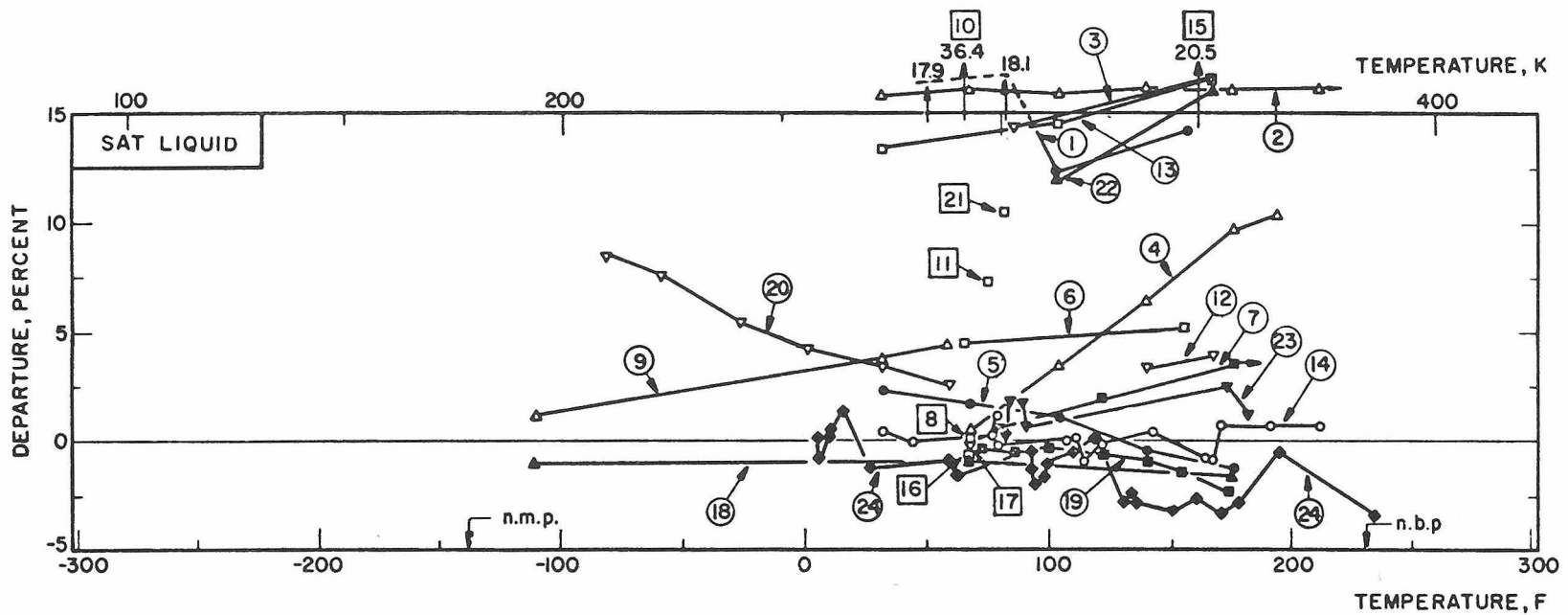


Fig. 16. Departure plot for thermal conductivity of liquid toluene. (From Touloukian, vol. 3, 1970).

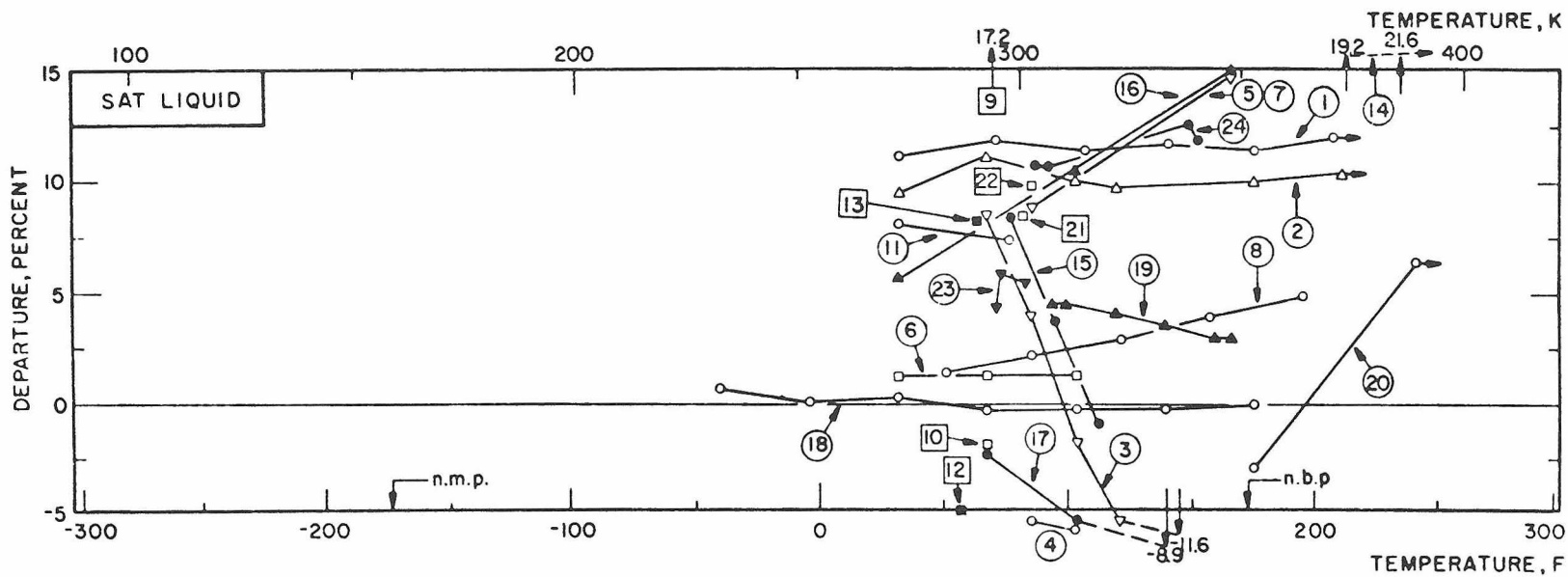


Fig. 17. Departure plot for thermal conductivity of liquid ethyl alcohol. (From Touloukian, vol. 3, 1970).

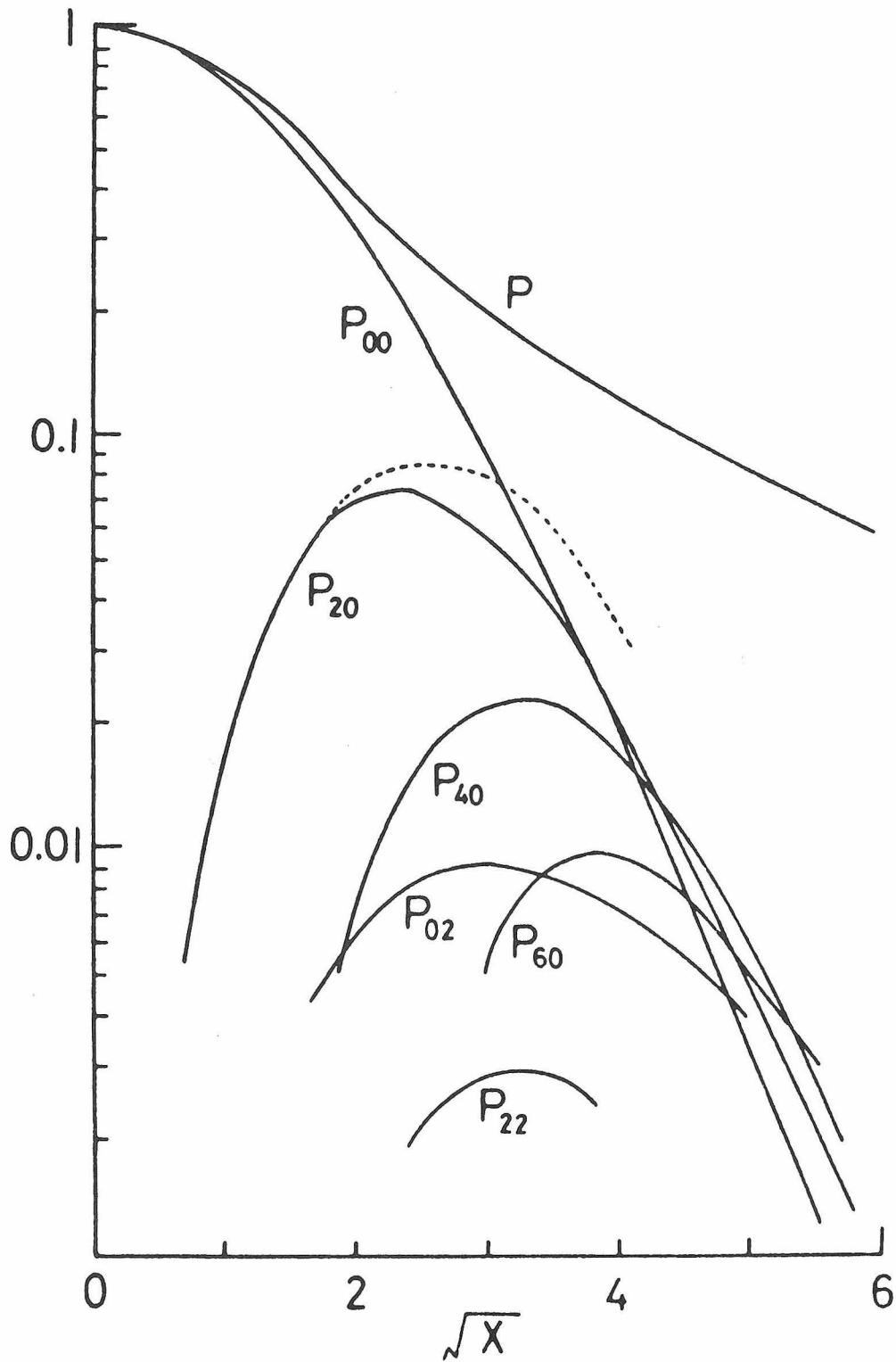


Fig. 18.  $P_{NM}(x)$  vs.  $x^{1/2}$  at  $\gamma L \gg 1$ . -----  $P_{20} + P_{40}$   
(From Fujime and Maruyama 1973).

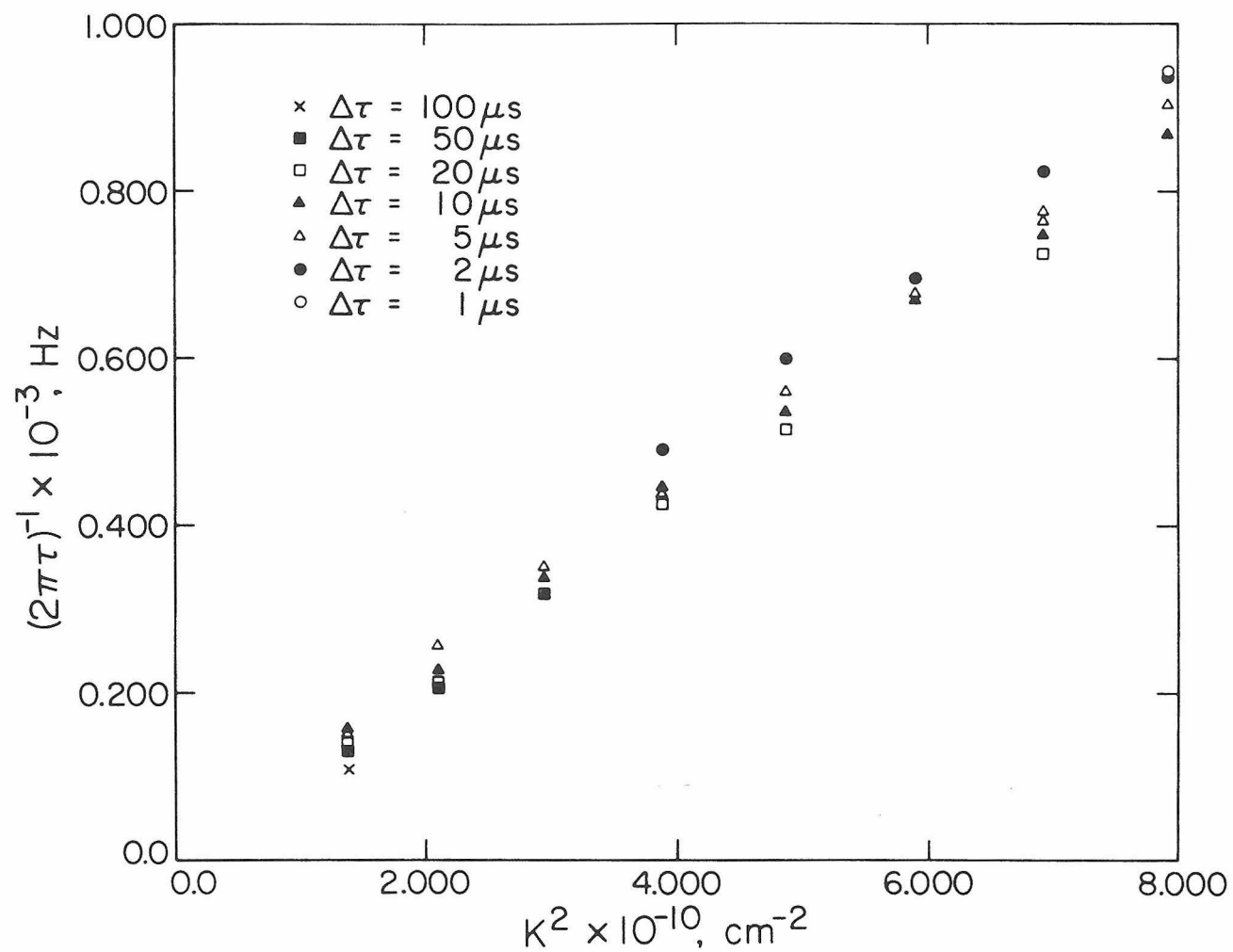


Fig. 19. Inverse decay times versus scattering wave vector squared for a solution of polystyrene latex spheres.  $\tau^{-1}$  is determined by an exponential fit with a variable baseline.

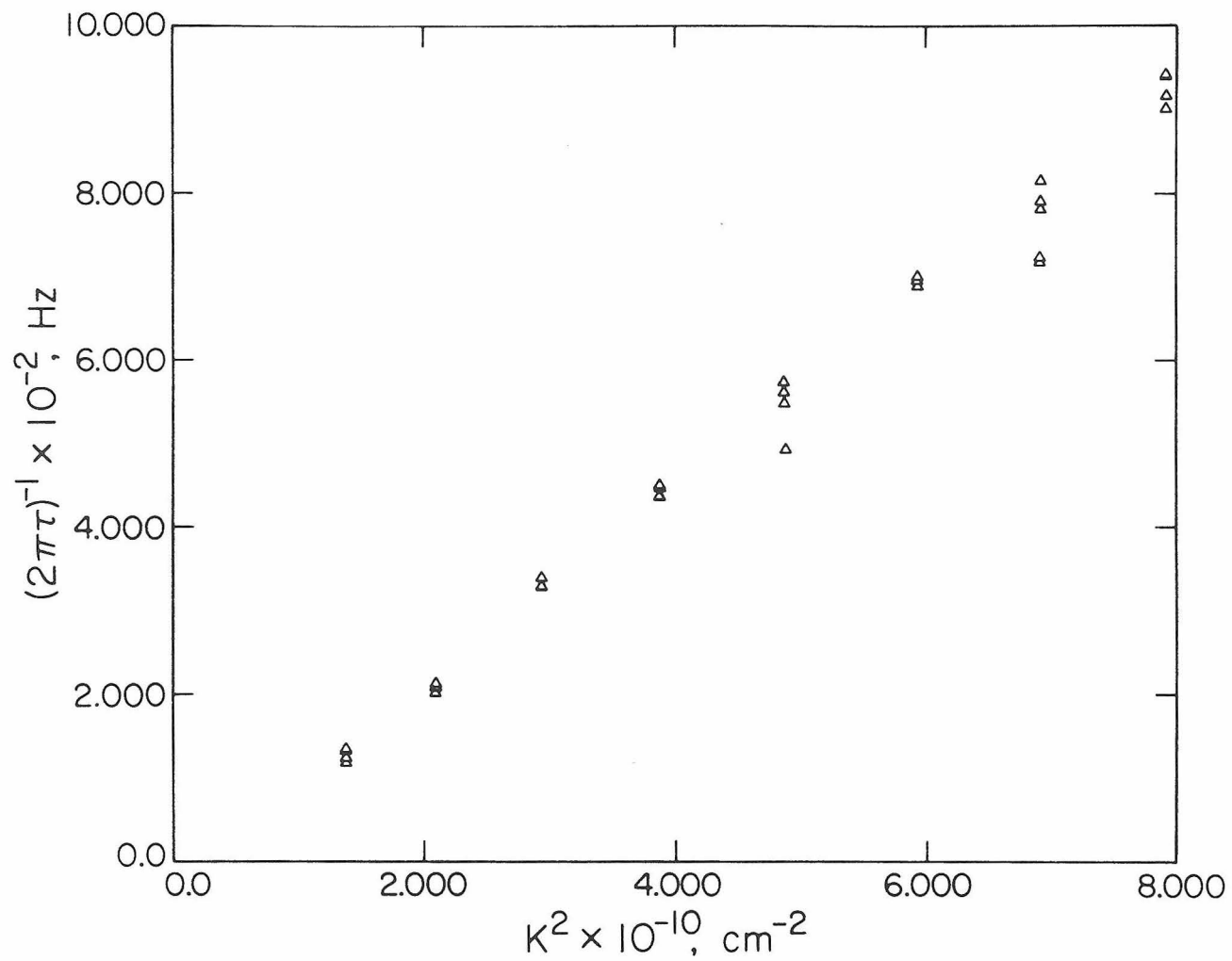


Fig. 20 Inverse decay times versus scattering wave vector squared for the same data as in Figure 19.  $\tau^{-1}$  is determined by an exponential fit with a zero baseline.

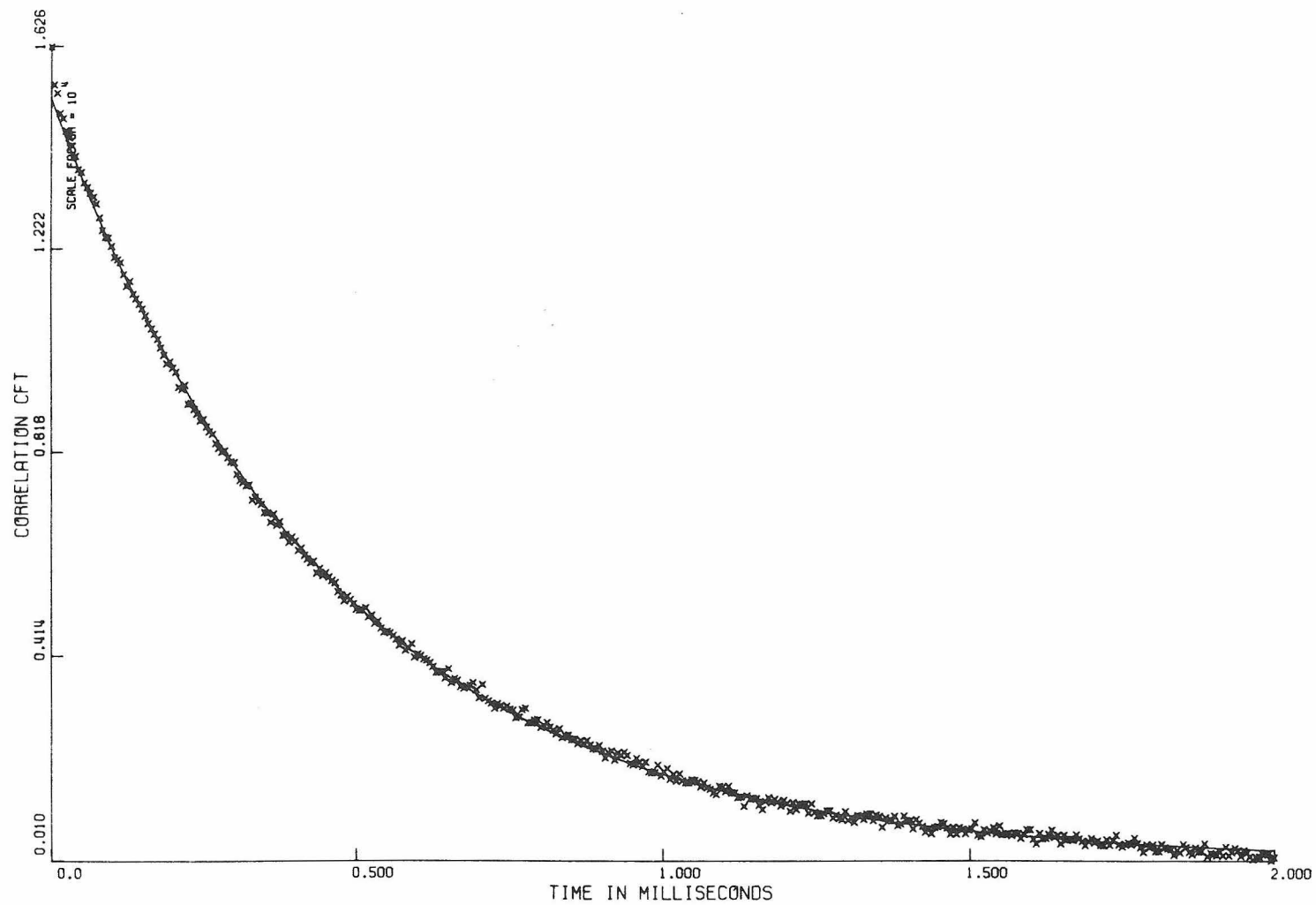


Fig. 21. A typical correlation function collected for a solution of polystyrene latex spheres. The sample time increment is  $5 \mu\text{s}$ . The solid line is a computer fit to the data.

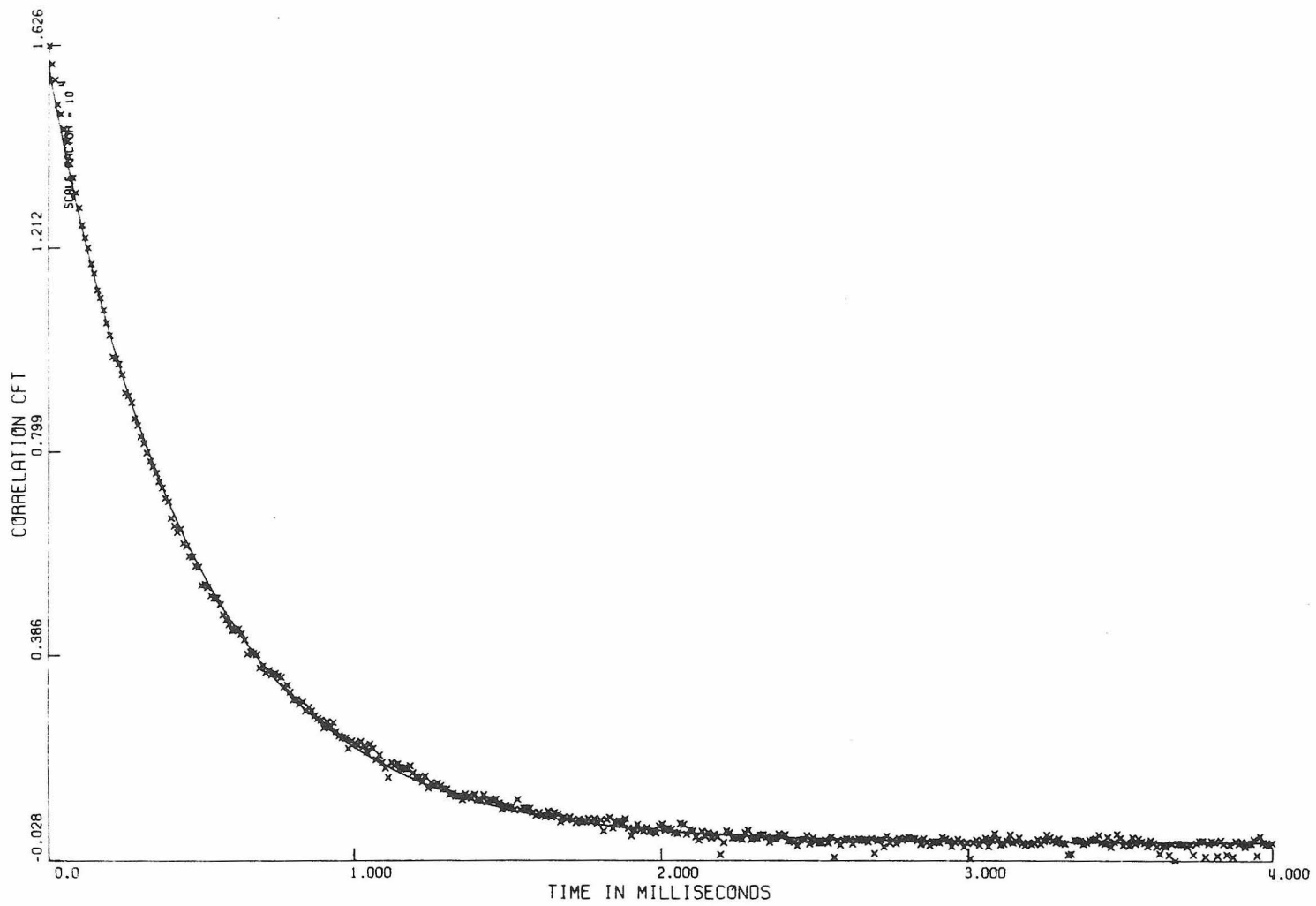


Fig. 22. A typical correlation function collected under conditions identical to those of Figure 21 except that  $\Delta\tau = 10 \mu\text{s}$ .

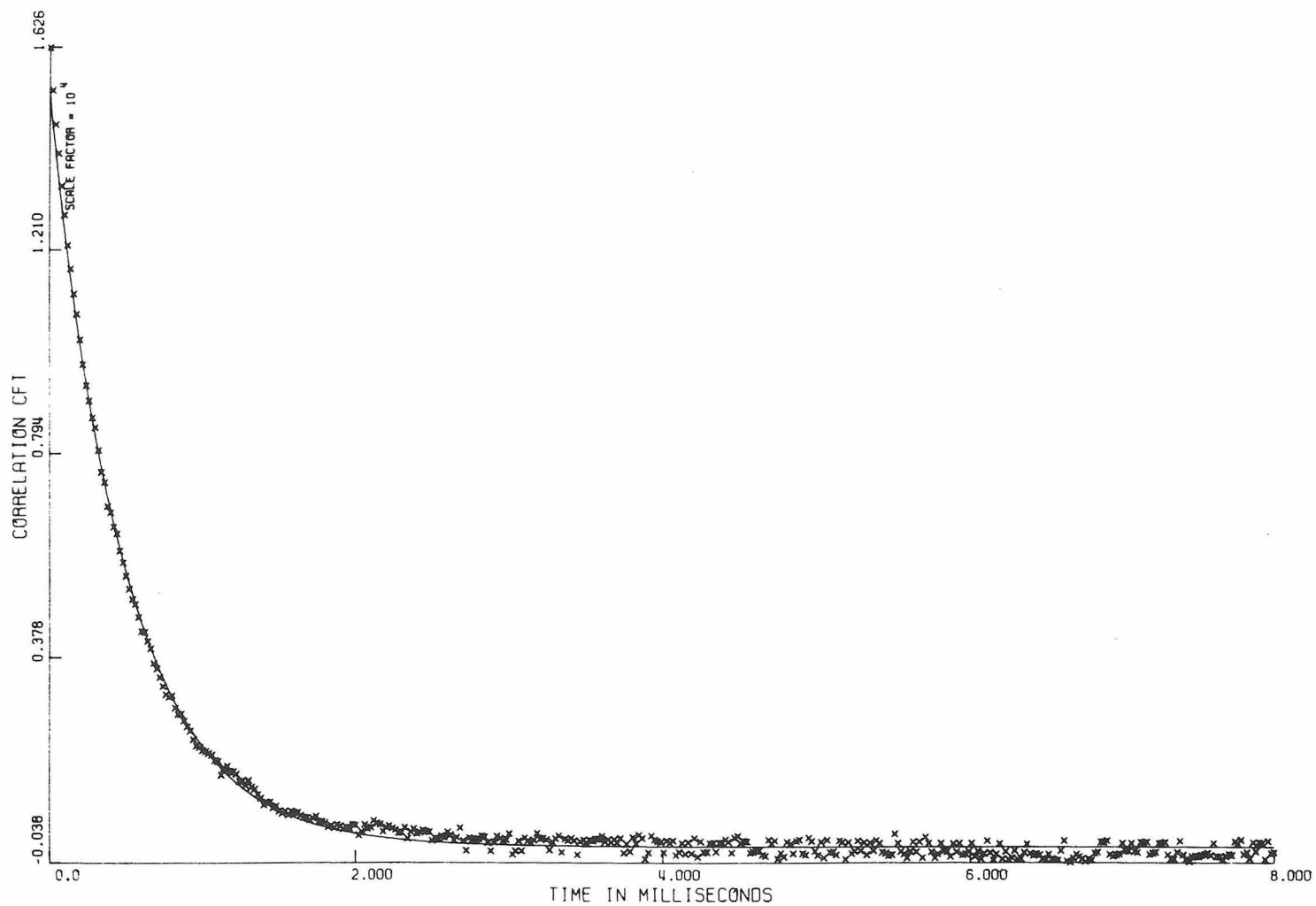


Fig. 23. A typical correlation function collected under conditions identical to those of Figure 21 except that  $\Delta\tau = 20 \mu\text{s}$ .

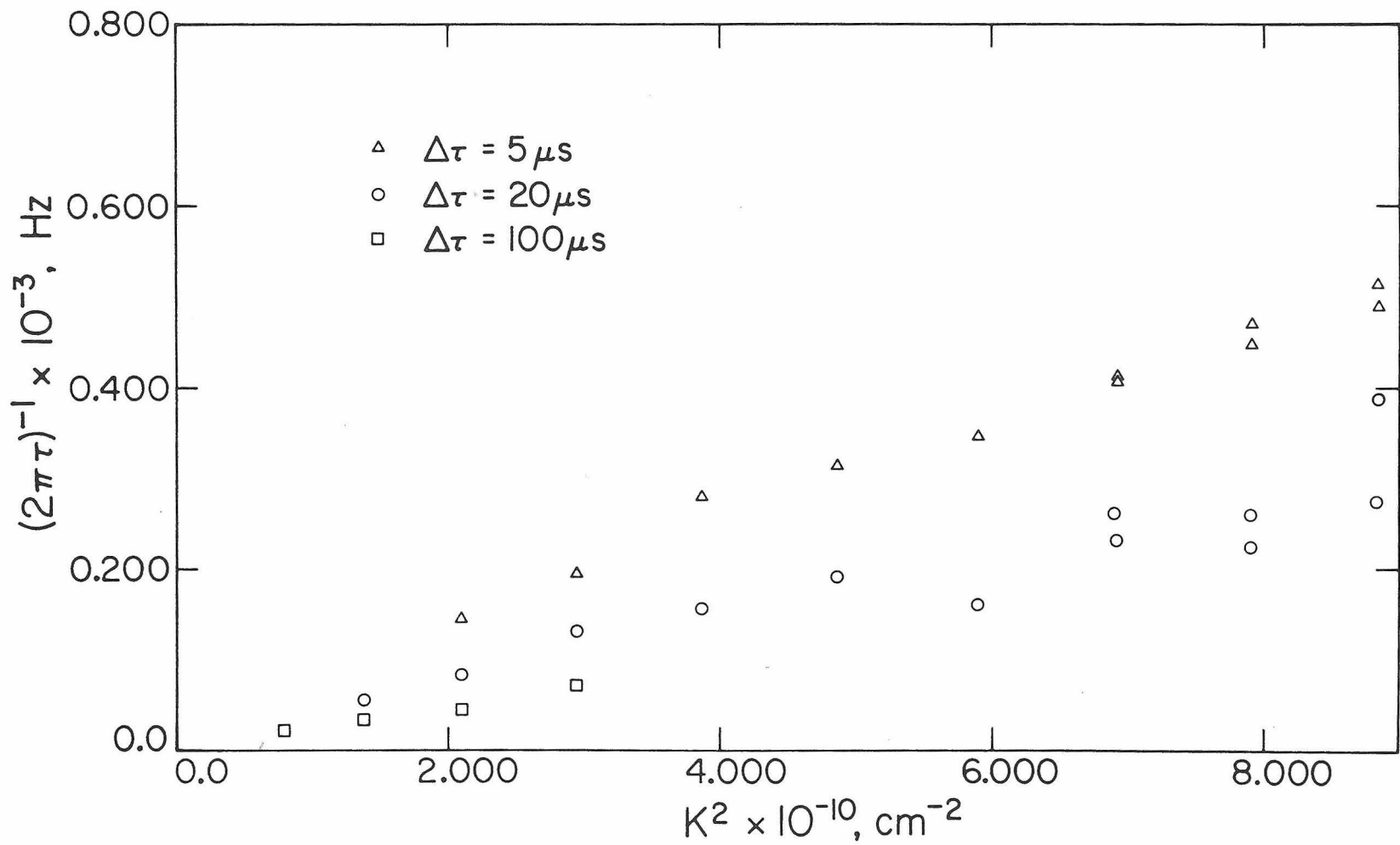


Fig. 24. Inverse decay times versus scattering wave vector squared for a solution of  $\phi$ X174 RF I and II DNA.

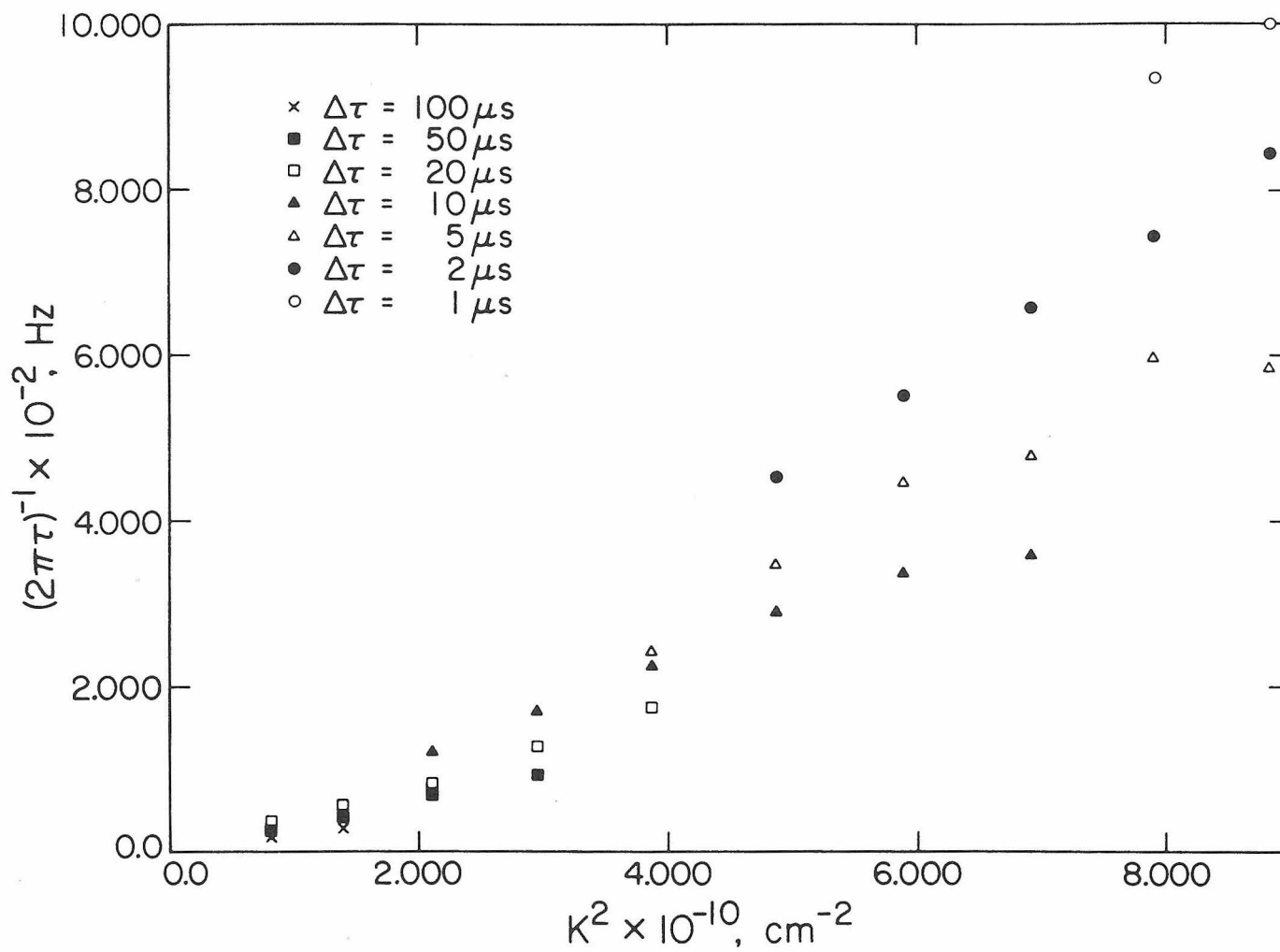


Fig. 25. Inverse decay times versus scattering wave vector squared for a solution of PM2 I DNA.

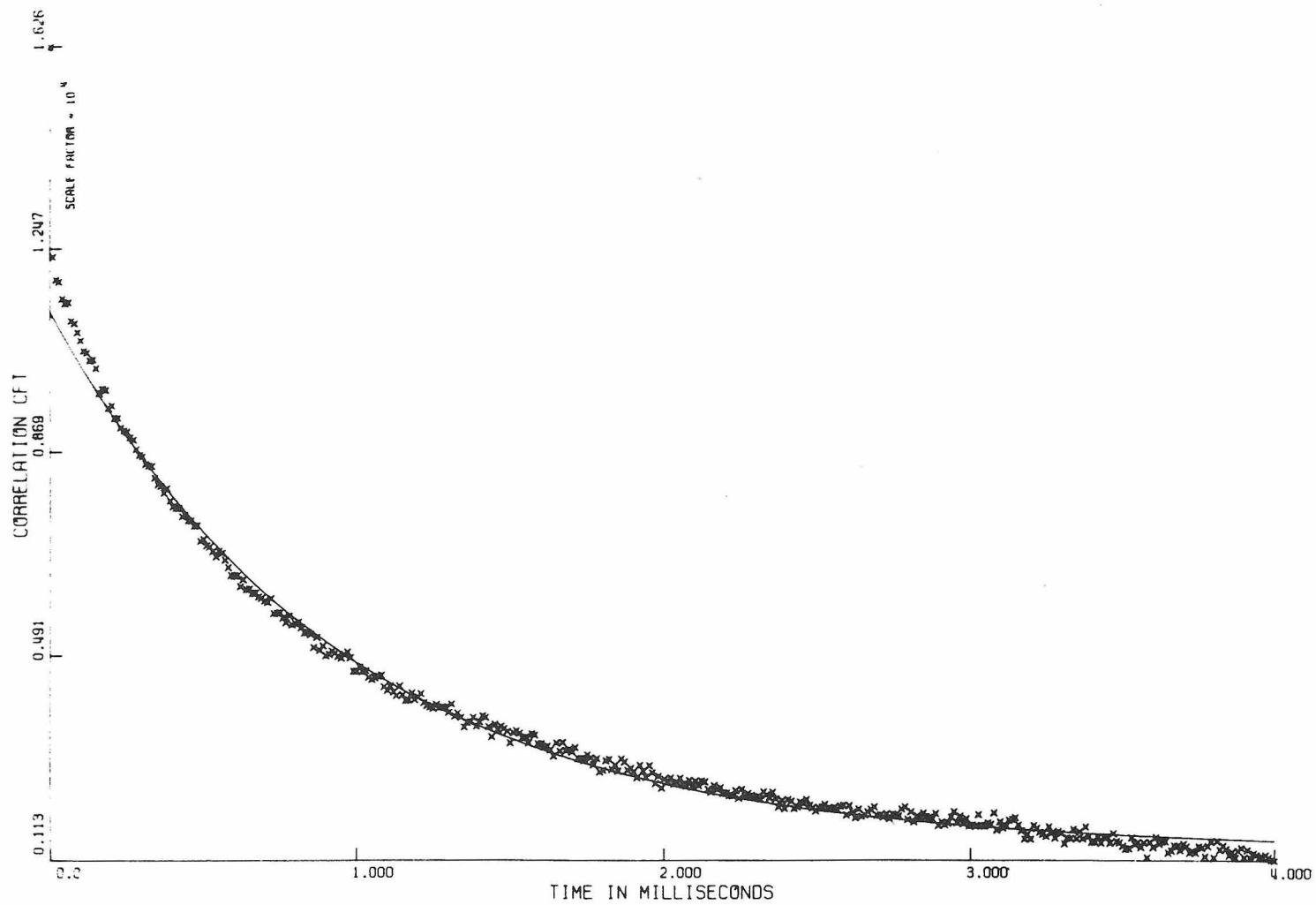


Fig. 26 A typical correlation function collected from a solution of PM2 I DNA. The sample time increment is 10  $\mu$ s. The solid line is a computer fit to the data.

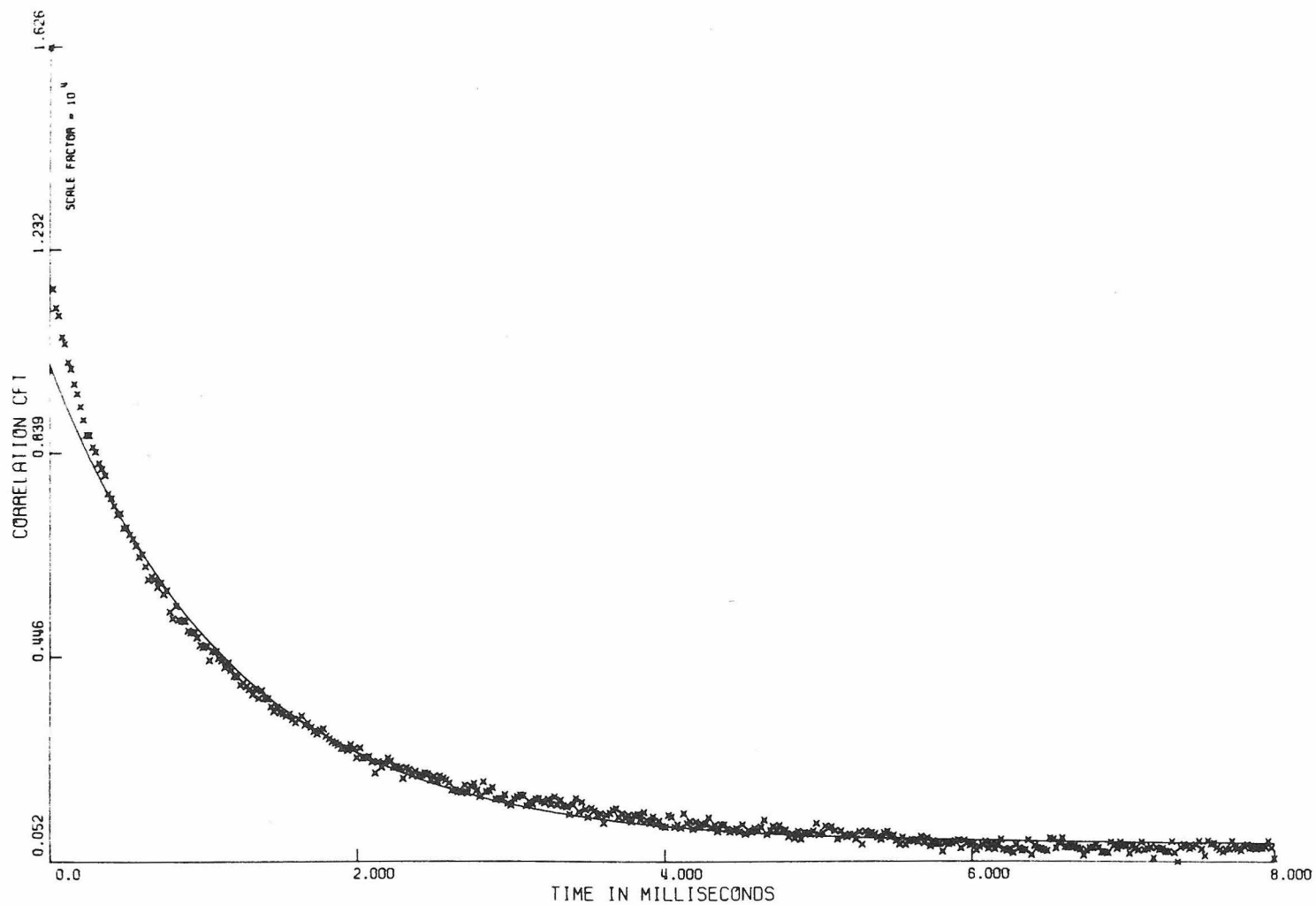


Fig. 27 A typical correlation function for PM2 I DNA collected under conditions identical to those of Figure 26 except that  $\Delta\tau = 20 \mu\text{s}$ .

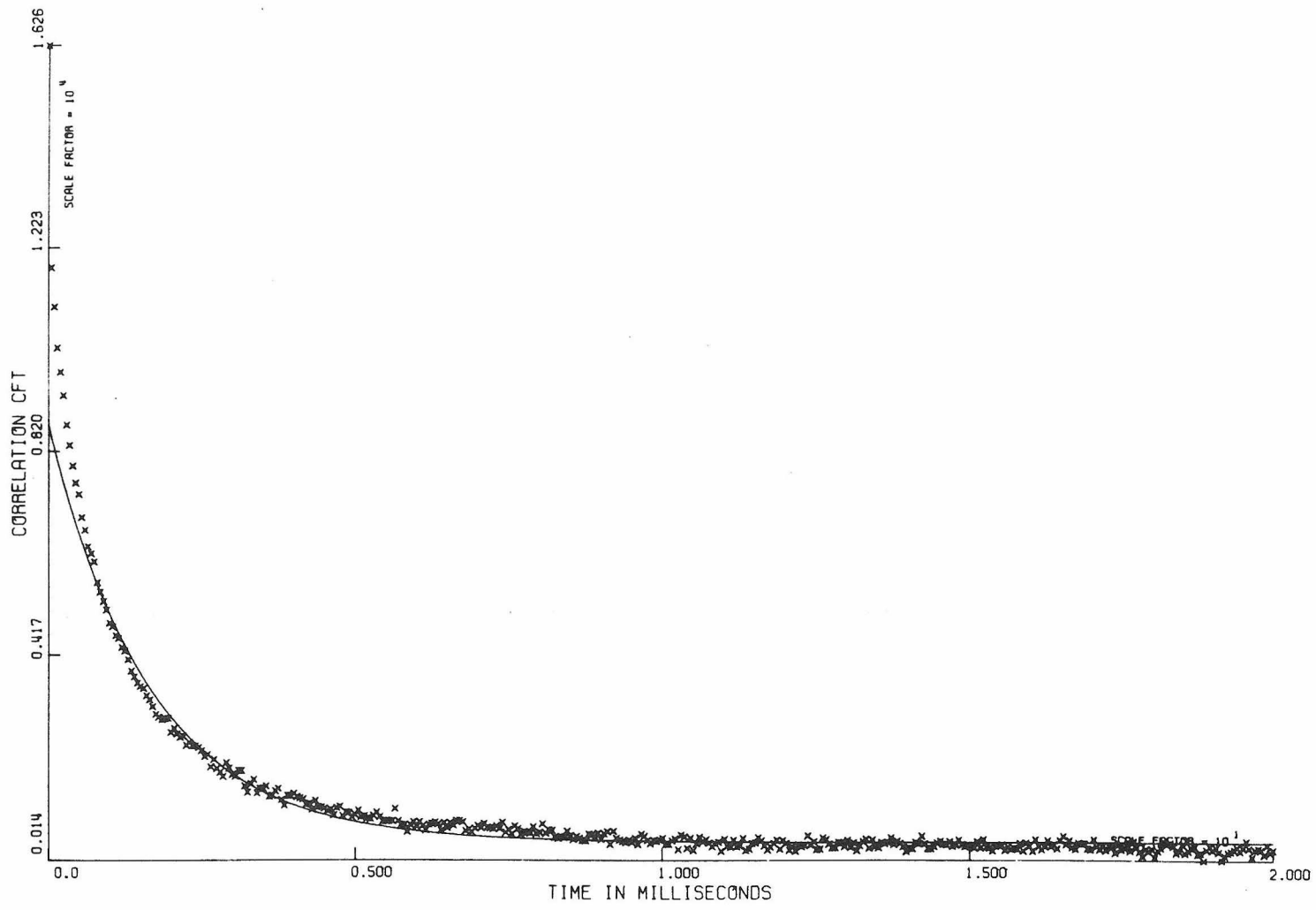


Fig. 28 A typical correlation function for PM2 I DNA collected under conditions identical to those of Figure 26 except that  $\Delta\tau = 50 \mu\text{s}$ .

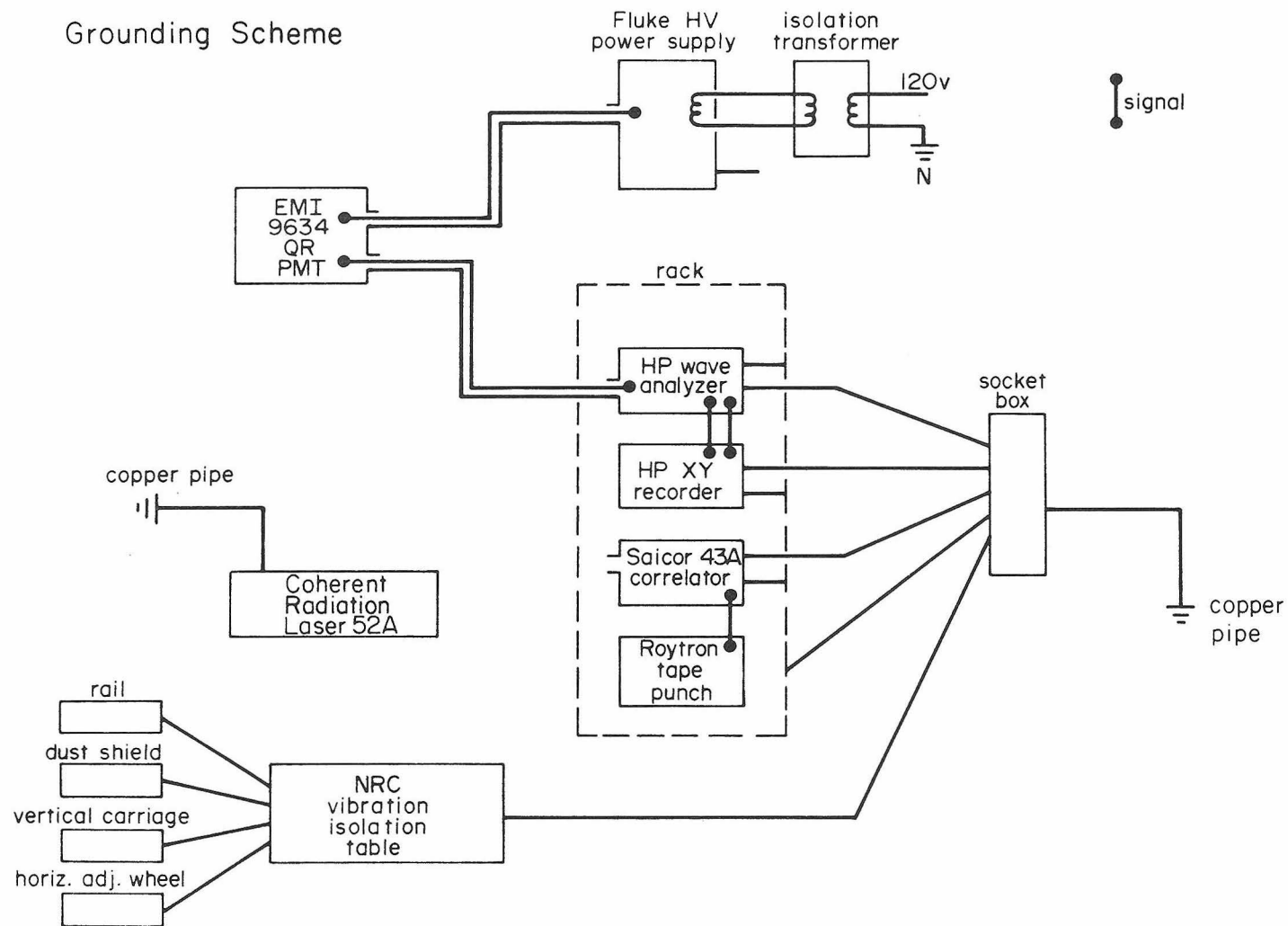


Fig. II.1. Details of the grounding scheme for the light scattering spectrometer

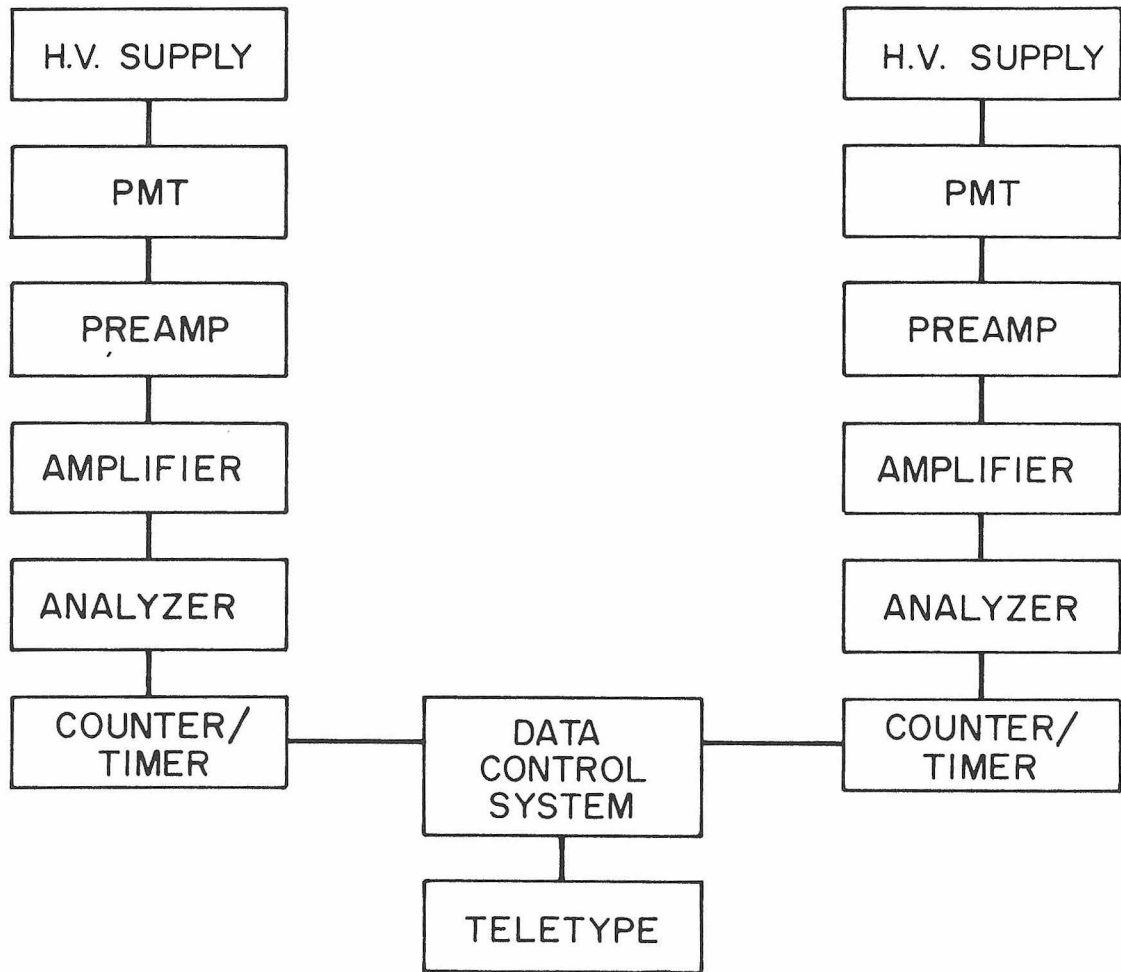


Fig. III.1. Block diagram of the photon counting and data collection systems

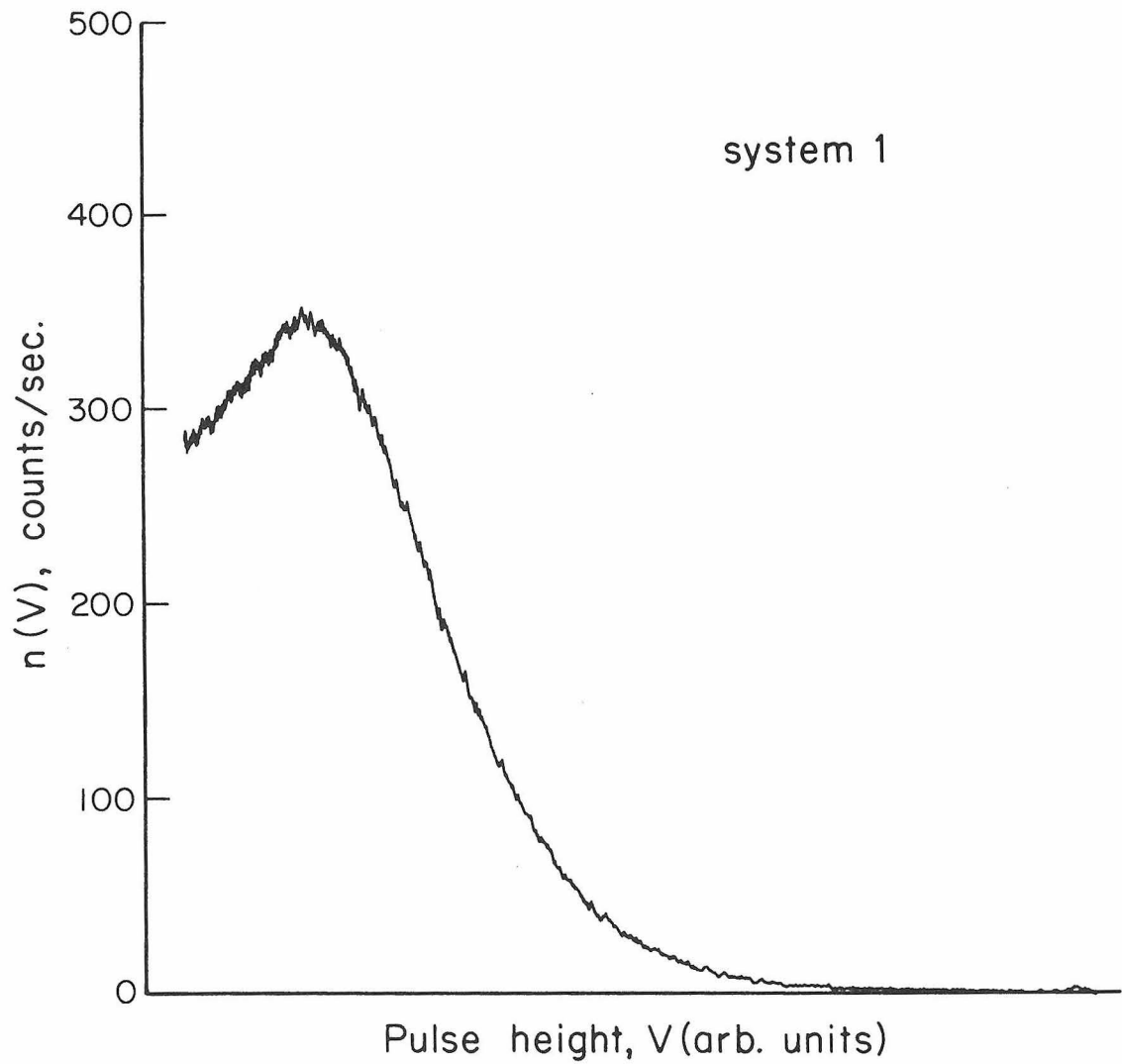


Fig. III.2. A pulse height distribution for the EMI 9789B photo-multiplier tube in system 1, obtained using the E sweep with a window width of 0.04 volts and a power supply voltage of 1350.

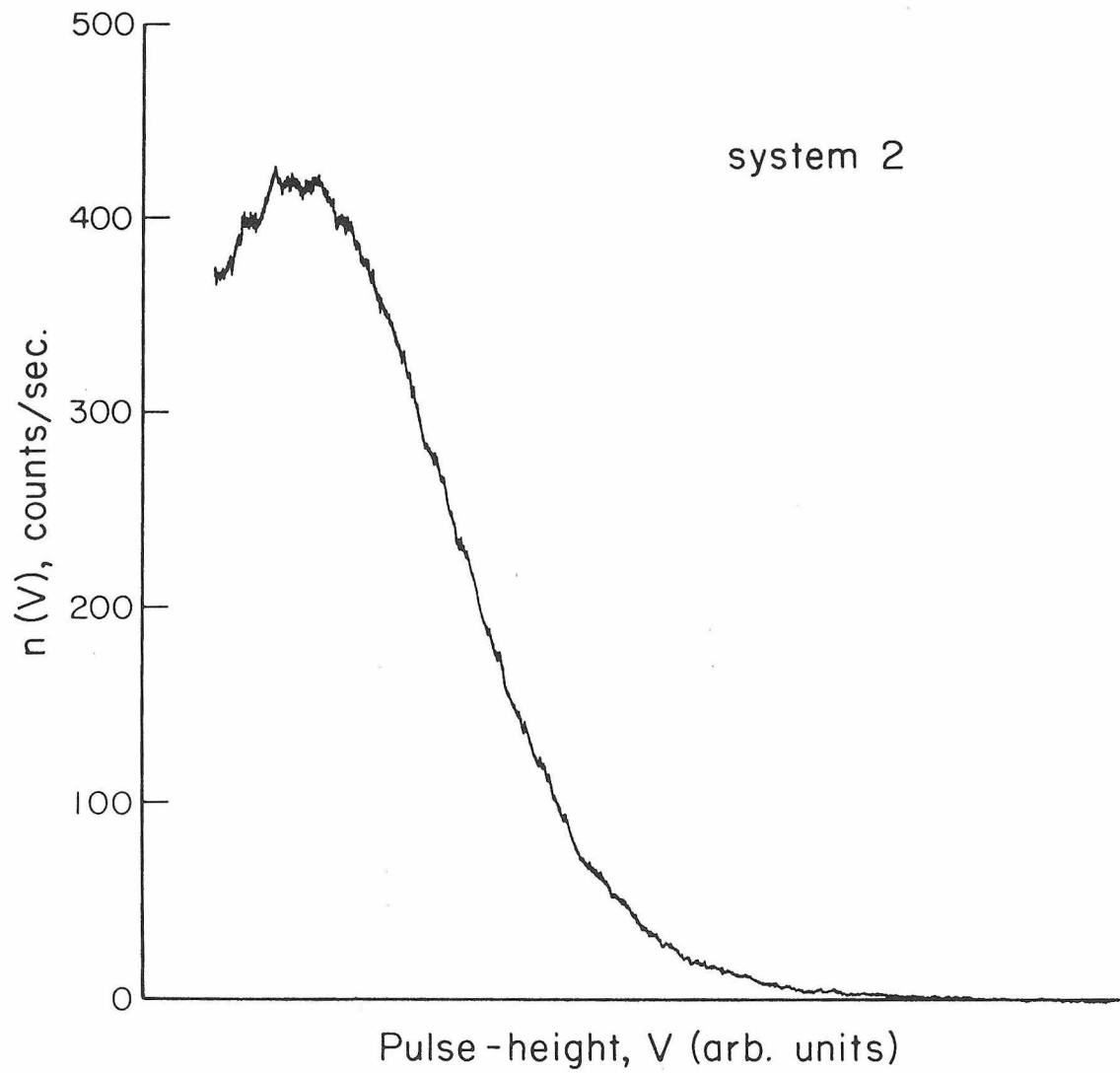


Fig. III.3. A pulse height distribution for the EMI 9789B photo-multiplier tube in system 2, obtained using the E-sweep with a window width of 0.04 volts and a power supply voltage of 1250.

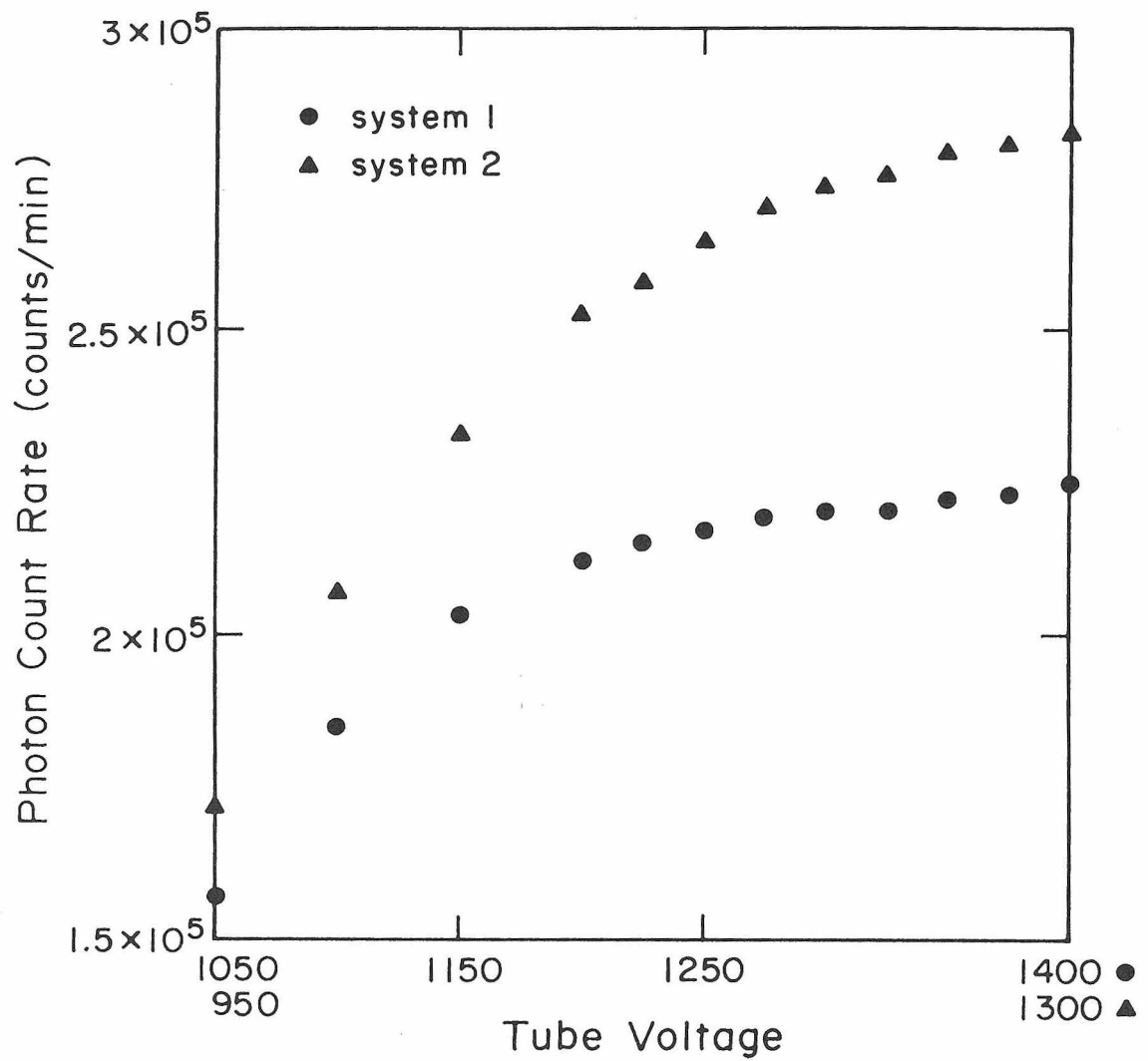


Fig. III.4. The photon count rate as a function of high voltage applied to the photomultiplier tubes. All other variables are fixed.

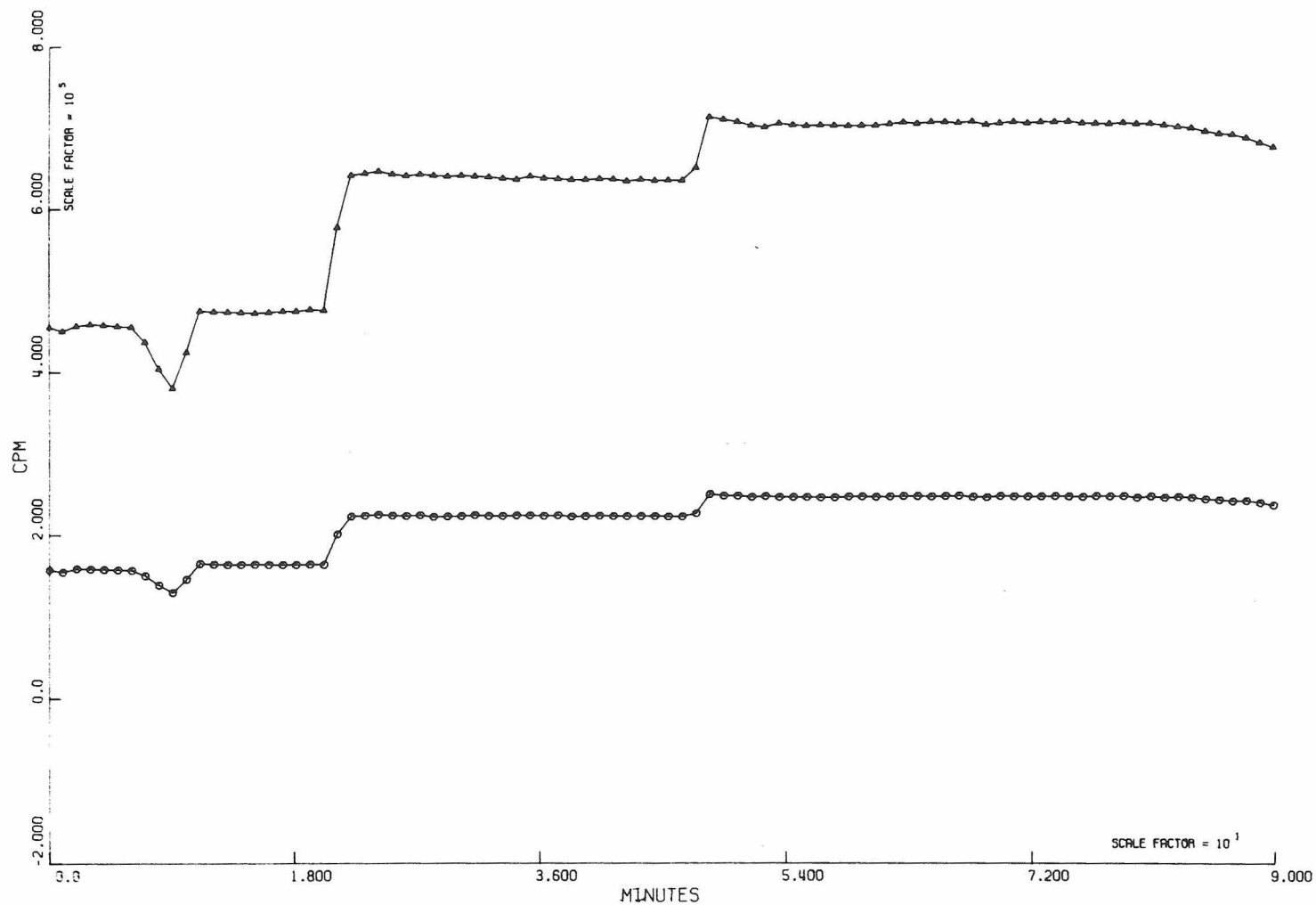


Fig. III.5. Counts per minute interval versus elapsed time. The upper curve corresponds to the reference channel and the lower curve represents the analytical channel. The source is a sample of fluorescein irradiated by laser light and modulated with a variable attenuator.

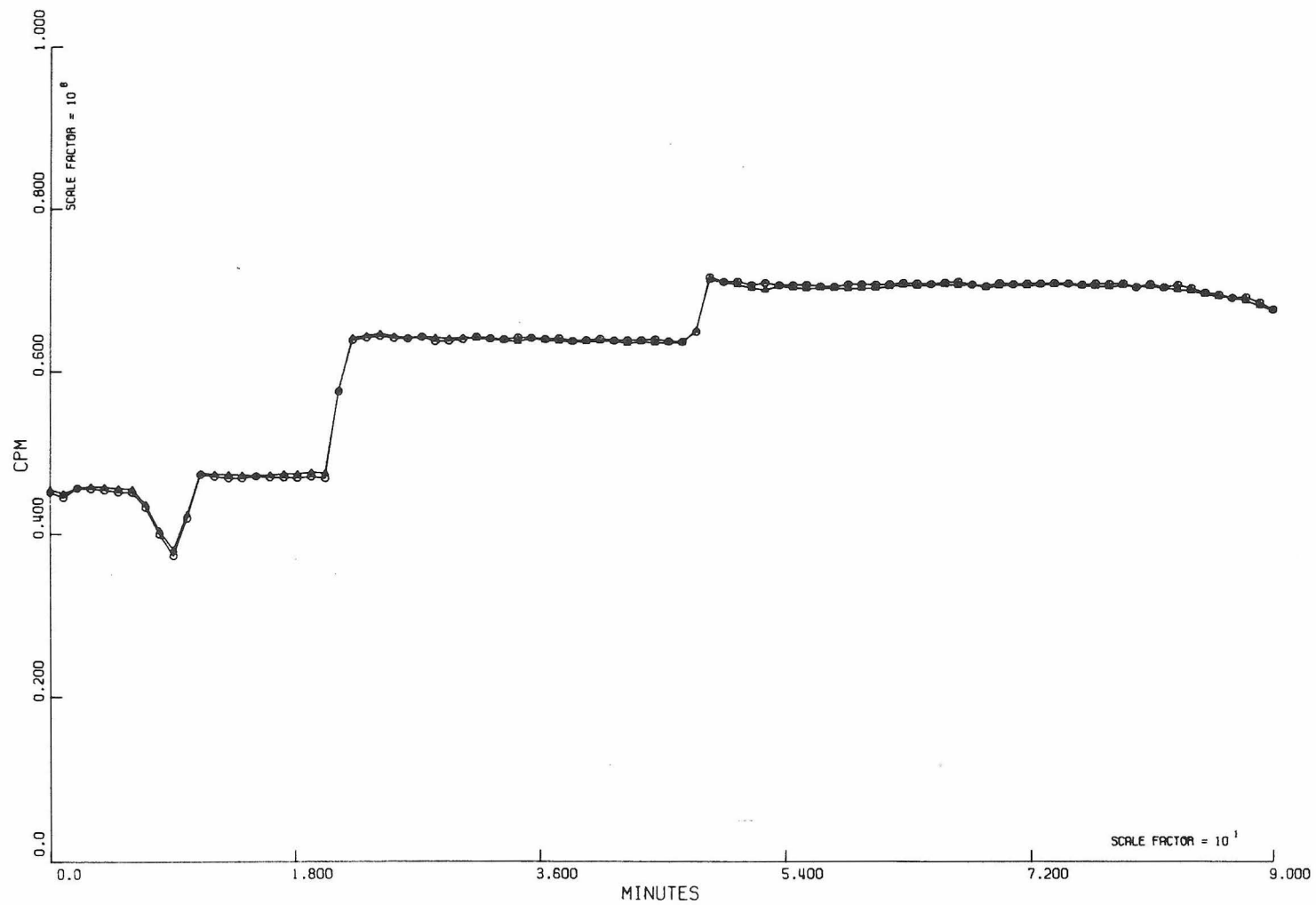


Fig. III.6. Counts per minute interval versus elapsed time. The analytical count rate is normalized to the reference channel. Fluorescein source.

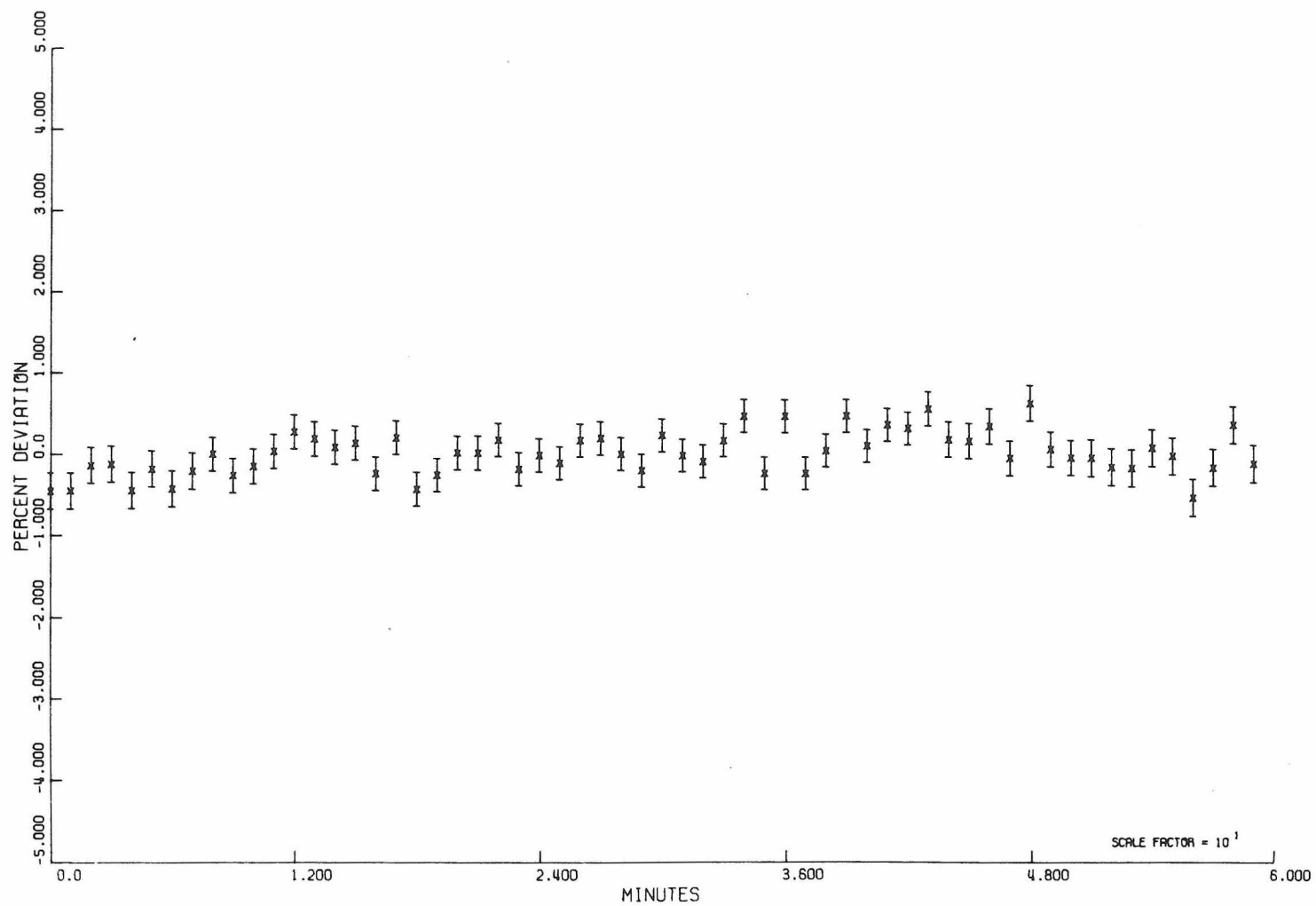


Fig. III.7. Percent departure of the analytical count rate from the reference count rate. Error bars represent one sigma due to counting statistics. Fluorescein source.

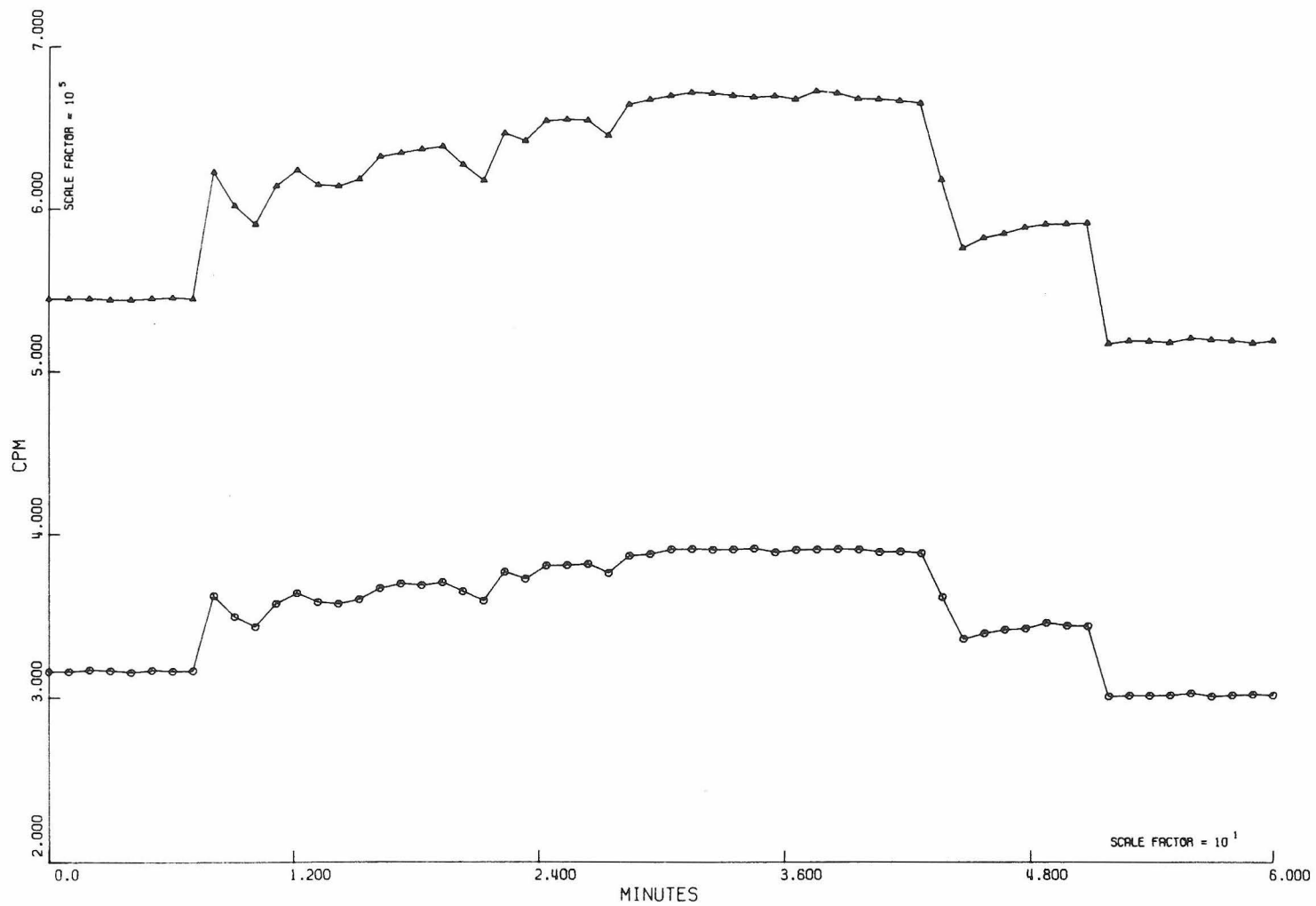


Fig. III.8. Counts per minute interval versus elapsed time. The upper curve corresponds to the reference channel and the lower curve represents the analytical channel. The source is a white light bulb powered by a battery and regulated with a variable resistor.

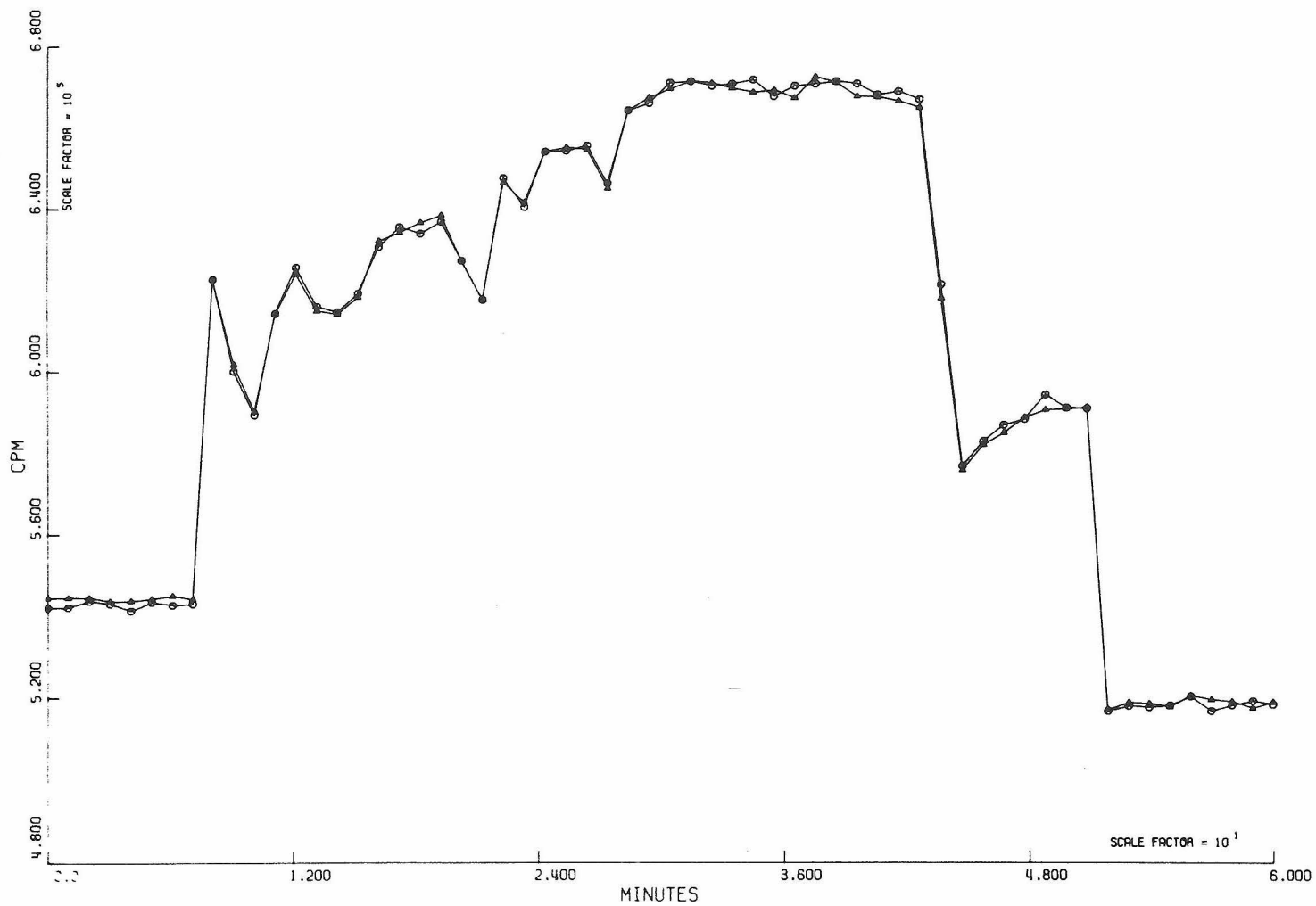


Fig. III.9. Counts per minute interval versus elapsed time. The analytical count rate is normalized to the reference channel. White light source.

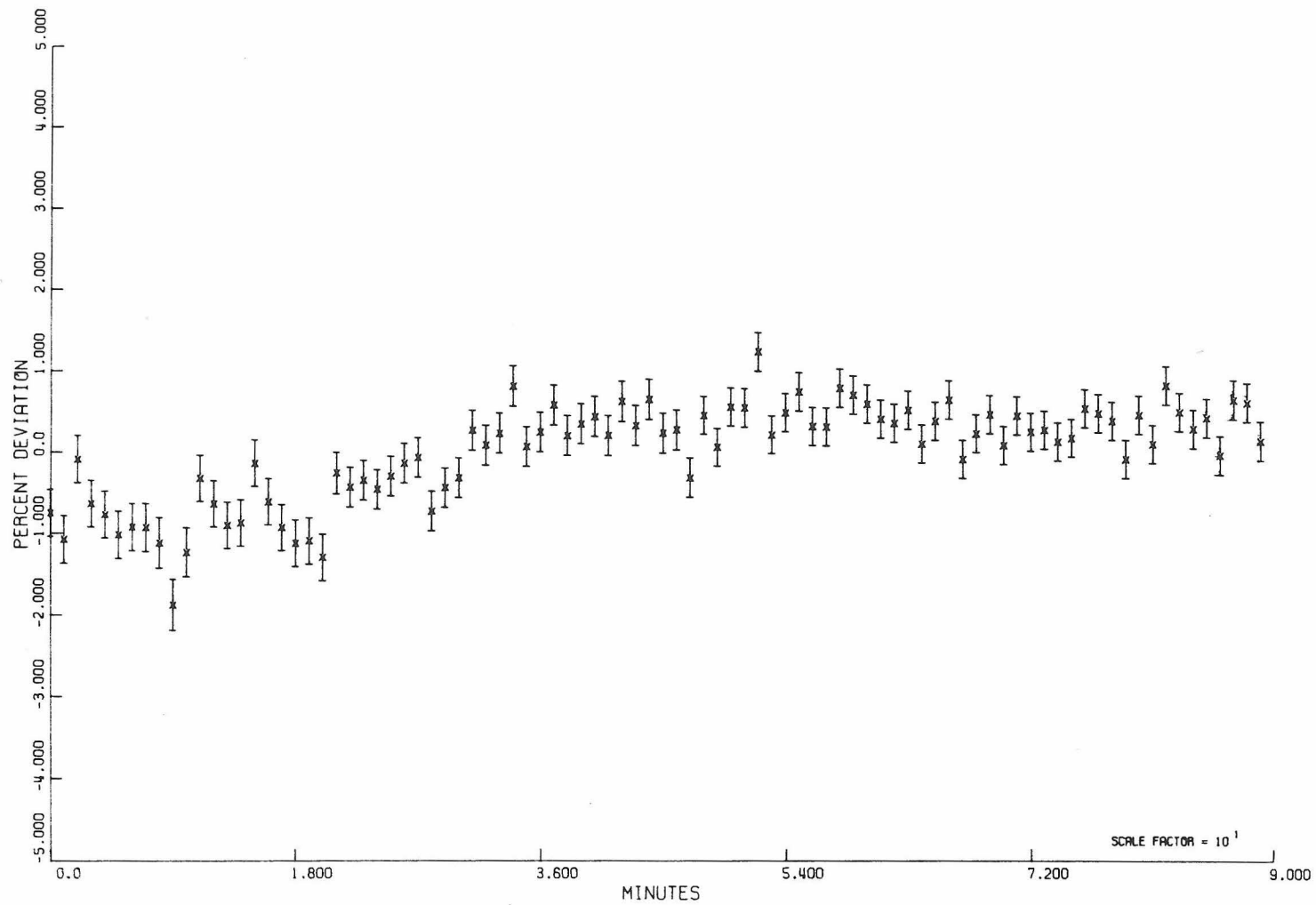


Fig. III.10. Percent departure of the analytical count rate from the reference count rate. Error bars represent one sigma due to counting statistics. White light source.

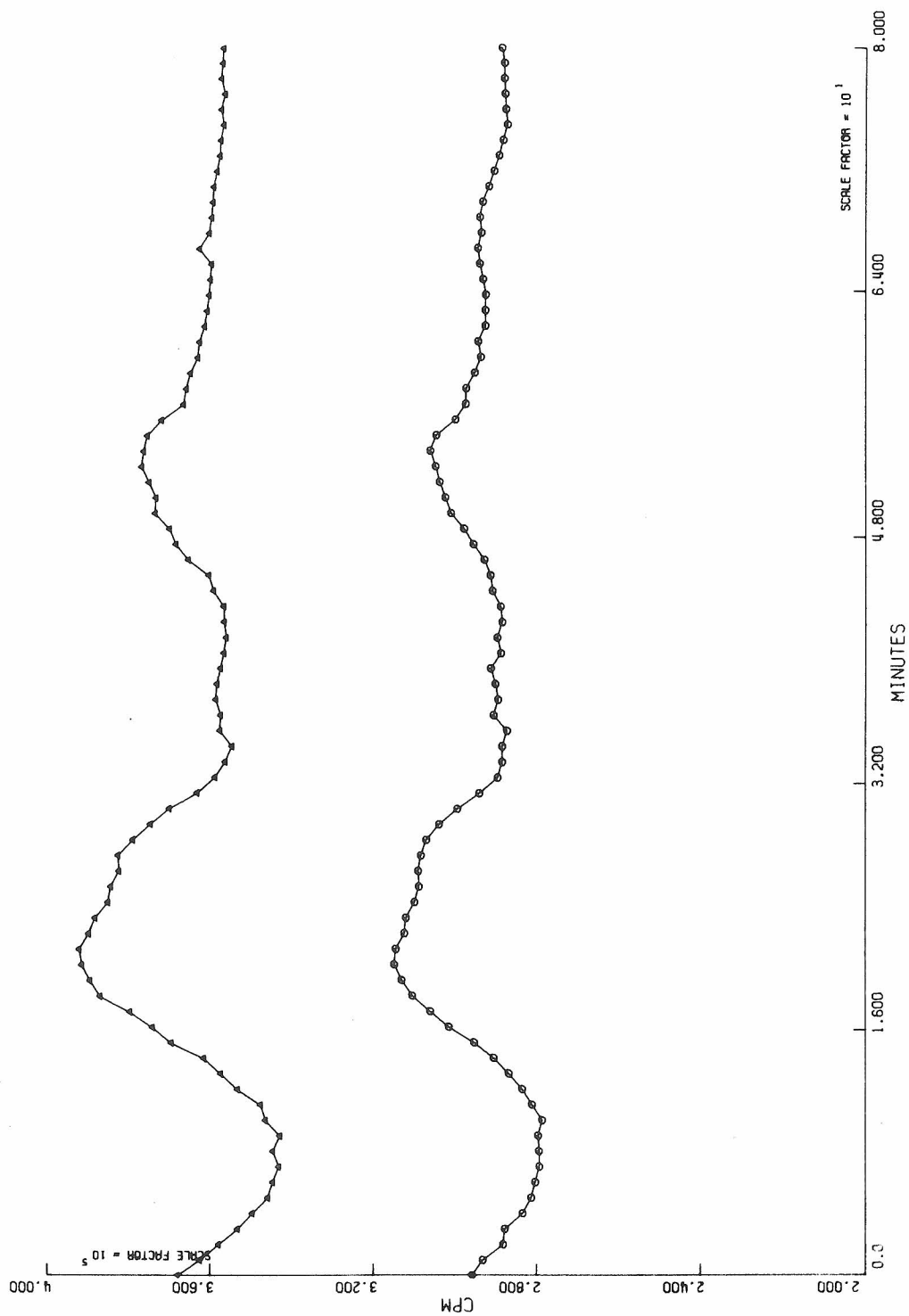


Fig. III.11. Counts per minute interval versus elapsed time. The upper curve corresponds to the reference channel and the lower curve represents the analytical channel. The source is an aqueous solution of polystyrene latex spheres.

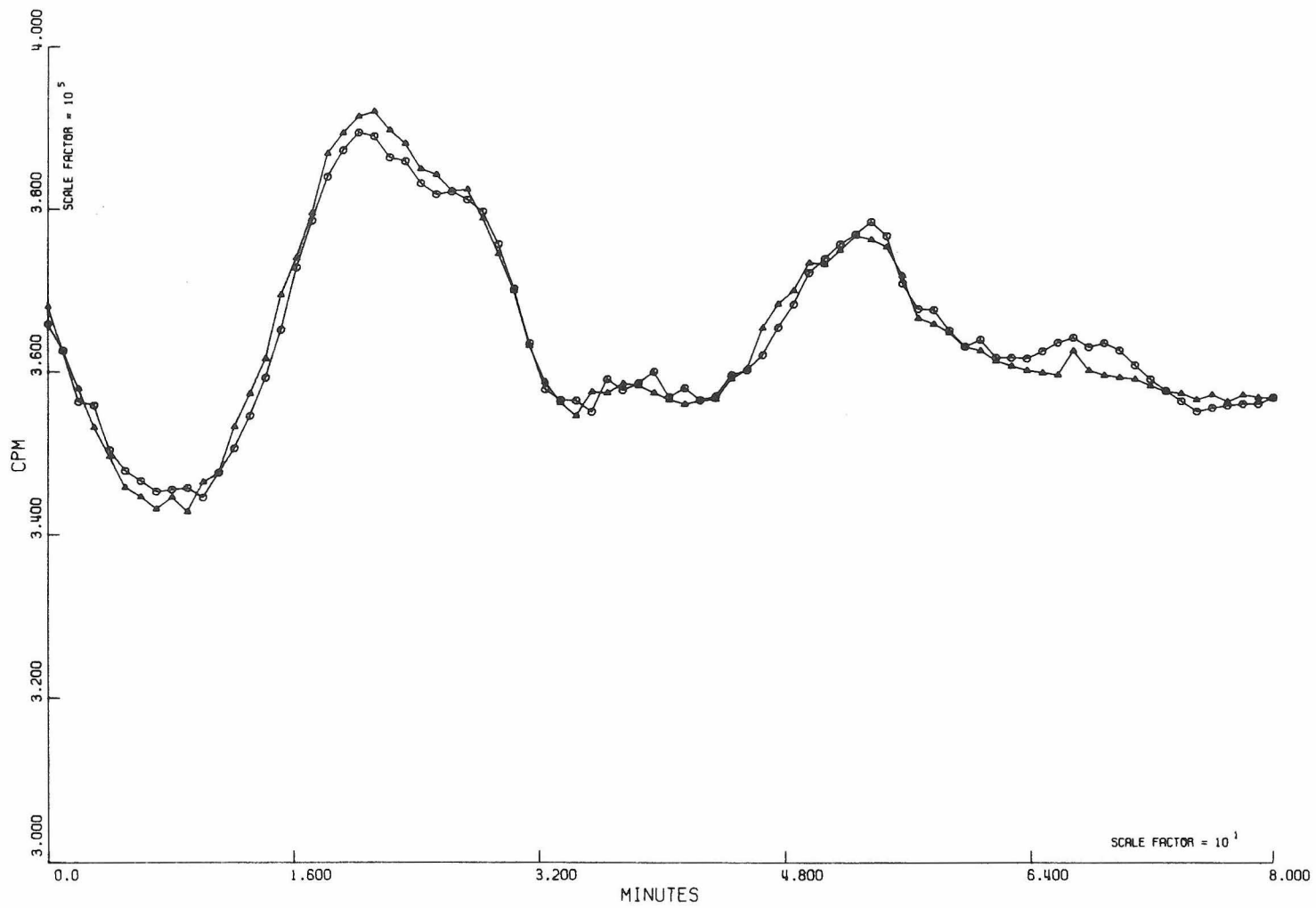


Fig. III.12. Counts per minute interval versus elapsed time. The analytical count rate is normalized to the reference channel. Sphere solution source.

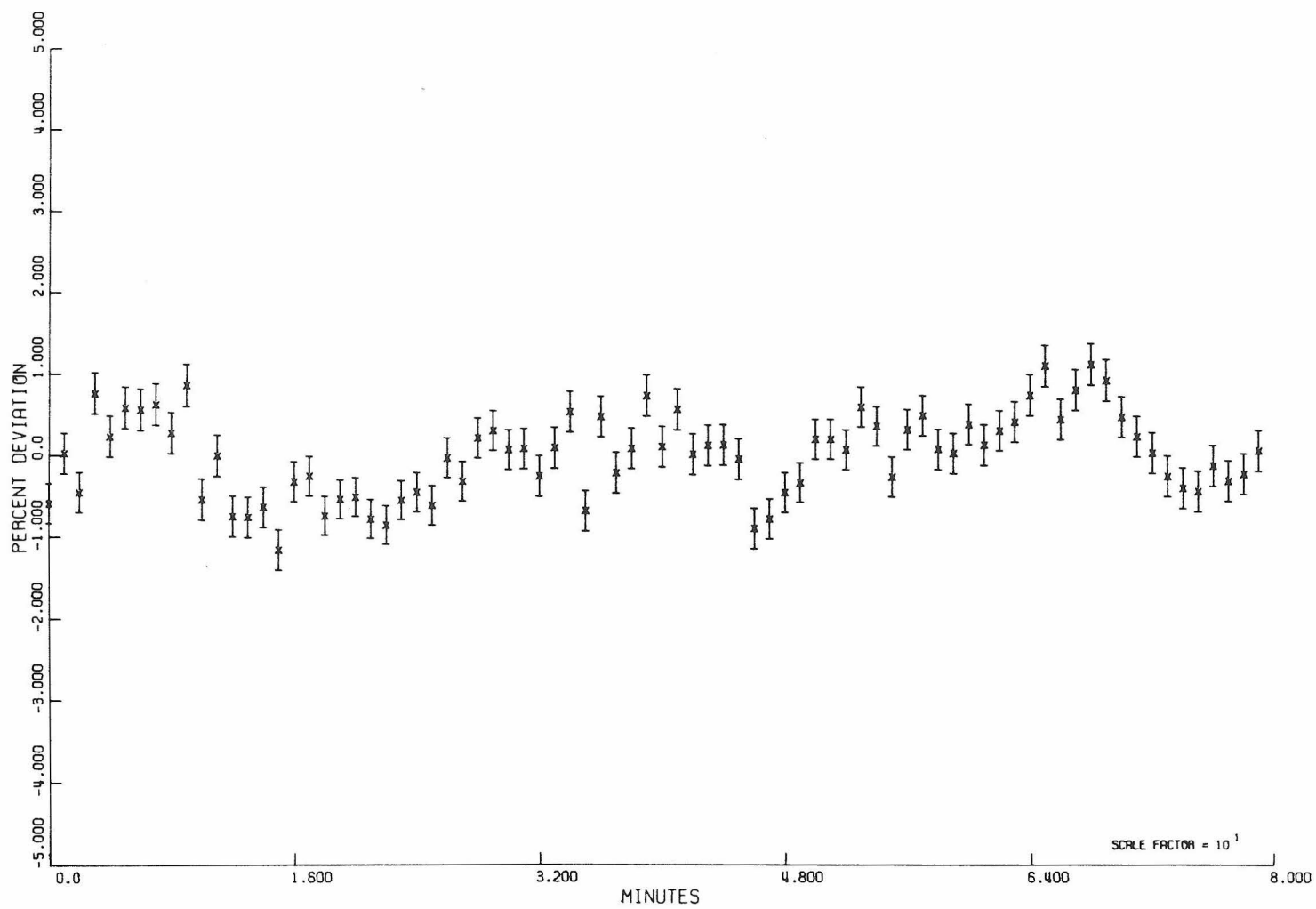


Fig. III.13. Percent departure of the analytical count rate from the reference count rate. Error bars represent one sigma due to counting statistics. Sphere solution source.

A PROPOSAL TO STUDY  
THE  $\lambda$  DNA CYCLIZATION REACTION  
BY CLASSICAL LIGHT SCATTERING

The two cohesive ends of the linear  $\lambda$  DNA molecule are known to be short segments of probably less than ten nucleotides, and are capable of joining intramolecularly to form closed circular monomers. The cyclization of these molecules has been carefully studied by Wang and Davidson (1966a, 1966b). The purpose of this proposition is to show that the cyclization equilibrium and kinetics may be readily studied with a laser light source and conventional light scattering theory and techniques.

According to the theory for scattering from polymer molecules with dimensions comparable to the wavelength of radiation,

$$E_{\text{scat}} \propto \alpha_0 \sum_{j=1}^{\sigma} e^{-i\bar{s} \cdot \bar{r}_j} \quad (1)$$

where  $\alpha_0$  is the polarizability of a monomer unit,  $\bar{r}_j$  is the location of the  $j^{\text{th}}$  segment,  $\sigma$  represents the number of statistical segments in the molecule, and  $\bar{s}$ , the Bragg wave vector, is equal to  $4\pi/\lambda \sin(\theta/2)$ .  $P(\theta)$ , the ratio of scattered intensity with interference to scattered intensity without interference is then

$$P(\theta) = \frac{1}{\sigma^2} \sum_{j=1}^{\sigma} \sum_{k=1}^{\sigma} \cos(\bar{s} \cdot \bar{r}_{jk}) \quad (2)$$

where  $\bar{r}_{jk} = \bar{r}_j - \bar{r}_k$  is the vector leading from the  $j^{\text{th}}$  to  $k^{\text{th}}$  scattering point. Equation (2) represents the value of  $P(\theta)$  for a rigid scattering particle fixed in space, but we are interested in a value of  $P(\theta)$  averaged over all possible orientations and configurations of the molecule. Defining  $\psi$  as the angle between  $\bar{s}$  and  $\bar{r}_{jk}$ , the average over all orientations of  $\cos \bar{s} \cdot \bar{r}_{jk}$  becomes

$$\langle \cos \bar{s} \cdot \bar{r}_{jk} \rangle = \frac{\int_{\psi=0}^{\psi=\pi} \cos(sr_{jk} \cos \psi) \sin \psi d\psi}{\int_{\psi=0}^{\psi=\pi} \sin \psi d\psi}$$

$$\langle \cos s \cdot r_{jk} \rangle = \frac{\sin(sr_{jk})}{sr_{jk}} \quad (3)$$

and substitution in Equation (2) leads to the value of  $P(\theta)$  based on random orientation of the scattering particle,

$$P(\theta) = \frac{1}{\sigma^2} \sum_{j=1} \sum_{k=1} \frac{\sin sr_{jk}}{sr_{jk}}$$

This relation was first derived by Debye for X-ray scattering.

In the process of obtaining a  $P(\theta)$  averaged over all configurations of the molecule, the theory of linear polymer statistics is employed. In particular, we initially treat the linear  $\lambda$  DNA molecules as flexible, random Gaussian coils; the distribution function for end-to-end distances is given by (Jacobson and Stockmayer 1950)

$$W(h)dh \approx \left\{ \frac{3}{2\pi(\ell b)} \right\}^{3/2} \{ \exp(-3h^2/2\ell b) \} 4\pi h^2 dh \quad (4)$$

$\ell$  is the contour length,  $b$  represents the random coil segment length, and  $h$  is the end-to-end distance. Observe that  $\ell b$  equals the mean square end-to-end distance  $\langle h^2 \rangle$ . Again from polymer statistics (Tanford 1961) we know that

$$R_G^2 = \langle R^2 \rangle = \langle h^2 \rangle / 6 \quad (5)$$

where  $R_G$  is the radius of gyration, hence

$$R_G^2 = \lambda b / 6$$

for the linear  $\lambda$  DNA.

Zimm and Stockmayer (1949) have shown that the distribution function for dimensions of a circular molecule is also expressed as a Gaussian, but the mean square end-to-end distance of the circular molecule is reduced by 2 from that of a linear molecule of the length. Thus, for the circular  $\lambda$  DNA

$$R_G^2 = \lambda b / 12$$

The differing radii of gyration for the two molecules account for the difference in their respective scattering envelopes.

With a knowledge of the segment distribution function we are able to perform the averaging over all possible configurations of the molecule. The result, originally derived by Debye, is

$$P(\theta) = (2/u^2) (e^{-u} + u - 1) \quad (6)$$

where

$$u = s^2 R_G^2$$

Using Equation (6) it is possible to compare  $P(\theta)$ 's for the circular and linear molecules. The results of this comparison appear as Figure 1. Values for the two radii of gyration are based on a contour length of  $13.2\mu$  (MacHattie and Thomas 1964) and a statistical segment length

of  $717\text{\AA}$  (Hearst and Stockmayer 1962).

The preceding treatment is oversimplified; we have assumed that  $\lambda$  DNA can be adequately represented as a Gaussian random coil. For the more realistic model of a wormlike coil with excluded volume, Sharp and Bloomfield (1968) have described the light scattering form factors. The qualitative features of the linear and circular form factors do not change dramatically.

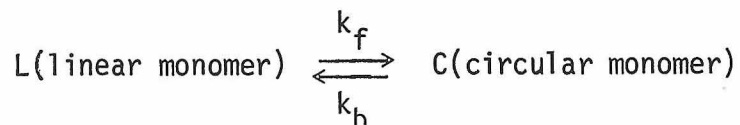
Dawson and Harpst (1971) have reported light scattering measurements on  $\lambda$  DNA. While a number of their conclusions based on low angle extrapolations are questionable (Schmid et al. 1971), they have been able to confirm our expectation of a significant difference between the linear and circular DNA form factors. In the calculations that follow we shall assume that the  $P(\theta)$ 's are experimental values as they are presumably the most accurate.

Experimentally, we observe  $I(\theta)$ , the time averaged intensity at scattering angle  $\theta$ . For the cyclization reaction,  $I(\theta)$  may be expressed as

$$I(\theta) = I_L(\theta) + I_C(\theta)$$

$$I(\theta) = K' \{P_L(\theta) (L) + P_C(\theta) (C)\} \quad (7)$$

$K'$  is a proportionality constant;  $(L)$  and  $(C)$  are the concentrations of linear and circular DNA molecules, respectively. The cyclization process



can be described by a single equilibrium constant

$$K = (C)/(L)$$

Thus scattering at two angles provides enough information to estimate the equilibrium constant of the reaction. Alternatively, all linear or circular DNA could be used initially, eliminating the requirement of a second scattering angle.

The rate constants for the linear relaxation of the system to equilibrium can be studied by following the decay of scattered intensity as a function of time. The cyclization reaction is characterized by the relaxation time  $\tau_R$ , where

$$\tau_R = \frac{1}{k_f + k_b}$$

The time rate of change in intensity is

$$\begin{aligned} \frac{dI}{dt} &= K' \left\{ P_L(\theta) \frac{d(L)}{dt} + P_C(\theta) \frac{d(C)}{dt} \right\} \\ &= K' \frac{d(L)}{dt} \{ P_L(\theta) - P_C(\theta) \} \end{aligned} \quad (8)$$

Defining a configurational factor  $Z$  as

$$Z = P_L(\theta) - P_C(\theta)$$

and integrating Equation (8), we arrive at the expression

$$I_t - I_0 = K'Z x_{L_0} \{ e^{-t/\tau_R} - 1 \} \quad (9)$$

where  $x_{L_0}$  is the initial extent of reaction,  $(L)_0 - (L)_\infty$  (a similar relation holds for circular DNA). Determination of  $\tau_R$  (and therefore  $k_f$  and  $k_b$ ) from the data obtained by continuously monitoring intensity as a function of time follows directly from Equation (9).

The principal advantages of this approach to the study of DNA ring closure are the ease of data acquisition and the accuracy of the method. The entire experiment can be performed without removing the sample from the light scattering apparatus; previous techniques required a sedimentation analysis for each data point. The extreme intensity of the laser light provides the sensitivity required--small relative changes in intensity are easily detected.

In summary, conventional light scattering techniques in conjunction with a laser light source offer an alternate approach to the study of  $\lambda$  DNA cyclization. Classical scattering theory, polymer statistics, and relaxation kinetics provide the foundation for the technique.

LITERATURE CITED

- Dawson, J. R., and J. A. Harpst, *Biopolymers* 10, 2499 (1971)
- Hearst, J. and W. H. Stockmayer, *J. Chem. Phys.* 37, 1425 (1962)
- Jacobson, H., and W. H. Stockmayer, *J. Chem. Phys.* 18, 1600 (1950)
- MacHattie, L. A., and C. A. Thomas, *Science* 144, 1142 (1964)
- Schmid, C. W., F. P. Rhinehart, and J. E. Hearst, *Biopolymers* 10,  
883 (1971)
- Sharp, P. and V. A. Bloomfield, *Biopolymers* 6, 1201 (1968)
- Tanford, C., Physical Chemistry of Macromolecules. Wiley & Sons  
Publishers, NewYork (1961)
- Wang, J. C., and N. Davidson, *J. Mol. Biol.* 15, 111 (1966);  
*Ibid.* 19, 469 (1966)
- Zimm, B., and W. H. Stockmayer, *J. Chem. Phys.* 17, 1301 (1949)

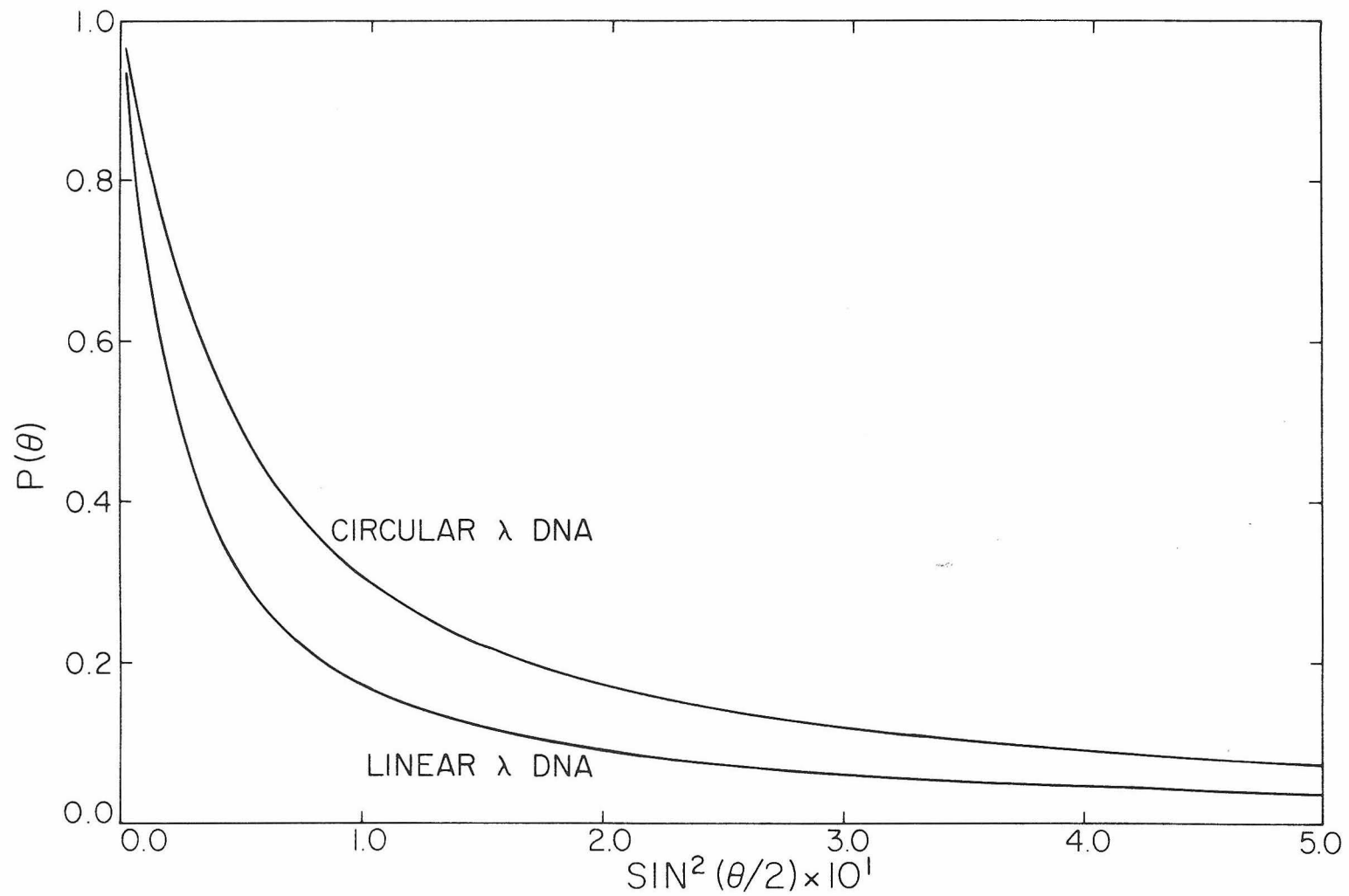


Fig. 1. Scattering form factors for linear and circular  $\lambda$  DNA